UNIVERSIDADE ESTADUAL DE CAMPINAS
FACULDADE DE ENGENHARIA MECÂNICA

Arthur Guilherme Mereles

Mathematical Modeling of Rotor Systems by the Continuous Segment Method

Modelagem Matemática de Rotores pelo Método do Segmento Contínuo

CAMPINAS

2021

Arthur Guilherme Mereles

Mathematical Modeling of Rotor Systems by the Continuous Segment Method

Modelagem Matemática de Rotores pelo Método do Segmento Contínuo

Dissertation presented to the School of Mechanical Engineering of the University of Campinas in partial fulfillment of the requirements for the degree of Master in Mechanical Engineering, in the area of Solid Mechanics and Mechanical Design.

Dissertação apresentada à Faculdade de Engenharia Mecânica da Universidade Estadual de Campinas como parte dos requisitos exigidos para obtenção do título de Mestre em Engenharia Mecânica, na Área de Mecânica dos Sólidos e Projeto Mecânico

Orientadora: Profa. Dra. Katia Lucchesi Cavalca Dedini.

ESTE TRABALHO CORRESPONDE À VERSÃO FINAL DA DISSERTAÇÃO DEFENDIDA PELO ALUNO ARTHUR GUILHERME MERELES, E ORIENTADA PELA PROFA. DRA. KATIA LUCCHESI CAVALCA DEDINI

CAMPINAS

2021

Ficha catalográfica
Universidade Estadual de Campinas
Biblioteca da Área de Engenharia e Arquitetura
Rose Meire da Silva - CRB 8/5974

M541m

Mereles, Arthur Guilherme, 1997-
Mathematical modeling of rotor systems by the continuous segment method / Arthur Guilherme Mereles. – Campinas, SP : [s.n.], 2021.

Orientador: Katia Lucchesi Cavalca Dedini.
Dissertação (mestrado) – Universidade Estadual de Campinas, Faculdade de Engenharia Mecânica.

1. Rotores. 2. Análise no domínio do tempo. 3. Rotores - Dinâmical. 4. Análise modal. 5. Sistemas de parâmetros distribuídos. 6. Equações de movimento. I. Dedini, Katia Lucchesi Cavalca, 1963-. II. Universidade Estadual de Campinas. Faculdade de Engenharia Mecânica. III. Título.

Informações para Biblioteca Digital

Título em outro idioma: Modelagem matemática de rotores pelo método do segmento contínuo
Palavras-chave em inglês:
Rotors
Time domain analysis
Rotor - Dynamics
Modal analysis
Distributed parameter systems
Equations of motion
Área de concentração: Mecânica dos Sólidos e Projeto Mecânico
Titulação: Mestre em Engenharia Mecânica
Banca examinadora:
Katia Lucchesi Cavalca Dedini [Orientador]
Josué Labaki Silva
Carlos Alberto Bavastri
Data de defesa: 25-02-2021
Programa de Pós-Graduação: Engenharia Mecânica

Identificação e informações acadêmicas do(a) aluno(a)
- ORCID do autor: https://orcid.org/0000-0002-1921-7934
- Currículo Lattes do autor: http://lattes.cnpq.br/7275080884849491

UNIVERSIDADE ESTADUAL DE CAMPINAS
FACULDADE DE ENGENHARIA MECÂNICA

DISSERTAÇÃO DE MESTRADO ACADÊMICO

Mathematical Modeling of Rotor Systems by the Continuous Segment Method

Modelagem Matemática de Rotores pelo Método do Segmento Contínuo

Autor: **Arthur Guilherme Mereles**

Orientador: **Profa. Dra. Katia Lucchesi Kavalca Dedini**

A Banca Examinadora composta pelos membros abaixo aprovou esta Dissertação:

Profa. Dra. Katia Lucchesi Cavalca Dedini

Prof. Dr. Josué Labaki Silva

Prof. Dr. Carlos Alberto Bavastri

A Ata de Defesa com as respectivas assinaturas dos membros encontra-se no SIGA/Sistema de Fluxo de Dissertação/Tese e na Secretaria do Programa da Unidade.

Campinas, 25 de fevereiro de 2021

Acknowledments

Gostaria de agradecer a todos que contribuíram direta ou indiretamente na concepção deste trabalho.

Agradeço à minha orientadora, profa. Dra. Katia, pelos conhecimentos passados e pela confiança no meu trabalho.

Agradeço à minha companheira, Victória, por sempre estar a meu lado e me animar em tempos difíceis. Sem você tudo seria muito mais difícil.

Em especial, gostaria de agradecer meus pais, Ivone e Evelio, por terem me criado e me incentivado sempre em minhas conquistas. Sem o constante suporte de vocês não conseguiria ir longe, agradeço de coração.

Agradeço também à Universidade de Campinas (UNICAMP) e a Faculdade de Engenharia Mecânica (FEM) pela oportunidade.

O presente trabalho foi realizado com apoio da Conselho Nacional de Desenvolvimento Científico e Tecnológico (CNPq), processo no 133719/2019-7.

Resumo

Neste trabalho, apresenta-se um novo método aplicado na modelagem de rotores. Uma vez que o processo de modelagem matemática é essencial em aplicações de engenharia, a contribuição deste trabalho é providenciar uma abordagem alternativa para o estudo de máquinas rotativas, considerando reduzido número de graus de liberdade essenciais à representação da dinâmica destas. Estas máquinas são majoritariamente compostas por eixos, modelados como vigas, impulsores ou pás, modelados como discos rígidos, e mancais, modelados como um sistema mola-amortecedor. O método, denominado Método do Segmento Contínuo (MSC ou CSM em inglês), pode ser aplicado em sistemas com um número arbitrário de eixos segmentados, discos e mancais. O modelo do eixo considera a flexão e a deformação por cisalhamento, porém ignora os movimentos axiais e torcionais. Os discos são modelados com massas rígidas, e podem ter geometrias assimétricas. Os mancais são molas e amortecedores lineares com coeficientes equivalentes de rigidez e amortecimento que podem ser isotrópicos ou anisotrópicos. Por meio do MSC, soluções analíticas fechadas podem ser obtidas para rotores com geometrias segmentadas. Isso é feito, primeiramente, resolvendo o problema de auto-valor do sistema, onde obtém-se as auto-funções e os auto-valores, que representam os modos de vibrar e as frequências naturais, respectivamente. Com as auto-funções, a análise modal pode ser aplicada para discretizar as equações de movimento levando a equações diferenciais desacopladas para as coordenadas modais. O número de equações é igual ao número de modos de vibrar necessários para se obter a resposta, que pode ser pequeno dependendo do intervalo de rotação estudado. O MSC é avaliado comparando seus resultados ao amplamente conhecido e consolidado Método dos Elementos Finitos (MEF ou FEM em inglês), este bem estabelecido e aplicado em dinâmica de rotores. Os resultados das frequências naturais, formas modais e resposta forçada são comparados, mostrando-se a eficácia do MSC em modelar uma grande variedade de rotores e estabelecendo-o como uma ferramenta alternativa para o estudo de máquinas rotativas.

Palavras Chaves: rotores com mancais, dinâmica de rotores, análise modal, rotores multissegmentados, estudo numérico.

Abstract

In this work, a new method for the modeling of rotor systems is presented. Since process of mathematical modeling is essential in engineering applications, the contribution of this work is to provide an alternative approach to study rotating machines, taking into account reduced number of degrees of freedom, essentials to represent the system dynamics. These machines are composed for the most part of shafts, modeled as beams, impellers or blades, modeled as rigid disks and bearings, being these represented as a spring-damper system. The method, named Continuous Segment Method (CSM), can be applied to systems with an arbitrary number of segmented shafts, disks and bearings. The shaft model considers bending and shear deformation but neglects torsional and axial motions. The disks are modeled as rigid masses, and can have asymmetric geometries. The bearings are linear springs and dampers with equivalent dynamic coefficients that can be isotropic or anisotropic. By means of the CSM, closed-form solutions of rotor systems with stepped geometries can be obtained. This is done by first solving the eigenvalue problem of the system and obtaining the eigenfunctions and eigenvalues, that represent the mode shapes and natural frequencies, respectively. With the eigenfunctions, modal analysis can be applied to discretize the equations of motion leading to uncoupled differential equations for the modal coordinates. The number of equations equals the number of modes of vibration needed for the response, which can be a small number depending on the rotational speed range studied. The CSM is evaluated by comparing its results with the Finite Element Method (FEM), which is a very well established method and it is commonly used in rotordynamics. The results of natural frequencies, mode shapes and forced response are compared, showing the effectiveness of the CSM to model a great variety of rotor systems and establishing it as an alternative tool to study rotating machines.

Keywords: rotor-bearing systems; rotordynamics; modal analysis; multi-stepped rotor; numerical study.

List of Figures

List of Tables

Nomenclature

Acronyms

CSM	Continuous segment method
DWL	Dry-friction whirl
DWP	Dry-friction whip
EHP	Extended Hamilton principle
FEM	Finite element method
$FWAR$	Forward annular rub
$FWPR$	Forward partial rub
TMM	Transfer matrix method

Variables

$\bar{A}(x)$	Distributed cross-sectional area
$\bar{c}_{ij}(x)$	Distributed bearing damping
$\bar{I}(x)$	Distributed area moment of inertia
$\bar{J}_d(x)$	Distributed diametral moment of inertia
$\bar{J}_p(x)$	Distributed polar moment of inertia
$\bar{k}_{ij}(x)$	Distributed bearing stiffness
$\chi(t)$	Indentation on contact
$\delta_d(x)$	Dirac's delta function
δ_i, ε_i	Mode shape parameters
δ_{ij}	Kronecker delta
$\dot{\theta}(t)$	Whirl speed
κ	Shear correction factor
λ	Eigenvalue
μ_m	Maximum friction coefficient

Ω	Rotating speed
ω	Natural frequency (imaginary part of eigenvalue)
$\phi(x)$, $\eta(x)$	Eigenfunctions
ρ	Density of the rotor
σ	Damping parameter (real part of eigenvalue)
ξ_i	Local coordinate of segment i
b	Contact location along the rotor
c_h	Contact damping
E	Young Modulus
$f(x,t)$	Distributed external force function
$F_c(t)$	Contact force
$F_t(t)$	Tangential force
G	Shear Modulus
$H(x)$	Heaviside unit step function
k_h	Contact stiffness
K_i	Complex normalizing constant of mode i
L	Length of the rotor
$q(t)$	Modal coordinates
R	Shaft radius
T	Kinetic Energy
$u(x,t)$, $\psi(x,t)$	Displacement and bending angle fields
V	Potential Energy
$v_{rel}(t)$	Relative velocity on contact point
W_{nc}	Work of non-conservative forces

Matrices and Vectors

$[A]$, $[B]$	Matrices of boundary conditions
$[c]$	Distributed damping and/or gyroscopic matrix
$[H_i]$	Transfer matrix between segments i and $i+1$
$[h_i]$	Matrix of continuity conditions
$[K]$	Stiffness matrix in state-space
$[k]$	Distributed stiffness matrix
$[L]$	Matrix of Laplace transform coefficients
$[M]$	Mass matrix in state-space
$[m]$	Distributed mass matrix
$\{\hat{\Phi}(s)\}$	Vector of Laplace transform
$\{\Phi_i(x)\}$	Vector of eigenfunctions
$\{W(x,t)\}$	Distributed state vector
$\{w(x,t)\}$	Distributed vector of displacements and slope
$\{X(\xi_i)\}$	Vector of local eigenfunctions

Operations

$(')$	Spatial derivative (see text for variable)
$(\dot{})$	Time derivative (d/dt)
$(\tilde{})$	Adjoint parameter
$(^*)$	Complex conjugate
$[\cdot]$	Matrix
$[\cdot]^H$	Conjugate transpose of matrix
$[\cdot]^T$	Transpose of matrix
$\langle\cdot\rangle$	Internal product
$\{\cdot\}$	Vector

Summary

1 Introduction

Mathematical modeling is an essential process in engineering applications, as it not only provides means to predict faults in the machines but also allows insights into the dynamics of the systems. Engineers can then use such insights to develop better and more efficient machines, which in turn will require better and more complex models. The first mathematical models developed to study rotating machines were mainly to understand the functioning of them. This was required as these machines showed complex behavior that were unique early on. After the establishment of the models and the introduction of the main concepts in rotordynamics such as critical speeds and mass unbalance, more elaborate models were needed to further optimize these machines and even use them in airplanes. The two main approaches used to model these machines were the Transfer Matrix Method (TMM) and the Finite Element Method (FEM). When it comes to the design of rotating machines, the FEM has long been established as the main tool due to its versatility in modeling complex geometry systems.

Despite the several advantages of the FEM, it generally gives a large number of degrees of freedom (DOFs), specially for systems with complex geometry. Thus, one generally needs a model reduction technique, in order to obtain a reduced number of equations. This facilitates, for example, in the design of controllers for vibration attenuation and the identification of parameters in the systems.

Rotating machines can also be modeled by means of a continuous model. In this approach, the system is discretized by means of eigenfunctions, that give the mode shapes, and are obtained by means of separation of variables from the equations that govern the

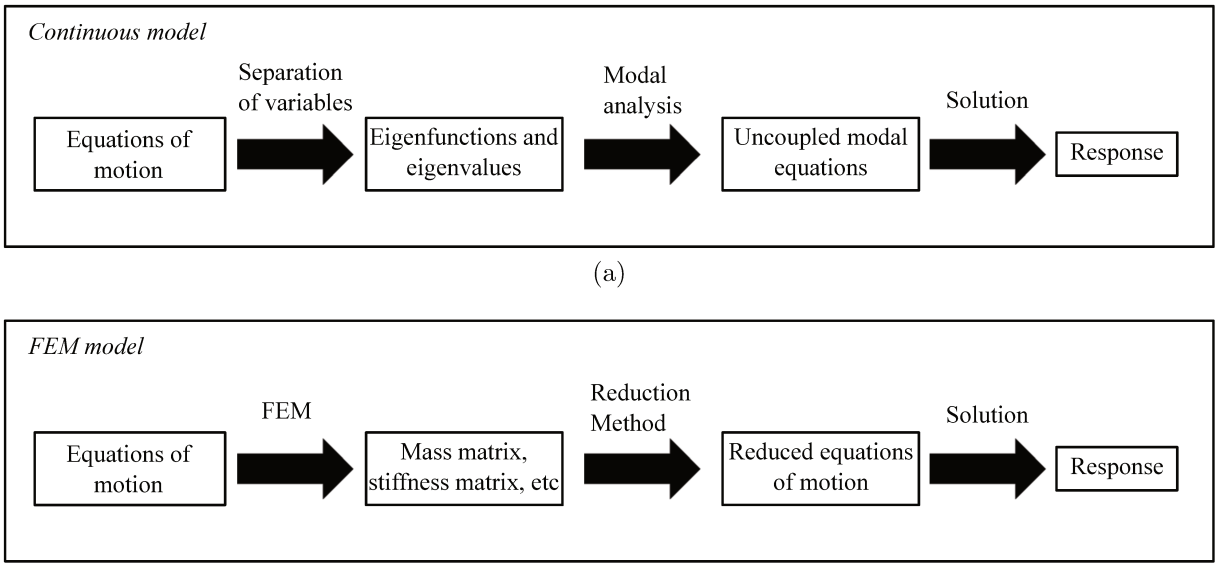

Figure 1: Continuous and FEM model fluxogram.

system. With the eigenfunctions, one can then apply modal analysis to arrive at uncoupled differential equations for the modal coordinates, which can be solved to obtain the response of the continuous system. Figure 1 illustrates the approaches taken in the continuous model in comparison to a model based on the FEM. As mentioned above, in the continuous model one starts with the equations of motion, in this case partial differential equations, and applies the separation of variables to obtain the eigenfunctions and eigenvalues. This first step is the main disadvantage of the continuous approach, since it can be done only for systems with simple geometry that can be modeled by beams or plates. In the FEM model, the equations of motion, traditionally transformed in the weak form, are discretized using shape functions. These are comparison functions, and only satisfy the geometric boundary conditions of the system. The domain is divided into elements, where one obtains local mass, stiffness, damping, and gyroscopic matrices. These matrices can be assembled to represent the entire system, which is now a discrete system instead of a continuous one. The assembled matrices give the global equations of motion, that can be reduced by means of modal analysis or Guyan static reduction, for example, before performing the solution. From the above discussion, the main distinction between the continuous model and FEM model is in the discretization of the continuous system. The discretization done in the FEM facilitates the introduction of complex geometries.

In this work, a method is introduced that uses the continuous approach to model multi-stepped rotor systems with multiple bearings and disks. The method, named Continuous Segment Method (CSM), extends the continuous approach to more complex geometry systems. By means of the CSM, eigenfunctions of rotors with multiple segments can be obtained, allowing the obtention of critical speeds, mode shapes and unbalance response. The system is still required to have segments with constant cross-sections, but the CSM can be applied to rotor systems with anisotropic bearings, asymmetric rigid disks and multiple segments.

1.1 Objectives

This work presents a new method, namely the CSM, to model multi-stepped rotor systems with several disks and bearings. The method is valid for a wide range of systems such as with isotropic and anisotropic bearings and with asymmetric disks and shafts. By means of the CSM, exact solutions can be obtained for rotors with segments of constant cross-section. By means of numerical simulations, the CSM is evaluated by comparing its results with the ones given by the FEM, showing the effectiveness of the method in modeling rotor systems of several kind.

The results that will be presented are: Campbell diagrams to compare the natural frequencies for different rotational speeds, logarithmic decrements to compare the damping

and the possible unstable regimes given by the methods, and the response of the system due to mass unbalance. These parameters are the basis in the design of any rotating machine, and thus required by any method intended to study such systems.

1.2 Manuscript outline

The present manuscript is divided into different chapters: in Chapter 2 a brief literature review is presented, where some concepts necessary for the understanding of the method are presented as well as the discussion of previous works. Chapter 3 introduces the CSM to isotropic rotors. The expansion to anisotropic and asymmetric rotors are presented in Chapters 4 and 5, respectively. These chapters present in depth how to obtain the eigenfunctions from the equations of motion and how to apply the modal analysis. Chapter 6 presents an overview of rotor-stator rubbing, a major phenomenon in rotordynamics, and a contact model that will be used to study the outcomes of the CSM to nonlinear applications. Chapter 7 shows several results obtained with the proposed method and the comparisons with the FEM. The work then ends with some final remarks in Chapter 8.

2 Literature review

This chapter presents a general review on major topics of concern regarding the present work. The aim is to present some background for the upcoming chapters, as well as review important contributions in the literature that are relevant to this work. For the sake of brevity, the topics are discussed in a shallow way, but references are indicated if further information is needed.

Section 2.1 presents some major methods and ideas used for the development of the Continuous Segment Method (CSM). These methods are commonly used in mechanical vibration analysis. The application of these in rotor systems are presented in Sec. 2.2, where some definitions used throughout this work are established. A review on related works is presented in Sec. 2.3; starting from the modeling of multi-stepped beams to the applications of rotor-bearing systems.

2.1 Concepts of mechanical vibrations

Vibrations are defined as oscillatory movements due to external actions on a system, and may or may not persist indefinitely through exchange of energy by different means and mechanisms. A classic example is the swing of a pendulum. Mechanical vibrations is a subdiscipline that is concerned in the oscillations of mechanical systems such as beams, plates, shafts, and other type of structures. The forms of energy that are of most interest in mechanical vibrations are kinetic and potential energy. Some important elements of mechanical systems are inertia, stiffness and damping, which dictates in many ways how such systems will vibrate. These properties allows the exchange between kinetic energy in the motion of inertia elements into potential energy, which is stored in stiffness elements. Damping elements are mainly responsible in dissipate energy, commonly through heat. The study of mechanical vibration is mainly concerned in how these elements affect the behavior of systems. There are many great books that present this topic, among these are presented in Rao (2004, 2007), Balachandran and Magrab (2008), Inman (2008), Meirovitch (1975) and Hartog (1985).

In the study of mechanical vibrations, the systems are divided in two categories: discrete and continuous systems. In the first kind, also known as lumped parameter systems, the coordinates needed to describe their motion, namely their Degree of Freedom (DOF), is finite. This approach is valid when a system has a dimension with much greater importance then others, or when it posses large concentrated properties. Continuous systems, also known as distributed parameter systems, have an infinite number of DOFs. Due to the limited solutions available for such systems, they are commonly discretized into finite systems (MEIROVITCH, 1980). An example of a discrete system is the already

mentioned pendulum, which is modeled as a concentrated mass (inertia element) attached to a massless string and acted upon gravity (stiffness element). In case the dynamics of the string becomes important, such as when the concentrated mass is not large enough, the system is most adequately modeled as a continuous system, where the string now has distributed inertia and stiffness.

The analysis of vibratory systems is mostly concerned on how a system — possessing mass, stiffness and damping — will react by the action of an external force. To achieve this, analysts rely on mathematical models that best describes the physical system at hand. The conception of the models starts with assumptions, such as the use of discrete or continuous models, that lead to equations of motion describing mathematically the vibrating system. These equations can then be solved to obtain the responses, and a careful analysis of the results is performed. Depending on the assumptions used, the models are distinguished in various ways. A common distinction is linear and nonlinear models. In the former kind, the principle of superposition applies, and the solutions are possible in most cases. In nonlinear systems, however, the solutions are not possible in the majority of cases, and the responses are obtained only approximately or by numerical procedures (NAYFEH; PAI, 2008).

2.1.1 Eigenvalue problem

Two concepts that will be constantly discussed in this work are eigenvalues and eigenfunctions. These terms are borrowed from pure mathematics, and in vibration analysis mainly represent natural frequencies and mode shapes of systems, which, in turn, are obtained from an eigenvalue or characteristic-value problem (RAO, 2007). The solutions of these problems are unique, and depends on the mass, stiffness and damping properties of the vibrating system. The eigenvalue problem is obtained directly from the equations of motion that govern the system's dynamics. Consider a discrete system with a mass matrix $[m]$ and stiffness matrix $[k]$ governed by the following equation,

$$[m]\{\ddot{w}(t)\} + [k]\{w(t)\} = \{f(t)\} \tag{2.1}$$

being t time, $\{w(t)\}$ the vector of displacements, $\{f(t)\}$ the vector of external forces and the dots denote a derivative with respect to time t. Throughout this work, a term in brackets $[\cdot]$ means a matrix and a term in braces $\{\cdot\}$ means a vector. The eigenvalue problem associated with the above equation is,

$$\Big([k] - \lambda^2[m]\Big)\{X\} = 0 \tag{2.2}$$

where $\{X\}$ is the eigenvector. The above equation is obtained assuming $\{f(t)\} = 0$ and $\{w(t)\} = \{X\}e^{\lambda t}$ in Eq. (2.1). In order to Eq. (2.2) to have non-trivial solutions, the determinant of the coefficient matrix must be zero, which leads to,

$$det\Big([k] - \lambda^2[m]\Big) = 0 \tag{2.3}$$

where *det* denotes the determinant. This determinant leads to a polynomial equation, known as the characteristic equation, which roots give the eigenvalues λ. After λ is obtained, the corresponding eigenvector is obtained from Eq. (2.2) by substituting the value of λ. This discussion is very basic and the reader is referred to Rao (2007) or Meirovitch (1998) for a more in depth approach.

In case of continuous systems, instead of obtaining eigenvectors, one obtains eigenfunctions (RAO, 2007). The process is somewhat similar as above. Consider a one dimensional beam based on the Euler-Bernoulli theory, which has the following equation of motion,

$$[m]\ddot{w}(x,t) + [k]w(x,t) = f(x,t) \tag{2.4}$$

which has the same form as Eq. (2.1), but now the displacement $w = w(x,t)$ is a displacement field and it is also dependent on the space variable $x \in [0,\ L]$; being L the length of the beam. The matrices $[m]$ and $[k]$ are now 1×1 matrices given as,

$$[m] = \bar{m}(x), \quad [k] = \frac{\partial^2}{\partial x^2}\left(E\bar{I}(x)\frac{\partial^2}{\partial x^2}\right)$$

being $\bar{m}(x)$ and $E\bar{I}(x)$ the distributed mass and stiffness, respectively. Although the form of Eqs. (2.1) and (2.4) are similar, the latter is now a partial differential equation. The eigenvalue problem of Eq. (2.4) is obtained by letting $f(x,t) = 0$ and $w(x,t) = \phi(x)e^{\lambda t}$, leading to,

$$\left[\frac{\partial^2}{\partial x^2}\left(E\bar{I}(x)\frac{\partial^2}{\partial x^2}\right) - \lambda^2\bar{m}(x)\right]\phi(x) = 0 \tag{2.5}$$

note that the problem now is a differential equation, which solution gives the eigenfunctions $\phi(x)$ and eigenvalues λ. To solve this differential equation, one needs additional equations that specify the boundary conditions at both ends, that can be written as (MEIROVITCH, 1998),

$$B_i w(x,t)\Big|_{x=0,L}, \quad \text{for } i = 1,2 \tag{2.6}$$

where B_i are differential operators. Equations (2.4) and (2.6) are denoted as a boundary-value problem. The method presented in this work, namely the Continuous Segment Method (CSM), basically provides a mean to solve an eigenvalue problem such as the one given by Eq. (2.5), but for rotor systems. The eigenvalues are obtained after solving the differential equation and applying the boundary conditions. The characteristic equations

are now of transcendental kind instead of polynomial, which posses a infinite number of roots or zeros. The reader is referred to Rao (2007) and Magrab (2012) for more information on vibration of continuous systems.

The method used to arrive at Eq. (2.5) is known as separation of variables (STRAUSS, 2007). In this way, the displacement field $w(x,t)$ was separated as a product of two functions, namely $\phi(x)$ and $e^{\lambda t}$, which are functions of only the space variable x or the time variable t. If one is able to solve the differential equations given in (2.5), then the solution is labeled exact. However, there are many cases where this is not possible, and one needs to rely on approximate solutions such as Rayleigh-Ritz-based methods (MEIROVITCH; KWAK, 1991). In such cases, the function $\phi(x)$ is obtained from a simplified problem or is simply assumed as having some form. Meirovitch (1980) provides several approximate methods for discrete and continuous vibrating systems.

2.1.2 Modal analysis

There are many methods to obtain the response of discrete and continuous systems under external forcing. A well known method is the modal analysis, where the displacements are written as a linear combination of the normal modes of the system (EWINS, 2000). These normal modes, also known as modes of vibration, are obtained from the eigenvalue problem, and represent the relative amplitudes of the system. By means of modal analysis, the equations of motion, that can be coupled and have an arbitrary number, can be transformed to uncoupled differential equations for the modal coordinates. This uncoupling is possible due to the orthogonality property of the eigenfunctions (or eigenvectors for discrete systems).

Consider the beam equation shown in Eq. (2.4). To apply modal analysis, supposing that the eigenfunctions $\phi(x)$ are already at hand, one first assumes,

$$w(x,t) = \sum_{i=1}^{\infty} \phi_i(x) q_i(t) \tag{2.7}$$

being q_i the modal coordinates and ϕ_i the ith eigenfunction. Substituting Eq. (2.7) into (2.4), leads to

$$\sum_{i=1}^{\infty} \Big\{ [m]\phi_i(x)\ddot{q}_i(t) + [k]\phi_i(x)q_i(t) \Big\} = f(x,t) \tag{2.8}$$

The eigenfunctions ϕ_i, which are assumed to be normalized, have the following orthogonality properties,

$$\int_0^L \phi_j[m]\phi_i = \delta_{ij}, \quad \int_0^L \phi_j[k]\phi_i = \lambda^2 \delta_{ij}, \tag{2.9}$$

where δ_{ij} is the Kronecker delta. These conditions are obtained from Eq. (2.5). Now,

multiplying Eq. (2.8) by ϕ_j, integrating from $x = 0$ to $x = L$, and taking into account the orthogonality conditions, one arrives at,

$$\ddot{q}_i(t) + \lambda_i^2 q_i(t) = \int_0^L \phi_i(x) f(x,t) dx, \quad i = 1, 2, ... \tag{2.10}$$

which is infinite second order differential equations for the modal coordinates q_i. It is important to note the importance of the orthogonality condition to uncouple Eq. (2.8). Also, note that the external force is weighted by the eigenfunction of mode i.

In case the system posses damping or gyroscopic effect, the orthogonality conditions above are not valid, and one needs to treat the system in state-space (MEIROVITCH, 1980). This approach will be first shown in Chapter 3 and the subsequent chapters, where modal analysis is applied to a much more complex continuous systems. Nonetheless, the ideas outlined above are very important for the analysis of these kind of systems.

2.2 Overview on rotordynamics

Rotordynamics is mainly concerned in the study of rotating machines. These machines consist essentially of rotating parts, such as shafts, bladed disks, impellers, and so on; and stationary parts, like bearings housings, seals and foundations. Some examples of rotating machines are steam turbines, compressors, pumps, internal combustion engines, electric motors and generators. The unique interaction between the different parts in the machine gives rise to a number of phenomena that are not seen in other structures. Besides the interactions between rotors and stators, the fluid media often present between these components adds even more complexity and dynamic richness for these kind of machines. Some books devoted exclusively to the study of rotordynamics are Gasch et al. (1975), Lee (1993), Childs (1993), Krämer (1993), Lalanne e Ferraris (1998), Muszynska (2005), Vance et al. (2010), Genta (2007), Ishida and Yamamoto (2012), Friswell et al. (2010) and Tiwari (2017).

The modeling of rotors started in the mid 1800s, and many authors consider the paper by Rankine (1869) to be the first paper published on the topic, where the concept of critical speed was already established. However, Rankine wrongly predicted that this speed was impossible to reach. Notwithstanding, because of this prediction many early rotating machines were "forbidden" to run pass the critical speed. According to Vance et al. (2010), DeLaval proved in the late 1890s that the supercritical operation was possible. Shortly after that, Jeffcott (1919) introduced the Jeffcott rotor, which was able to represent a great deal of phenomenon seen in rotating machines, as Krämer (1993), Gasch et al. (1975), Genta (2007) and Lalanne e Ferraris (1998) show. As the machines started to rotate at ever faster speeds, engineers faced several kinds of instabilities, such as whirl

instability due to fluid related phenomena and due to rotating internal damping of the shaft. The understanding and prevention of such instabilities proved to be very important for the correct functioning of rotating machines.

In order to adequately predict the phenomena seen in real machines, more suitable mathematical models were needed. The rotordynamics models can be divided into two groups: rigid and flexible rotors. In the first kind, the rotor is considered as a rigid body; thus it hypothetically does not suffer deformation of any kind. Rigid rotors can model effectively rotating machines that operate at low speeds or have a shaft much stiffer than the supporting bearings. In case the shaft whirl becomes important, one needs to apply flexible rotor models that account for the shaft distributed inertia and stiffness, leading to a continuous vibrating system. The equations of motion of these systems are partial differential equations, which required a discretization procedure. The two main approaches developed for that matter were the transfer matrix method (TMM) (LUND, 1974; HSIEH et al., 2006; LEE; LEE, 2018; CHEN et al., 2020) and the finite element method (FEM) (NELSON; MCVAUGH, 1976; KU, 1998).

2.2.1 Nonlinear phenomena in rotordynamics

The inherent complexity of rotating machines and the interaction between its different parts give rise to a number of nonlinear phenomena. Although linear rotordynamics models provide great insights in the functioning of the machines, they may predict wrong behaviors in many situations and are thus not suitable when some kind of nonlinearity is at play. Common sources of nonlinearities are fluid-related phenomena (CASTRO et al., 2008; MENDES; CAVALCA, 2014; RIEMANN et al., 2013) and rubbing between rotating and stationary parts (JACQUET-RICHARDET et al., 2013; VARANIS et al., 2018; WANG et al., 2020; ALBER; MARKERT, 2014). In case the shaft presents large deformations, one needs to account the stiffening effect in the modeling of them, as shown by Ishida et al. (1996) and Shad et al. (2011). More information on nonlinear rotordynamics can be found in the papers by Ishida (1994), Shaw and Balachandran (2008) and Prabith and Krishna (2020).

Giving the importance of nonlinear phenomena, that in some cases can lead to the complete failure of the machines, the introduction of them in the mathematical modeling is very important. For this reason, this work also introduces the use of the CSM to study the rubbing phenomenon. A review of rotor to stator rub is presented in Chapter 6, where the nonlinear model used is also introduced. The idea is to present the application of nonlinear phenomena using the present method and apply to multi-stepped rotor systems.

2.3 Modeling of multi-stepped rotor systems

Flexible rotors are commonly modeled as beams, since the bending effect is generally more prevalent than other effects. Hence, it is worth reviewing some models of multi-stepped beams, as they can be applied to rotors with some adaptations. Researchers have long been interested in beams with stepped sections, as they can be used to model a great deal of structures and machine parts. Some early works by Taleb and Suppiger (1961), Klein (1974), Levinson (1976) and Jang and Bert (1989a, 1989b) show examples of solutions of single-stepped beams. Koplow et al. (2006) and Jaworski and Dowel (2008) present experimental results of multi-stepped beams. The latter study compared results from several different models, including 1-D beams, 2-D shells and 3-D solids with experimental results; showing that 1-D beams can give good results provided the stepping cross section is not excessively high.

The expansion from single-stepped beams to multi-stepped was performed by several authors. Vaz and Junior (2016) presented a systematic method to model multi-stepped beam with variable cross-sections and material properties by means of the Euler-Bernoulli beam theory. Farghaly and El-Sayed (2016) and Torabi et al. (2013) presented approaches to model multi-stepped beams using Timoshenko beams with multiple attachments. These works mostly consider the undamped beams. Sorrentino et al. (2003) presented an approach were the damping, which can be viscous, hysteretic and even fractional, is included in the eigenvalue problem. The general steps used in these works are: (i) solve the eigenvalue problem for a single uniform segment, (ii) apply the continuity conditions to relate the mode shapes of the different segments and (iii) apply the boundary conditions to obtain the eigenvalues. It is worth metioning that condition (ii) requires that the segments have a collinear neutral axis. In case this assumption is not valid, such as when large manufacture errors are present, the coupling between bending and axial modes need to be taken into account, as discussed by Ju et al. (1994).

A different approach to model multi-stepped beams is to use receptances methods based on time transformations by means of Laplace or Fourier transforms. This idea is used in the Spectral Element Method (SEM) (LEE, 2009), where the Fourier transform is used to obtain the results in the frequency domain. The application of this method for multi-stepped beams consist in assembling a global dynamic matrix, similar to the FEM. Lin and Ng (2017) used an approach by impedance matrices to obtain the solution of multi-span beams with attachments using the Euler-Beronoulli beam theory. A similar approach is given by Chen et al. (2020), where a TMM is established for multi-stepped beams with concentrated masses and springs using the Timoshenko beam theory. Some additional works that are worth mentioning utilize approximate methods in the modeling of stepped beams, such as the differential quadrature method, Wang (2013), and composite element model, Lu et al. (2009).

The modeling of rotor systems can be done positioning 1-D beams in the two orthogonal directions. These directions, however, are coupled due to the gyroscopic effects and, in some cases, the bearings. The gyroscopic effect makes the application of modal analysis a bit more challenging, as the eigenvalue problem is non-self-adjoint (MEIROVITCH, 1980). The eigenfunctions obtained from this kind of problems are not orthogonal, requiring the use of adjoint quantities. Lee (1991), Sawicki and Genta (2001) and Genta (1992) provided important insights into the modal analysis applied to discrete rotor systems. These systems are commonly obtained through the discretization by the FEM. The expansion of the modal analysis for continuous rotors were presented by Lee and Jei (1988) for symmetric rotors on anisotropic supports and by Jei and Lee (1992b) for asymmetric rotors. Eshleman and Eubanks (1967, 1969) presented the solution of continuous rotors considering several effects such as shear deformation, rotary inertia, disk diameter and driving torque.

Multi-stepped rotors can be approached in a similar way as beams, using the conditions (i)-(iii) discussed above. In spite of this, the number of works devoted to the modeling of rotors is more scarce than for beams. Jun and Kim (1999) presented the modeling of multi-stepped rotors considering rotary inertia, shear deformation and driving torque. More recently, Torabi et al. (2017), Afshari and Rahaghi (2018), and Afshari et al. (2020), showed similar methods in the modeling of multi-stepped rotors using the Timoshenko theory with multiple disks and bearings and with axial force. Szolc (2000) presented the modeling of rotor systems with nonlinear bearings and coupled lateral-torsional vibrations. Chasalevris and Papadopoulos (2010, 2014) studied nonlinear whirling due to oil-film bearing using a method similar to component modal analysis.

Similarly to what was done in beams, the modeling of rotors in the frequency domain was also studied by many authors. Fang and Yang (1998) and Hong and Park (1999) presented similar approaches where the Laplace transform is used to solve the eigenvalue problem of the multi-stepped rotor. This allows the construction of local dynamic stiffness matrices, that can be assembled to represent the multi-stepped rotor in a process similar to the SEM (LEE, 2009). Since the response in such methods are obtained first in the frequency domain, the application of nonlinear forces becomes challenging; although it is still possible. Özcsahin et al. (2014) utilized the receptances of the rotor to account for multi-stepped cross-sections, disks and bearings. Exact dynamic elements were obtained by Hong and Park (2001), which can be used to establish finite elements for rotor systems.

The method presented here has similar features to previous works, most notably Özcsahin et al. (2014) and Torabi et al. (2017). However, while these works did not considered damping in their modeling, the CSM includes general non-proportional damping and gyroscopic effect. The main difference to the CSM to previous works is the use of

the complex notation, which facilitates the analysis of rotating machines. In addition to this, the present method is also valid for multi-stepped rotors on anisotropic bearings and with asymmetric shafts.

3 Modeling of isotropic rotor systems

This chapter presents the application of the Continuous Segment Method (CSM) to isotropic rotor systems. These type of rotor systems consist of axisymmetric shafts, symmetric rigid disks and isotropic bearings. When a system with such properties is excited by an external force, the direction of the displacement will be the same as the exciting force (LEE, 1993; GENTA, 2007). Due to this fact, a synchronous external force, such as unbalance force, will not excite the backward natural frequencies of the system, and the rotor's orbit will be circular. Another important fact of isotropic rotors is their axisymmetry, which allows the reduction of the number of equations through the use of complex variables.

The current chapter is divided as follows: first the equations of motion are derived in Section 3.1. After that, the approach used to obtain the eigenfunctions are presented in Section 3.2. The final step is shown in Section 3.3, where the eigenfunctions are used to discretize the partial differential equations by means of modal analysis and uncoupled equations for the modal coordinates are obtained.

3.1 Equations of motion

The rotor system considered in this chapter is depicted in Fig. 2. It consist of a shaft of length L divided into n segments, each of which has a length L_i and constant cross-section area A_i and area moment of inertia I_i $(i = 1, 2, ..., n)$. An arbitrary number Q of disks and P of bearings are placed along the shaft, which locations are given by the local coordinates b_i and a_i, respectively. Each segment has also a local coordinate system $\xi_i \in [0,\ L_i]$ that is used to describe the local mode shape. Also, the rotor is considered homogeneous with density ρ, Young's modulus E, shear constant κ and shear modulus G. The displacements and bending angles in the y and z directions are denoted as $u_y(x,t)$, $u_z(x,t)$, $\psi_y(x,t)$ and $\psi_z(x,t)$, respectively, with the directions shown in Fig. 2.

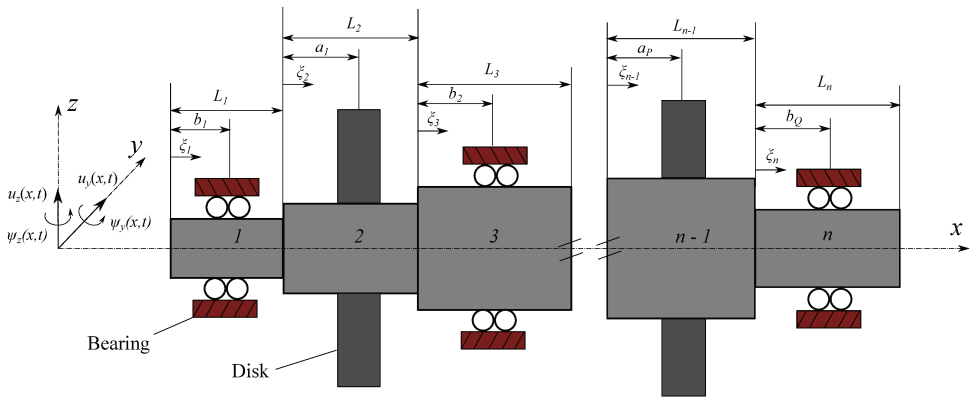

Figure 2: Multi-stepped rotor system

The shaft is modeled as a beam in the two orthogonal directions. The equations of motion of the system can be obtained through the Extended Hamilton Principle (EHP), which is a variational method commonly used in continuous systems and can be stated as (RAO, 2007; NAYFEH; PAI, 2008),

$$\delta \int_{t_1}^{t_2} \Big(T - V + W_{nc} \Big) = 0 \tag{3.1}$$

where $\delta(\cdot)$ denotes the virtual displacement, T is the kinetic energy, V is the potential energy and W_{nc} the virtual work of the non-conservative forces. The kinetic energy of the system, considering only terms up to second order, can be written as,

$$T = \frac{1}{2}\int_0^L \bar{m}(x) \left[\left(\frac{\partial u_y}{\partial t} \right)^2 + \left(\frac{\partial u_z}{\partial t} \right)^2 \right] dx + \frac{1}{2}\int_0^L \bar{J}_d(x) \left[\left(\frac{\partial \psi_y}{\partial t} \right)^2 + \left(\frac{\partial \psi_z}{\partial t} \right)^2 \right] dx$$
$$+ \int_0^L \bar{J}_p(x) \left(\Omega + \psi_y \frac{\partial \psi_z}{\partial t} \right)^2 dx \tag{3.2}$$

being $\bar{m}(x)$ the mass per unit length; $\bar{J}_d(x)$ and $\bar{J}_p(x)$ the diametral and polar mass moment of inertia per unit length and Ω the shaft rotating speed. Note that the functional dependency (x, t) of the displacements and bending angles were omitted for the ease of notation. The contribution of the disks are included in the distributed properties as shown in Eq. (3.14). The last term in Eq. (3.2) is due to the gyroscopic effect, and its form may be different depending on the angles used to describe the rotation of the shaft in 3-D space. However, the form of the final equations of motion will be the same regardless the angles used, at least for terms up to second order, as shown by Raffa and Vatta (1999). The potential energy consist of the contribution of the shaft and the bearings $V = V_s + V_b$; the potential energy of the shaft can be obtained as,

$$V_s = \frac{1}{2}\int_0^L E\bar{I}(x) \left[\left(\frac{\partial \psi_y}{\partial x} \right)^2 + \left(\frac{\partial \psi_z}{\partial x} \right)^2 \right] dx + \frac{1}{2}\int_0^L \kappa G\bar{A}(x) \left(\frac{\partial u_y}{\partial x} - \psi_z \right)^2 dx$$
$$+ \frac{1}{2}\int_0^L \kappa G\bar{A}(x) \left(\frac{\partial u_z}{\partial x} + \psi_y \right)^2 dx \tag{3.3}$$

being the first term due to bending and the last two terms due to shear deformation. The contribution of the bearings is written as,

$$V_b = \frac{1}{2}\int_0^L \left(\bar{k}_m(x) u_y^2 + \bar{k}_m(x) u_z^2 + \bar{k}_t(x) \psi_y^2 + \bar{k}_t(x) \psi_z^2 \right) dx \tag{3.4}$$

The bearings are modeled as concentrated isotropic springs and dampers, with transverse ($\bar{k}_m$ and $\bar{c}_m$) and torsional ($\bar{k}_t$ and $\bar{c}_t$) coefficients. The work of the non conservative forces

is given as,

$$W_{nc} = \frac{1}{2}\int_0^L \left[\bar{c}_m(x)\left(\frac{\partial u_y}{\partial t}\right)^2 + \bar{c}_m(x)\left(\frac{\partial u_z}{\partial t}\right)^2 + \bar{c}_t(x)\left(\frac{\partial \psi_y}{\partial t}\right)^2 + \bar{c}_t(x)\left(\frac{\partial \psi_z}{\partial t}\right)^2\right] dx$$

$$+ \int_0^L \left(f_y u_y + f_z u_z\right) dx \tag{3.5}$$

where $f_y = f_y(x,t)$ and $f_z = f_z(x,t)$ are the distributed force components. The equations of motion can be obtained by substituting Eqs. (3.2)-(3.5) into the EHP shown in Eq. (3.1), which gives (for a derivation the reader is referred to Tiwari (2017), chapter 10),

$$\bar{m}(x)\frac{\partial^2 u_y}{\partial t^2} + \frac{\partial}{\partial x}\left[\kappa G\bar{A}(x)\left(\psi_z - \frac{\partial u_y}{\partial x}\right)\right] + \bar{k}_m(x)u_y + \bar{c}_m(x)\frac{\partial u_y}{\partial t} = f_y(x,t) \tag{3.6}$$

$$\bar{m}(x)\frac{\partial^2 u_z}{\partial t^2} - \frac{\partial}{\partial x}\left[\kappa G\bar{A}(x)\left(\psi_y + \frac{\partial u_z}{\partial x}\right)\right] + \bar{k}_m(x)u_z + \bar{c}_m(x)\frac{\partial u_z}{\partial t} = f_z(x,t) \tag{3.7}$$

$$\bar{J}_d(x)\frac{\partial^2 \psi_y}{\partial t^2} + \Omega\bar{J}_p(x)\frac{\partial \psi_z}{\partial t} - \frac{\partial}{\partial x}\left[E\bar{I}(x)\frac{\partial \psi_y}{\partial x}\right] + \kappa G\bar{A}(x)\left[\psi_y + \frac{\partial u_z}{\partial x}\right]$$

$$- \bar{k}_t(x)\psi_y - \bar{c}_t(x)\frac{\partial \psi_y}{\partial t} = 0 \tag{3.8}$$

$$\bar{J}_d(x)\frac{\partial^2 \psi_z}{\partial t^2} - \Omega\bar{J}_p(x)\frac{\partial \psi_y}{\partial t} - \frac{\partial}{\partial x}\left[E\bar{I}(x)\frac{\partial \psi_z}{\partial x}\right] + \kappa G\bar{A}(x)\left[\psi_z - \frac{\partial u_y}{\partial x}\right]$$

$$- \bar{k}_t(x)\psi_z - \bar{c}_t(x)\frac{\partial \psi_z}{\partial t} = 0 \tag{3.9}$$

By introducing the complex displacements,

$$u = u_y + ju_z \tag{3.10}$$

$$\psi = \psi_z - j\psi_y \tag{3.11}$$

with $j = \sqrt{-1}$, Eqs. (3.6)-(3.9) can be rewritten in the complex form as,

$$\bar{m}(x)\frac{\partial^2 u}{\partial t^2} + \frac{\partial}{\partial x}\left[\kappa G\bar{A}(x)\left(\psi - \frac{\partial u}{\partial x}\right)\right] + \bar{k}_m(x)u + \bar{c}_m(x)\frac{\partial u}{\partial t} = f(x,t) \tag{3.12}$$

$$\bar{J}_d(x)\frac{\partial^2\psi}{\partial t^2} - j\Omega\bar{J}_p(x)\frac{\partial\psi}{\partial t} - \frac{\partial}{\partial x}\left[E\bar{I}(x)\frac{\partial\psi}{\partial x}\right] + \kappa G\bar{A}(x)\left[\psi - \frac{\partial u}{\partial x}\right]$$
$$- \bar{k}_t(x)\psi - \bar{c}_t(x)\frac{\partial\psi}{\partial t} = 0 \tag{3.13}$$

being $f(x,t) = f_y(x,t) + jf_z(x,t)$. The functions of the rotor's properties represent a model where the parameters of the shaft are distributed in a step-wise manner and the disks and bearings are concentrated at their location points. The following functions are assumed,

$$\bar{A}(x) = \sum_{i=1}^{n} A_i H_i(x), \quad \bar{I}(x) = \sum_{i=1}^{n} I_i H_i(x), \quad \bar{m}(x) = \sum_{i=1}^{n} \rho A_i H_i(x) + \sum_{j=1}^{P} M^j \delta_d(x - x_a^j)$$

$$\bar{J}_d(x) = \sum_{i=1}^{n} \rho A_i r_i^2 H_i(x) + \sum_{j=1}^{P} J_d^j \delta_d(x - x_a^j), \quad \bar{J}_p(x) = \sum_{i=1}^{n} 2\rho A_i r_i^2 H_i(x) + \sum_{j=1}^{P} J_p^j \delta_d(x - x_a^j) \tag{3.14}$$

where δ_d is the Dirac's delta function, $r_i^2 = I_i/A_i$ is the radius of gyration and x_a^j are the coordinates of the disks. Note that the rigid disks are encoded in the distributed masses and moments of inertia through the use of δ_d. The function H_i is given as,

$$H_i(x) = H(x - x_i) - H(x - x_{i+1}) \quad \text{for} \quad i = 1, 2, ..., n \tag{3.15}$$

being H the Heaviside unit step function and x_i the coordinates of the nodes or boundaries between segments. The functions $\bar{k}_m$, $\bar{c}_m$, $\bar{k}_t$ and $\bar{c}_t$ are given as,

$$\bar{k}_m(x) = \sum_{l=1}^{Q} k_m^l \delta_d(x - x_b^l), \quad \bar{c}_m(x) = \sum_{l=1}^{Q} c_m^l \delta_d(x - x_b^l)$$

$$\bar{k}_t(x) = \sum_{l=1}^{Q} k_t^l \delta_d(x - x_b^l), \quad \bar{c}_t(x) = \sum_{l=1}^{Q} c_t^l \delta_d(x - x_b^l) \tag{3.16}$$

being x_b^l the coordinates of the bearings and k and c the stiffness and damping coefficients, respectively. In case cross coupled effects must be added, the coefficients can be assumed as $k = k_d + jk_c$ and $c = c_d + jc_c$, where the subscripts d and c denote the direct and cross coupled coefficients, respectively. Also, the effect of internal damping can be included by considering the Young's modulus in the formulation as $E = E(1 + j\Omega c_i)$, being c_i the internal damping coefficient. The boundary conditions, which are also given by the EHP, can be stated as,

$$\left[E\bar{I}(x)\frac{\partial\psi(x,t)}{\partial x}\delta\psi(x,t)\right]_{x=0,L} = 0 \tag{3.17}$$

$$\left[\kappa G\bar{A}(x)\left(\psi(x,t)-\frac{\partial u(x,t)}{\partial x}\right)\delta u(x,t)\right]_{x=0,L}=0 \tag{3.18}$$

Equations (3.12), (3.13), (3.17) and (3.18) denote the boundary-value problem of the rotor system. Close-form solutions of such problems are possible only for a few particular cases; for example, when the boundary conditions are not complicated and the distribution of mass and stiffness is constant. For the particular system presented, one can obtain exact solutions by means of separation of variables, since each segment has constant cross-section, the shaft is homogeneous and the boundary conditions are simple. However, one should note that the present approach can be applied to rotors with non-uniform cross-section or other complicating property; but then the solutions would be approximate rather than exact. By means of the modal expansion or assumed modes method, the displacement and slope fields can be written as,

$$u(x,t)=\sum_{i=1}^{\infty}[\phi_i^F(x)q_i^F(t)+\phi_i^B(x)q_i^B(t)]\approx\sum_{i=1}^{N}[\phi_i^F(x)q_i^F(t)+\phi_i^B(x)q_i^B(t)] \tag{3.19}$$

$$\psi(x,t)=\sum_{i=1}^{\infty}[\eta_i^F(x)q_i^F(t)+\eta_i^B(x)q_i^B(t)]\approx\sum_{i=1}^{N}[\eta_i^F(x)q_i^F(t)+\eta_i^B(x)q_i^B(t)] \tag{3.20}$$

being $\phi_i(x)$ and $\eta_i(x)$ the eigenfunctions, $q_i(t)$ the modal coordinates, N the number of modes used, and F and B denote the forward and backward modes, respectively. What makes the approach exact (at least for the system shown in Fig. 2) is that the eigenfunctions $\phi_i(x)$ and $\eta_i(x)$ are obtained directly from the equations of motion (3.12) and (3.13) through separation of variables. They also satisfy the boundary conditions shown in Eqs. (3.17) and (3.18).

3.2 Eigenfunctions and eigenvalues

The free vibration of the system can be obtained as,

$$\bar{m}(x)\frac{\partial^2 u}{\partial t^2}+\frac{\partial}{\partial x}\left[\kappa G\bar{A}(x)\left(\psi-\frac{\partial u}{\partial x}\right)\right]+\bar{k}_m(x)u+\bar{c}_m(x)\frac{\partial u}{\partial t}=0 \tag{3.21}$$

$$\bar{J}_d(x)\frac{\partial^2\psi}{\partial t^2}-j\Omega\bar{J}_p(x)\frac{\partial\psi}{\partial t}-\frac{\partial}{\partial x}\left[E\bar{I}(x)\frac{\partial\psi}{\partial x}\right]+\kappa G\bar{A}(x)\left[\psi-\frac{\partial u}{\partial x}\right]$$
$$-\bar{k}_t(x)\psi-\bar{c}_t(x)\frac{\partial\psi}{\partial t}=0 \tag{3.22}$$

The solutions are assumed as $u=\phi(x)q(t)=\phi(x)e^{\lambda t}$ and $\psi=\eta(x)q(t)=\eta(x)e^{\lambda t}$, being

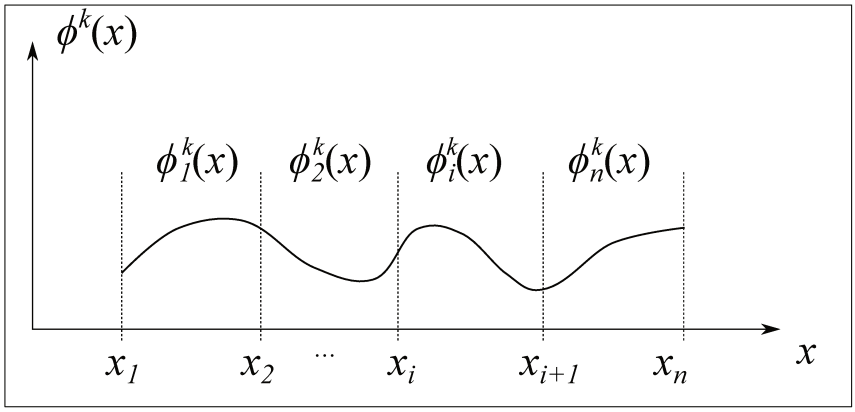

Figure 3: Eigenfunction of the rotor system.

λ the eigenvalue. After substituting these solutions, one arrives at,

$$\lambda^2 \bar{m}(x)\phi(x) + \frac{d}{dx}\left[\kappa G\bar{A}(x)\left(\eta(x) - \frac{d\phi(x)}{dx}\right)\right] + \left[\bar{k}_m(x) + \lambda\bar{c}_m(x)\right]\phi(x) = 0 \tag{3.23}$$

$$\lambda^2 \bar{J}_d(x)\eta(x) - j\lambda\Omega\bar{J}_p(x)\eta(x) - \frac{d}{dx}\left[E\bar{I}(x)\frac{d\eta(x)}{dx}\right] + \kappa G\bar{A}(x)\left(\eta(x) - \frac{d\phi(x)}{dx}\right) - \left[\bar{k}_t(x) + \lambda\bar{c}_t(x)\right]\eta(x) = 0 \tag{3.24}$$

Equations (3.23) and (3.24), together with the boundary conditions, constitute the eigenvalue problem of the system. Since each segment is uniform, with a disk or bearing, the problem can be solved for each segment individually. By doing this, one obtains the eigenfunctions $\phi_i^k(x)$ and $\eta_i^k(x)$ for mode k and for each segment $(i = 1, 2, ..., n)$ in the domain $x \in [x_i,\ x_{i+1}]$. The functions of the whole system are obtained by imposing continuity conditions between the local mode shapes, and a piecewise continuous function is obtained as illustrated in Fig. 3. This procedure has the advantage that the rotor can have an arbitrary number of segments, as well as disks and bearings.

Consider a arbitrary segment i, which position along the shaft is $x_i < x < x_{i+1}$ and the eigenfunctions are $\phi_i(\xi_i)$ and $\eta_i(\xi_i)$; where ξ_i is the local coordinate of the segment. In addition, consider this segment to have a kth disk and a lth bearing, which positions are given by the local coordinates a_k and b_l, respectively. The local eigenvalue problem can be written as,

$$\lambda^2\left[\rho A_i + M^k\delta_d(\xi_i - a_k)\right]\phi_i(\xi_i) + \kappa G A_i\left[\eta_i'(\xi_i) - \phi_i''(\xi_i)\right] + \left(k_m^l + \lambda c_m^l\right)\phi_i(\xi_i)\delta_d(\xi_i - b_l) = 0 \tag{3.25}$$

$$\lambda^2\left[\rho A_i r_i^2 + J_d^k\delta_d(\xi_i - a_k)\right]\eta_i(\xi_i) - j\lambda\Omega\left[2\rho A_i r_i^2 + J_p^k\delta_d(\xi_i - a_k)\right]\eta_i(\xi_i) - EI_i\eta_i''(\xi_i) + \kappa G A_i\left[\eta_i(\xi_i) - \phi_i'(\xi_i)\right] + \left(k_t^l + \lambda c_t^l\right)\eta_i(\xi_i)\delta_d(\xi_i - b_l) = 0 \tag{3.26}$$

where M^k, J_d^k and J_p^k denote the mass, diametral and polar moment of inertia of the

disk, respectively; and $' = d/d\xi_i$. Note that the local problem given by Eqs. (3.25) and (3.26) now has constant coefficients, and it is thus solvable. Here one should note that the problem could be reduced to only one equation by solving for $\eta_i'(\xi_i)$ in Eq. (3.25); this, however, would lead to a complicated equation for ϕ_i with multiple derivatives of δ_d. Therefore, it is advisable to solve both equations simultaneously, since the final result will be the same. After applying the Laplace Transform to the spatial variable ξ_i in Eqs. (3.25) and (3.26), one may have,

$$\lambda^2\rho A_i\hat{\phi}_i(s) + \kappa GA_i\left[s\hat{\eta}_i(s) - \eta_i(0)\right] - \kappa GA_i\left[s^2\hat{\phi}_i(s) - \phi_i'(0) - s\phi_i(0)\right] + \lambda^2 M^k\phi_i(a_k)e^{-sa_k} + \left(k_m^l + \lambda c_m^l\right)\phi_i(b_l)e^{-sb_l} = 0 \tag{3.27}$$

$$\left(\lambda^2 - 2j\lambda\Omega\right)\rho A_i r_i^2\hat{\eta}_i(s) - EI_i\left[s^2\hat{\eta}_i(s) - \eta_i'(0) - s\eta_i(0)\right] + \kappa GA_i\hat{\eta}_i(s) - \kappa GA_i\left[s\hat{\phi}_i(s) - \phi_i(0)\right] + \left(\lambda^2 J_d^k - j\lambda\Omega J_p^k\right)\eta_i(a_k)e^{-sa_k} - \left(k_t^l + \lambda c_t^l\right)\eta_i(b_l)e^{-sb_l} = 0 \tag{3.28}$$

where $\hat{\phi}_i(s)$ and $\hat{\eta}_i(s)$ are the Laplace transform of $\phi_i(\xi_i)$ and $\eta_i(\xi_i)$, respectively. The above equations can be written in matrix form as,

$$[L]\{\hat{\Phi}(s)\} = \{b\} \tag{3.29}$$

being,

$$[L] = \begin{bmatrix} \rho A_i\lambda^2 - \kappa GA_i s^2 & \kappa GA_i s \\ -\kappa GA_i s & \left(\lambda^2 - 2j\lambda\Omega\right)\rho A_i r_i^2 - EI_i s^2 + \kappa GA_i \end{bmatrix} \tag{3.30}$$

$$\{\hat{\Phi}(s)\} = \begin{Bmatrix} \hat{\phi}_i(s) & \hat{\eta}_i(s) \end{Bmatrix}^T \tag{3.31}$$

$$\{b\} = \begin{Bmatrix} \kappa GA_i\left[\eta_i(0) - \phi_i'(0) - s\phi(0)\right] - \lambda^2 M^k\phi_i(a_k)e^{-sa_k} \\ -\left(k_m^l + \lambda c_m^l\right)\phi_i(b_l)e^{-sb_l} \\ -\kappa GA_i\phi_i(0) - EI_i\left[\eta_i'(0) + s\eta_i(0)\right] - \left(\lambda^2 J_d^k - j\lambda\Omega J_p^k\right)\eta_i(a_k)e^{-sa_k} \\ +\left(k_t^l + \lambda c_t^l\right)\eta_i(b_l)e^{-sb_l} \end{Bmatrix} \tag{3.32}$$

Equation (3.29) can be solved for $\hat{\phi}_i(s)$ and $\hat{\eta}_i(s)$ by multiplying both sides by $[L]^{-1}$. Recall that the inverse of a matrix can be written as $[L]^{-1} = adj([L])/det([L])$, where *adj* denotes the adjoint matrix and *det* the determinant. The determinant of the matrix $[L]$ will give the mode shape parameters of segment i through the solution of the following polynomial equation,

$$s^4 + \left(\frac{\rho A_i r_i^2}{EI_i}\left(2j\lambda\Omega - \lambda^2\right) - \frac{\rho A_i\lambda^2}{\kappa GA_i}\right)s^2 + \frac{\rho A_i\lambda_i^2}{EI_i}\left(1 - \frac{\rho r_i^2}{\kappa G}\left(2j\lambda\Omega - \lambda^2\right)\right) = 0 \tag{3.33}$$

This equation has two roots for s^2, being one positive and other negative. Denoting these

roots as δ_i^2 and $-\varepsilon_i^2$, one may have,

$$\delta_i^2 = -\frac{a_i}{2} + \sqrt{\frac{a_i^2}{4} - b_i} \tag{3.34}$$

$$\varepsilon_i^2 = \frac{a_i}{2} + \sqrt{\frac{a_i^2}{4} - b_i} \tag{3.35}$$

with

$$a_i = \frac{\rho A_i r_i^2}{EI_i}\left(2j\lambda\Omega - \lambda^2\right) - \frac{\rho A_i \lambda^2}{\kappa G A_i} \tag{3.36}$$

$$b_i = \frac{\rho A_i \lambda_i^2}{EI_i}\left(1 - \frac{\rho r_i^2}{\kappa G}\left(2j\lambda\Omega - \lambda^2\right)\right) \tag{3.37}$$

Using the roots given above, one can write $det([L]) = (s^2 - \delta_i^2)(s^2 + \varepsilon_i^2)$, and apply the inverse Laplace transform in Eq. (3.29). By performing this, one arrives at,

$$\phi_i(\xi_i) = \eta_i(0)f_1(\xi_i) + \eta_i'(0)f_2(\xi_i) + \phi_i(0)f_3(\xi_i) + \phi_i'(0)f_4(\xi_i)$$
$$+\left[p_1^{a_k}(\xi_i)\phi_i(a_k) + h_1^{a_k}(\xi_i)\eta_i(a_k)\right]H(x-a_k) + \left[p_1^{b_l}(\xi_i)\phi_i(b_l) + h_1^{b_l}(\xi_i)\eta_i(b_l)\right]H(x-b_l) \tag{3.38}$$

$$\eta_i(\xi_i) = \eta_i(0)g_1(\xi_i) + \eta_i'(0)g_2(\xi_i) + \phi_i(0)g_3(\xi_i) + \phi_i'(0)g_4(\xi_i)$$
$$+\left[p_2^{a_k}(\xi_i)\phi_i(a_k) + h_2^{a_k}(\xi_i)\eta_i(a_k)\right]H(x-a_k) + \left[p_2^{b_l}(\xi_i)\phi_i(b_l) + h_2^{b_l}(\xi_i)\eta_i(b_l)\right]H(x-b_l) \tag{3.39}$$

the functions f_i, g_i $(i = 1, 2, 3, 4)$, p_j^m and h_j^m $(j = 1, 2$ and $m = a_k, b_l)$ are shown in Appendix A. Here one notes that the bearings and disks appear as Heaviside functions in the mode shapes together with the functions p and h. This allows them to be positioned anywhere along segment i.

Equations (3.38) and (3.39) have nine unknowns, namely, $\eta_i(0)$, $\eta_i'(0)$, $\phi_i(0)$, $\phi_i'(0)$, λ, $\eta_i(a_k)$, $\eta_i(b_k)$, $\phi_i(a_k)$ and $\phi_i(b_k)$. The first five unknowns, $\eta_i(0)$, $\eta_i'(0)$, $\phi_i(0)$, $\phi_i'(0)$ and λ; are obtained from the boundary conditions combined with the continuity conditions. The remaining four can be obtained directly from Eqs. (3.38) and (3.39) by the continuity of the functions ϕ_i and η_i at $\xi_i = a_k$ and $\xi_i = b_l$. However, if the bearing and disk are considered to be in the same segment i, one needs to assume $a_k < b_l$ or $a_k > b_l$. In order to avoid these assumptions, and to simplify the form of the local mode shapes, it is simpler to assume that each segment has only a bearing or a disk. Then one of the terms in brackets in Eqs. (3.38) and (3.39) vanish. Consider that the segment i has only a disk, then the function ϕ_i evaluated at $\xi_i = a_k$ is obtained as,

$$\phi_i(a_k) = \eta_i(0)f_1(a_k) + \eta_i'(0)f_2(a_k) + \phi_i(0)f_3(a_k) + \phi_i'(0)f_4(a_k)$$
$$+\left[\cancelto{0}{p_1^{a_k}(a_k)}\phi_i(a_k) + \cancelto{0}{h_1^{a_k}(a_k)}\eta_i(a_k)\right] = \eta_i(0)f_1(a_k) + \eta_i'(0)f_2(a_k) + \phi_i(0)f_3(a_k) + \phi_i'(0)f_4(a_k)$$

Thus, by doing the same procedure for $\eta_i(a_k)$, and substitute the result back in Eq. (3.38) and (3.39), one has,

$$\phi_i(\xi_i) = \eta_i(0)C_{1i}(\xi_i) + \eta_i'(0)C_{2i}(\xi_i) + \phi_i(0)C_{3i}(\xi_i) + \phi_i'(0)C_{4i}(\xi_i) = [C_i(\xi_i)]\{X_i(0)\} \quad (3.40)$$

$$\eta_i(\xi_i) = \eta_i(0)D_{1i}(\xi_i) + \eta_i'(0)D_{2i}(\xi_i) + \phi_i(0)D_{3i}(\xi_i) + \phi_i'(0)D_{4i}(\xi_i) = [D_i(\xi_i)]\{X_i(0)\} \quad (3.41)$$

being

$$\begin{cases} C_{ji}(\xi_i) = f_j(\xi_i) + [f_j(a_k)p_1^{a_k}(\xi_i) + g_j(a_k)h_1^{a_k}(\xi_i)]\, H(\xi_i - a_k) \\ D_{ji}(\xi_i) = g_j(\xi_i) + [f_j(a_k)p_2^{a_k}(\xi_i) + g_j(a_k)h_2^{a_k}(\xi_i)]\, H(\xi_i - a_k) \end{cases} \quad (3.42)$$

$$\text{for } j = 1,2,3,4; \;\; k = 1,2,...,P$$

$$[C_i(\xi)] = [C_{1i}(\xi) \;\; C_{2i}(\xi) \;\; \cdots \;\; C_{4i}(\xi)], \quad [D_i(\xi)] = [D_{1i}(\xi) \;\; D_{2i}(\xi) \;\; \cdots \;\; D_{4i}(\xi)], \quad (3.43)$$

$$\{X_i(\xi_i)\} = \{\eta_{1i}(\xi_i) \;\; \eta_i'(\xi_i) \;\; \phi_i(\xi_i) \;\; \phi_i'(\xi_i)\}^T \quad (3.44)$$

In case segment i has a bearing instead of a disk, one changes $p_1^{a_k}$ to $p_1^{b_l}$, $p_2^{a_k}$ to $p_2^{b_l}$, and so on. Note that if the segment i has no disk or bearing, $C_{ji} = f_j$ and $D_{ji} = g_j$, for $j = 1,2,3,4$. The form presented in Eqs. (3.40) and (3.41) will be valid for all segments $i = 1,2,...,n$, being the specific form of $[C_i(\xi_i)]$ and $[D_i(\xi_i)]$ dependent if the segment has a disk or bearing.

The continuity conditions, that relate the mode shapes of the different segments, are the continuity of the displacement, slope, bending moment and shear force, which can be written as,

$$\begin{cases} \eta_{i+1}(0) = \eta_i(L_i) \\ EI_{i+1}\eta_{i+1}'(0) = EI_i\eta_i'(L_i) \\ \phi_{i+1}(0) = \phi_i(L_i) \\ \kappa GA_{i+1}\Big(\eta_{i+1}(0) - \phi_{i+1}'(0)\Big) = \kappa GA_i\Big(\eta_i(L_i) - \phi_i'(L_i)\Big) \end{cases} \quad (3.45)$$

or, equivalently, in matrix form as,

$$\begin{Bmatrix} \eta_{i+1}(0) \\ \eta_{i+1}'(0) \\ \phi_{i+1}(0) \\ \phi_{i+1}'(0) \end{Bmatrix} = \begin{bmatrix} 1 & 0 & 0 & 0 \\ 0 & \beta_i & 0 & 0 \\ 0 & 0 & 1 & 0 \\ 1-\alpha_i & 0 & 0 & \alpha_i \end{bmatrix} \begin{Bmatrix} \eta_i(L_i) \\ \eta_i'(L_i) \\ \phi_i(L_i) \\ \phi_i'(L_i) \end{Bmatrix} = [h_i]\{X_i(L_i)\} \quad (3.46)$$

being $\beta_i = I_i/I_{i+1}$ and $\alpha_i = A_i/A_{i+1}$. By using the form given in Eqs. (3.40) and (3.41), the relation between $\{X_{i+1}(0)\}$ and $\{X_i(0)\}$ is found to be,

$$\{X_{i+1}(0)\} = [h_i]\Big[[D_i(L)] \;\; [D_i'(L)] \;\; [C_i(L)] \;\; [C_i'(L)]\Big]^T \{X_i(0)\} = [H_i]\{X_i(0)\} \quad (3.47)$$

Here it is worth mentioning that the disks and bearings are encoded into the matrices $[C_i(\xi_i)]$ and $[D_i(\xi_i)]$ by means of the functions p and h and the Heaviside function, as shown in Eq. (3.42). They can be placed anywhere along segment i, including the boundaries $\xi_i = 0, L_i$, by setting the local coordinates a_i or b_i. A different approach could have been taken where the disks and bearings are set only at the boundaries between the segments, and thus not included in the matrices $[C_i(\xi_i)]$ and $[D_i(\xi_i)]$. In this case, they would appear in the matrices $[h_i]$ in the boundary between segment i and $i+1$, as the continuity condition of the shear force and bending moment would be affected. Consider, for example, that in the boundary between segments i and $i+1$ there is a lth bearing; then the continuity of the shear force is now given as,

$$\kappa G A_{i+1}\Big(\eta_{i+1}(0) - \phi'_{i+1}(0)\Big) = \left(k_m^l + \lambda c_m^l\right)\phi_i(L_i) + \kappa G A_i\Big(\eta_i(L_i) - \phi'_i(L_i)\Big)$$

from this condition, the matrix $[h_i]$ need to be modified as follows,

$$[h_i] = \begin{bmatrix} 1 & 0 & 0 & 0 \\ 0 & \beta_i & 0 & 0 \\ 0 & 0 & 1 & 0 \\ 1-\alpha_i & 0 & -\frac{\left(k_m^l+\lambda c_m^l\right)}{\kappa G A_{i+1}} & \alpha_i \end{bmatrix}$$

Similar results can be obtained if the boundary has disks. One should note that the result of including the disks in the matrices $[C_i(\xi_i)]$ and $[D_i(\xi_i)]$ or in $[h_i]$ are equivalent, and the final eigenfunctions and eigenvalues are the same no matter the approach taken.

The problem now consist in finding the constants $\{X_i(0)\}$, for each segment $i = 1, 2, ..., n$, as well as the eigenvalue λ. This can be done by using the continuity condition, Equation (3.47), for each segment up to segment n. By this procedure, only the constants of segment 1 will be left; two of these are eliminated by the boundary conditions specified at the boundary $x = 0$. The remaining constants are obtained from the resulting system of equations obtained from the boundary conditions specified $x = L$, and the determinant of the coefficient matrix from this system of equations then gives the eigenvalues λ. By following the first approach, the system of equations can be obtained as,

$$[A]\Big([H_{n-1}] \times [H_{n-2}] \times \cdots \times [H_2]\Big)[B]\{X\} = [G(\lambda)]\{X\} = 0 \tag{3.48}$$

where the matrices $[A]$ and $[B]$ and the vector $\{X\}$ depend upon the conditions specified at $x = 0, L$. The matrices $[A]$ and $[B]$ are just slight variations of the matrices $[H_i]$ that account for the specified boundary conditions. The steps needed to obtain these matrices are presented in the following. Consider the case where both ends are free; then the

boundary conditions can be stated as,

$$\begin{cases} \eta_1'(0) = \eta_n'(L_n) = 0 \\ \kappa G A_1 \Big(\eta_1(0) - \phi_1(0)\Big) = \kappa G A_n \Big(\eta_n(L_n) - \phi_n(L_n)\Big) = 0 \end{cases} \tag{3.49}$$

The eigenfunctions of segment n, using Eqs (3.40), (3.41) and (3.47), can be written as,

$$\phi_n(\xi_n) = [C_n(\xi_n)]\{X_n(0)\} = [C_n(\xi_n)]\Big([H_{n-1}] \times [H_{n-2}] \times \cdots \times [H_1]\Big)\{X_1(0)\}$$

$$\eta_n(\xi_n) = [D_n(\xi_n)]\{X_n(0)\} = [D_n(\xi_n)]\Big([H_{n-1}] \times [H_{n-2}] \times \cdots \times [H_1]\Big)\{X_1(0)\}$$

Using the boundary conditions and the form of $\phi_n(\xi_n)$ and $\eta_n(\xi_n)$ presented above, one obtains the following equation,

$$\begin{bmatrix} [D_n'(L_n)] \\ [D_n(L_n)] - [C_n'(L_n)] \end{bmatrix} \Big([H_{n-1}] \times [H_{n-2}] \times \cdots \times [H_1]\Big)\{X_1(0)\} = 0$$

where one can identify the first matrix as being $[A]$. Now, to obtain the form of $[B]$ and $\{X\}$, the matrix $[H_1]$ and the vector $\{X_1(0)\}$ need to be modified. From the boundary conditions shown in Eq. (3.49) one has $\eta_1'(0) = 0$ and $\eta_1(0) = \phi_1(0)$; thus, the following modifications are needed,

$$[H_1]\{X_1(0)\} = [H_1] \begin{Bmatrix} \eta_1(0) \\ \eta_1'(0) \\ \phi_1(0) \\ \phi_1'(0) \end{Bmatrix} = [H_1] \begin{Bmatrix} \phi_1'(0) \\ 0 \\ \phi_1(0) \\ \phi_1'(0) \end{Bmatrix} = [H_1] \begin{bmatrix} 0 & 1 \\ 0 & 0 \\ 1 & 0 \\ 0 & 1 \end{bmatrix} \begin{Bmatrix} \phi_1(0) \\ \phi_1'(0) \end{Bmatrix} = [B]\{X\}$$

by substituting the above in the previous equation, one obtains the system of equation presented in Eq. (3.48). From the above steps, one can easily obtain the form of $[A]$, $[B]$ and $\{X\}$ for different boundary conditions. In addition to the classical boundary conditions, namely, free, clamped and simply-supported; one can also set the bearings or disks at the boundaries, provided they are located at the segments 1 or n and the coordinates a or b are set accordingly.

The characteristic equation is obtained from the determinant of the coefficient matrix $[G(\lambda)]$ in Eq. (3.48), which must be zero for non-trivial solutions to exist. The eigenvalues will have the form

$$\lambda_i^k = \sigma_i^k \pm j\omega_i^k \quad \text{for } i = 1, 2, ..., N;\ k = F, B \tag{3.50}$$

where ω_i^k are the damped natural frequencies, σ_i^k are the damping parameters and F and B denote the forward and backward modes, respectively. Due to the complex notation, the

forward natural frequencies will be positive $+j\omega_i^F$ and the backward natural frequencies negative $-j\omega_i^B$ for $i = 1, 2, ..., N$. This differs if the real notation is used, where the complex conjugate of the eigenfunctions and eigenvalues need to be given so that the response becomes real (LEE, 1991). The use of complex notation, at least for isotropic rotors, has also the advantage that the number of equations in the eigenvalue problem is diminished by half due to the axisymmetry.

The mode shape of the entire system is obtained by the combination of the mode shapes of each segment. By using this systematic procedure, a rotor system with any number of stepped cross-section can be modeled. The mode shapes and the slope for the entire system is given as a continuous step-wise function, thus

$$\phi(x) = \begin{cases} \phi_1(x) & \text{for } x_1 < x < x_2 \\ \phi_2(x) & \text{for } x_2 < x < x_3 \\ & \vdots \\ \phi_n(x) & \text{for } x_n < x < x_{n+1} \end{cases} \tag{3.51}$$

$$\eta(x) = \begin{cases} \eta_1(x) & \text{for } x_1 < x < x_2 \\ \eta_2(x) & \text{for } x_2 < x < x_3 \\ & \vdots \\ \eta_n(x) & \text{for } x_n < x < x_{n+1} \end{cases} \tag{3.52}$$

3.3 Modal analysis

Now that the eigenfunctions are at hand, it is possible to use modal analysis to discretize the partial differential equations and obtain the differential equations for the modal coordinates. Firstly, the equations of motion given by Eqs. (3.12) and (3.13) are rewritten as,

$$[m]\{\ddot{w}(x,t)\} + [c]\{\dot{w}(x,t)\} + [k]\{w(x,t)\} = \{g(x,t)\} \tag{3.53}$$

where

$$[m] = \begin{bmatrix} \bar{m}(x) & 0 \\ 0 & \bar{J}_d(x) \end{bmatrix}, \quad [c] = \begin{bmatrix} \bar{c}_m(x) & 0 \\ 0 & -j\Omega\bar{J}_p(x) - \bar{c}_t(x) \end{bmatrix}$$

$$[k] = \begin{bmatrix} -\frac{\partial}{\partial x}\left(\kappa G\bar{A}(x)\frac{\partial}{\partial x}\right) + \bar{k}_m(x) & \frac{\partial}{\partial x}\left(\kappa G\bar{A}(x)\right) \\ -\kappa G\bar{A}(x)\frac{\partial}{\partial x} & -\frac{\partial}{\partial x}\left(E\bar{I}(x)\frac{\partial}{\partial x}\right) + \kappa G\bar{A}(x) - \bar{k}_t(x) \end{bmatrix} \tag{3.54}$$

$$\{w(x,t)\} = \{u(x,t)\ \ \psi(x,t)\}^T \tag{3.55}$$

$$\{g(x,t)\} = \{f(x,t)\ \ 0\}^T \tag{3.56}$$

being T the transpose and the dots time differentiation. The form of the equations of motion shown in Eq. (3.53) is similar to what is seen to discrete vibrating systems, but

it describes an infinite degree of freedom system. This form is very general, since the matrices $[m]$, $[c]$ and $[k]$ can be adapted to any vibrating continuous system. Due to the damping and the gyroscopic effect, encoded in the matrix $[c]$, Eq. (3.53) has to be put in a state-space form to apply the modal analysis method, which yields,

$$[M]\{\dot{W}(x,t)\} = [K]\{W(x,t)\} + \{F(x,t)\} \tag{3.57}$$

being,

$$\{W(x,t)\} = \Big\{\{\dot{w}(x,t)\}\ \{w(x,t)\}\Big\}^T \tag{3.58}$$

$$\{F(x,t)\} = \Big\{0\ 0\ \{g(x,t)\}\Big\}^T = \Big\{0\ 0\ f(x,t)\ 0\Big\}^T \tag{3.59}$$

$$[M] = \begin{bmatrix} [0]_{2\times 2} & [m] \\ [m] & [c] \end{bmatrix} \tag{3.60}$$

$$[K] = \begin{bmatrix} [m] & [0]_{2\times 2} \\ [0]_{2\times 2} & -[k] \end{bmatrix} \tag{3.61}$$

where $[0]_{2\times 2}$ its a 2×2 matrix of zeros. The matrices $[M]$ and $[K]$ are complex operator matrices, and the nature of these operators gives information about the eigenfunctions needed to solve the eigenvalue problem. Two important properties of these operators is *self-adjointness* and *positive-definiteness*. The adjoint of an operator $[D]$ can be obtained for any test function $\{v(x)\} = \{v_1(x)\ v_2(x)\ \cdots\}^T$ (MEIROVITCH, 1980) as,

$$\langle\, [D]\{v(x)\},\ \{v(x)\}\,\rangle = \langle\, \{v(x)\},\ [\tilde{D}]\{v(x)\}\,\rangle \tag{3.62}$$

where $[\tilde{D}]$ is the adjoint operator of $[D]$. If the operator is *self-adjoint*, one has $[\tilde{D}] = [D]$ (RAO, 2007). In case where $[\tilde{D}] \neq [D]$, the operator $[D]$ is said to be *non-self-adjoint*. In addition, $\langle\cdot\rangle$ is the internal product, which, for two complex vectors $\{a\} = \{a_1(x), a_2(x)\}^T$ and $\{b\} = \{b_1(x),\ b_2(x)\}^T$, with $x \in [0, L]$ is defined as

$$\langle\, \{a\},\ \{b\}\,\rangle := \int_0^L a_1(x)b_1^*(x)dx + \int_0^L a_2(x)b_2^*(x)dx \tag{3.63}$$

being * the complex conjugate. The positive-definiteness of an operator $[D]$ is found for an arbitrary test function $\{v(x)\}$, from

$$\langle\, [D]\{v(x)\},\ \{v(x)\}\,\rangle \geq 0 \tag{3.64}$$

the operator $[D]$ is said to be positive if the above condition is satisfied, and positive definite if the term on the left-hand side is zero only if $\{v(x)\}$ is zero. In the present case, one can show, through the conditions (3.62) and (3.64), that the operators $[M]$ and

$[K]$ in Eq. (3.57) are both positive-definite, and the former is non-self-adjoint while the latter self-adjoint. A non-self-adjoint continuous system is analogous to a non-symmetric matrix in a discrete system, and the eigenfunctions obtained from such problems are not orthogonal (MEIROVITCH, 1975). To decouple the equations in discrete systems one needs to use the left eigenvectors of the non-symmetric matrix. The analogous way to proceed in the continuous case is to use of the adjoint eigenfunctions, which are obtained from the adjoint eigenvalue problem. Consider the state vector $\{W(x,t)\}$ to be expanded as,

$$\{W(x,t)\} = \sum_{i=0}^{\infty} \{\Phi_i(x)\} q_i(t) \tag{3.65}$$

where,

$$\{\Phi_i(x)\} = \begin{Bmatrix} \lambda_i \phi_i(x) & \lambda_i \eta_i(x) & \phi_i(x) & \eta_i(x) \end{Bmatrix}^T \tag{3.66}$$

The solution of the homogeneous part of Eq. (3.57) can be found substituting $\{W(x,t)\}$ from (3.65) and assuming $q_i = e^{\lambda_i t}$, which leads to,

$$\lambda_i [M] \{\Phi_i(x)\} = [K] \{\Phi_i(x)\} \quad \text{for} \quad i = 1, 2, ... \tag{3.67}$$

one can prove that the eigenvalue problem shown in Eq. (3.67) is the same as the one given by Eqs. (3.23) and (3.24) in the preceding section. The adjoint eigenvalue problem is obtained as,

$$\lambda_i^* [\tilde{M}] \{\tilde{\Phi}_i(x)\} = [\tilde{K}] \{\tilde{\Phi}_i(x)\} \quad \text{for} \quad i = 1, 2, ... \tag{3.68}$$

being $[\tilde{M}]$, $[\tilde{K}]$ and $\{\tilde{\Phi}_i(x)\}$ the adjoint quantities of $[M]$, $[K]$ and $\{\Phi_i(x)\}$, respectively. In the present case, one can show that $[\tilde{M}] = [M]^H$ and $[\tilde{K}] = [K]^H$, being H the complex conjugate transpose, also known as hermitian transpose. The vector $\{\tilde{\Phi}_i(x)\}$ is given as,

$$\{\tilde{\Phi}_i(x)\} = \begin{Bmatrix} \lambda_i^* \tilde{\phi}_i(x) & \lambda_i^* \tilde{\eta}_i(x) & \tilde{\phi}_i(x) & \tilde{\eta}_i(x) \end{Bmatrix}^T \tag{3.69}$$

being $\tilde{\phi}(x)$ and $\tilde{\eta}(x)$ the adjoint eigenfunctions of $\phi(x)$ and $\eta(x)$, respectively. The functions $\{\Phi_i(x)\}$ and $\{\tilde{\Phi}_j(x)\}$ are *biorthogonal* and can be normalized so as to satisfy the following relations (LEE, 1993; MEIROVITCH, 1980),

$$\langle\, [M]\{\Phi_i(x)\},\, \{\tilde{\Phi}_j(x)\} \,\rangle = \delta_{ij} \tag{3.70a}$$

$$\langle\, [K]\{\Phi_i(x)\},\, \{\tilde{\Phi}_j(x)\} \,\rangle = \lambda_i \delta_{ij} \tag{3.70b}$$

where δ_{ij} is the Kronecker delta, which is one if $i = j$ and zero if $i \neq j$. After substituting $\{W(x,t)\}$ given by Eq. (3.65) in the state-space equation of motion (3.57), taking the internal product in both sides by $\{\tilde{\Phi}_i(x)\}$, and taking into account the orthogonality

conditions, one may have,

$$\dot{q}_i(t) = \lambda_i q_i(t) + \int_0^L \tilde{\phi}_i^*(x) f(x,t) dx \quad \text{for} \quad i = 1, 2, ... \tag{3.71}$$

Equation (3.71) consist of infinite first order complex modal equations, which are in reality truncated at N modes. In this case, each mode has a forward and backward case, each with a unique equation. After solving for the modal coordinates, the physical displacement and slope are obtained by,

$$u(x,t) = \sum_{i=0}^{\infty} \phi_i(x) q_i(t) \tag{3.72}$$

$$\psi(x,t) = \sum_{i=0}^{\infty} \eta_i(x) q_i(t) \tag{3.73}$$

The y and z components of the displacements and slopes are simply the real and imaginary parts of $u(x,t)$ and $\psi(x,t)$, respectively.

Since $\{\Phi_i(x)\}$ and $\{\tilde{\Phi}_i^*(x)\}$ are the result of the same eigenvalue problem, as noted by taking the complex conjugate transpose of Eq. (3.67) and comparing it with Eq. (3.68), they are the same within a constant, that is (LEE, 1993),

$$\{\Phi_i(x)\} = \frac{1}{K_i} \{\tilde{\Phi}_i^*(x)\} \tag{3.74}$$

being K_i a complex normalizing constant, that is obtained from Eqs. (3.70a) or (3.70b). The expansion of these equations are given as, respectively,

$$(\lambda_i + \lambda_j) \int_0^L \left[\bar{m}(x) \phi_i(x) \tilde{\phi}_j^*(x) + \bar{J}_d(x) \eta_i(x) \tilde{\eta}_j^*(x) \right] dx - j\Omega \int_0^L \bar{J}_d(x) \eta_i(x) \tilde{\eta}_j^*(x) dx$$

$$+ \int_0^L \bar{c}_m(x) \phi_i(x) \tilde{\phi}_j^*(x) dx + \int_0^L \bar{c}_t(x) \eta_i(x) \tilde{\eta}_j^*(x) dx = \delta_{ij} \tag{3.75}$$

$$\lambda_i \lambda_j \int_0^L \left[\bar{m}(x) \phi_i(x) \psi_j^*(x) + \bar{J}_d(x) \eta_i(x) \tilde{\eta}_j^*(x) \right] dx + \int_0^L \kappa G \bar{A}(x) \left[\eta_i(x) - \frac{d\phi_i(x)}{dx} \right] \frac{d\tilde{\phi}_j^*(x)}{dx} dx$$

$$- \int_0^L E\bar{I}(x) \frac{d\eta_i(x)}{dx} \frac{d\tilde{\eta}_j^*(x)}{dx} dx + \int_0^L \kappa G \bar{A}(x) \left[\frac{d\phi_i(x)}{dx} - \eta_i(x) \right] \tilde{\eta}_j^*(x) dx$$

$$- \int_0^L \bar{k}_m(x) \phi_i(x) \tilde{\phi}_j^*(x) dx - \int_0^L \bar{k}_t(x) \eta_i(x) \tilde{\eta}_j^*(x) dx = \lambda_i \delta_{ij} \tag{3.76}$$

Equation (3.75) or (3.76), together with the relation given by Equation (3.74), can be used to obtain the normalizing constant K_i for each mode. Since the properties of the shaft

are given in a step-wise manner, the integrals in Eqs. (3.75) and (3.76) can be evaluated for each segment individually and then summing the results.

The initial conditions for the modal coordinates can be obtained by multiplying Equation (3.65) by $[M]$, taking the product $\langle\cdot\rangle$ in both sides by $\{\tilde{\Phi}_j(x)\}$, and use the orthogonality condition. Considering the initial conditions as $u(x,0) = u_0(x)$, $\dot{u}(x,0) = \dot{u}_0(x)$, $\psi(x,0) = \psi_0(x)$, $\dot{\psi}(x,0) = \dot{\psi}_0(x)$, one may have,

$$q_i(0) = \langle\, [M]\{W(x,0)\}, \{\tilde{\Phi}_i(x)\}\,\rangle = \int_0^L \Big[\lambda_i \bar{m}(x)u_0(x) + \bar{m}(x)\dot{u}_0(x) + \bar{c}_m(x)u_0(x)\Big]\tilde{\phi}_i^*(x)dx$$

$$+ \int_0^L \Big[\lambda_i \bar{J}_d(x)\psi_0(x) + \bar{J}_d(x)\dot{\psi}_0(x) - j\Omega\bar{J}_p(x)\psi_0(x) + \bar{c}_t(x)\psi_0(x)\Big]\tilde{\eta}_i^*(x)dx \qquad (3.77)$$

It is noted that the initial conditions of the modal coordinates depend on the displacements and the linear and angular momentum of the rotor, as well as the damping on the bearings.

The CSM is now completely established for isotropic rotor systems. The analysis starts by setting the dimensions of the shaft and the division of it into segments. Each segment must have a constant-cross section and either a disk or bearing. If one has a bearing and a disk at the same location, it is possible to set them in different segments and then position them in the boundaries of the segments. It's important to note that the way the shaft is divided does not affect the final result, since the approach is exact, as far as the model shown in Fig. 2. Thus increasing or decreasing the number of segments does not affect the results. With the eigenvalues and the eigenfunctions at hand, the response is obtained solving the differential equations for the modal coordinates given by Eq. (3.71), which can be in close-form depending on the external force $f(x,t)$ considered. Note that for each mode there is a forward and backward case, where the former has positive frequency and the latter negative. The displacement and bending angle at any position along the shaft is then given by Eqs. (3.72) and (3.73).

As a final remark, one should note that the CSM gives a solution to a very general vibrating system, that is subjected to the gyroscopic effect and non-proportional damping, as well as posses multiple bearings and rigid disks. The difference between the CSM and other methods used to solve continuous systems is that the former is exact in nature. For example, the domain is not discretized in the CSM, but the boundary-value problem is solved in its entire form, using eigenfunctions obtained from the equations of motion. The next chapter expands the CSM even more to also account for anisotropic bearings.

4 Modeling of rotor systems on anisotropic bearings

In the previous chapter the modeling and analysis of isotropic rotor systems by the proposed method was presented. Since most rotors in real applications have some kind of asymmetry, this chapter presents the CSM applied to rotors with anisotropic bearings. The model of the shaft is still considered axisymmetric, that is, it has the same moments of inertia in the two orthogonal directions. But, due to the anisotropy of the bearings, the whole system is not axisymmetric and the use of complex notation no longer reduces the problem as in the isotropic case. However, the use of complex coordinates is still very useful as it will be shown, and it provides important insights into the effects of anisotropy in the response.

Different from isotropic systems, when anisotropy is present the direction of the displacement is no longer collinear with the applied force (GENTA, 2007). Thus, a synchronous force such as unbalance will excite not only the forward modes but also the backward ones. The effect of this is that now one finds additional critical speeds corresponding to the backward whirl frequencies, where the rotor whirls in a backward direction, or even the so called "mixed-modes" where some parts of the shafts whirls in forward directions and other parts in backward direction (MUSZYNSKA, 2005). Also, the whirl orbit will be an ellipse rather than a circle, with a major and a minor axis.

The division of this chapter is similar to the previous one: Section 4.1 presents the equations of motion that govern the rotor system, where the anisotropy consideration is clearly stated. The eigenfunctions and eigenvalues are obtained in Sec. 4.2 in a similar fashion as before, but with major differences due to the anisotropic bearings. The chapter finalizes with the modal analysis in Sec. 4.3, to obtain the response of the system.

4.1 Equations of motion

The rotor system dealt with in this chapter is the same as the one illustrated in Fig. 2. As a quick recall, the shaft is divided into n segments with lengths L_i, cross-section areas A_i and area moments of inertia I_i. The number of disks and bearings is P and Q, positioned along a segment i by the local coordinates a_i and b_i. Each segment has a local coordinate $\xi_i \in [0,\ L_i]$ that is used to describe the local mode shape. The displacements and bending angles in the y and z directions are denoted as $u_y(x,t)$, $u_z(x,t)$, $\psi_y(x,t)$ and $\psi_z(x,t)$, respectively, with the directions shown in Fig. 2. The equations of motion can be derived in the exact same way, using the EHP, but with the addition of the anisotropic

bearings, which gives the following,

$$\bar{m}(x)\frac{\partial^2 u_y}{\partial t^2} + \frac{\partial}{\partial x}\left[\kappa G\bar{A}(x)\left(\psi_z - \frac{\partial u_y}{\partial x}\right)\right] + \bar{k}_{yy}(x)u_y + \bar{c}_{yy}(x)\frac{\partial u_y}{\partial t} \tag{4.1}$$

$$\bar{k}_{yz}(x)u_z + \bar{c}_{yz}(x)\frac{\partial u_z}{\partial t} = f_y(x,t) \tag{4.2}$$

$$\bar{m}(x)\frac{\partial^2 u_z}{\partial t^2} - \frac{\partial}{\partial x}\left[\kappa G\bar{A}(x)\left(\psi_y + \frac{\partial u_z}{\partial x}\right)\right] + \bar{k}_{zz}(x)u_z + \bar{c}_{zz}(x)\frac{\partial u_z}{\partial t} \tag{4.3}$$

$$+\bar{k}_{zy}(x)u_y + \bar{c}_{zy}(x)\frac{\partial u_y}{\partial t} = f_z(x,t) \tag{4.4}$$

$$\bar{J}_d(x)\frac{\partial^2 \psi_y}{\partial t^2} + \Omega\bar{J}_p(x)\frac{\partial \psi_z}{\partial t} - \frac{\partial}{\partial x}\left[E\bar{I}(x)\frac{\partial \psi_y}{\partial x}\right] + \kappa G\bar{A}(x)\left[\psi_y + \frac{\partial u_z}{\partial x}\right]$$

$$-\bar{k}_t(x)\psi_y - \bar{c}_t(x)\frac{\partial \psi_y}{\partial t} = 0 \tag{4.5}$$

$$\bar{J}_d(x)\frac{\partial^2 \psi_z}{\partial t^2} - \Omega\bar{J}_p(x)\frac{\partial \psi_y}{\partial t} - \frac{\partial}{\partial x}\left[E\bar{I}(x)\frac{\partial \psi_z}{\partial x}\right] + \kappa G\bar{A}(x)\left[\psi_z - \frac{\partial u_y}{\partial x}\right]$$

$$-\bar{k}_t(x)\psi_z - \bar{c}_t(x)\frac{\partial \psi_z}{\partial t} = 0 \tag{4.6}$$

Recall that $\bar{m}(x)$ is the mass per unit length; $\bar{J}_d(x)$ and $\bar{J}_p(x)$ are the diametral and polar mass moment of inertia per unit length; Ω is the shaft rotating speed; and $f_y(x,t)$ and $f_z(x,t)$ are the distributed force components. The properties of the shaft are given in a step-wise manner as shown in Eq. (3.14) and repeated here in the following,

$$\bar{A}(x) = \sum_{i=1}^{n} A_i H_i(x), \quad \bar{I}(x) = \sum_{i=1}^{n} I_i H_i(x), \quad \bar{m}(x) = \sum_{i=1}^{n} \rho A_i H_i(x) + \sum_{j=1}^{P} M^j \delta_d(x - x_a^j)$$

$$\bar{J}_d(x) = \sum_{i=1}^{n} \rho A_i r_i^2 H_i(x) + \sum_{j=1}^{P} J_d^j \delta_d(x - x_a^j), \quad \bar{J}_p(x) = \sum_{i=1}^{n} 2\rho A_i r_i^2 H_i(x) + \sum_{j=1}^{P} J_p^j \delta_d(x - x_a^j)$$

(3.14 repeated)

The bearings have now direct distributed coefficients $\bar{k}_{yy}$, $\bar{k}_{zz}$, $\bar{c}_{yy}$ and $\bar{c}_{zz}$ as well as cross-coupled coefficients $\bar{k}_{yz}$, $\bar{k}_{zy}$, $\bar{c}_{yz}$ and $\bar{c}_{zy}$. Figure 4 illustrates the bearing model, which can represent a great variety of bearings (CHILDS, 1993). The torsional coefficients are still considered isotropic with distributed coefficients $\bar{k}_t$ and $\bar{c}_t$. Its possible to write the above equations in complex form using Eqs. (3.10) and (3.11), which gives,

$$\bar{m}(x)\frac{\partial^2 u}{\partial t^2} + \frac{\partial}{\partial x}\left[\kappa G\bar{A}(x)\left(\psi - \frac{\partial u}{\partial x}\right)\right] + \bar{k}_f(x)u + \bar{c}_f(x)\frac{\partial u}{\partial t}$$

$$+ \bar{k}_b(x)u^* + \bar{c}_b(x)\frac{\partial u^*}{\partial t} = f(x,t) \tag{4.7}$$

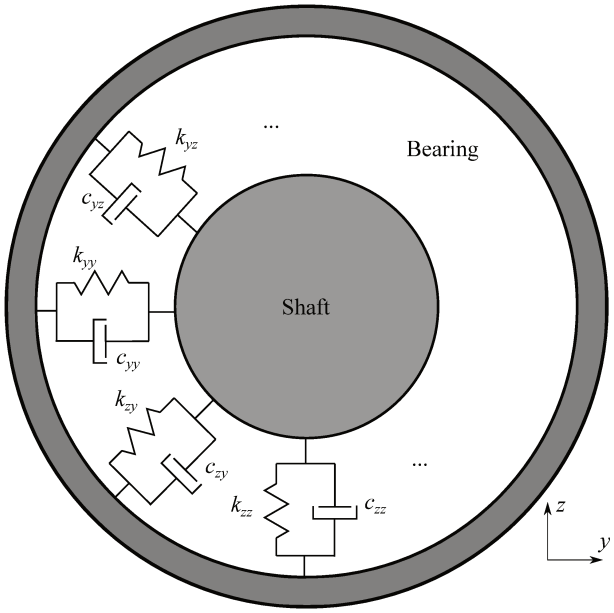

Figure 4: General anisotropic bearing

$$\bar{J}_d(x)\frac{\partial^2\psi}{\partial t^2} - j\Omega\bar{J}_p(x)\frac{\partial\psi}{\partial t} - \frac{\partial}{\partial x}\left[E\bar{I}(x)\frac{\partial\psi}{\partial x}\right] + \kappa G\bar{A}(x)\left[\psi - \frac{\partial u}{\partial x}\right] - \bar{k}_t(x)\psi - \bar{c}_t(x)\frac{\partial\psi}{\partial t} = 0 \tag{4.8}$$

where $u = u_y + ju_z$, $u^* = u_y - ju_z$ and $\psi = \psi_z - j\psi_y$. Also, the functions $\bar{k}_f$, $\bar{k}_b$, $\bar{c}_f$ and $\bar{c}_b$ are complex and given as,

$$\begin{aligned}
\bar{k}_f(x) &= \sum_{l=1}^{Q} k_f^l\delta_d(x-x_b^l) = \sum_{l=1}^{Q}\frac{1}{2}\Big(k_{yy}^l + k_{zz}^l - j(k_{yz}^l - k_{zy}^l)\Big)\delta_d(x-x_b^l)\\
\bar{c}_f(x) &= \sum_{l=1}^{Q} c_f^l\delta_d(x-x_b^l) = \sum_{l=1}^{Q}\frac{1}{2}\Big(c_{yy}^l + c_{zz}^l - j(c_{yz}^l - c_{zy}^l)\Big)\delta_d(x-x_b^l)\\
\bar{k}_b(x) &= \sum_{l=1}^{Q} k_b^l\delta_d(x-x_b^l) = \sum_{l=1}^{Q}\frac{1}{2}\Big(k_{yy}^l - k_{zz}^l + j(k_{yz}^l + k_{zy}^l)\Big)\delta_d(x-x_b^l)\\
\bar{c}_b(x) &= \sum_{l=1}^{Q} c_b^l\delta_d(x-x_b^l) = \sum_{l=1}^{Q}\frac{1}{2}\Big(c_{yy}^l - c_{zz}^l + j(c_{yz}^l + c_{zy}^l)\Big)\delta_d(x-x_b^l)
\end{aligned} \tag{4.9}$$

being x_b^l the coordinates of the bearings and k and c the stiffness and damping coefficients, respectively. The complex coefficients k_f^l and c_f^l denote the mean stiffness and damping coefficients while k_b^l and c_b^l the deviatoric coefficients (GENTA, 2007). Note that in case of isotropic bearings, $k_{yy}^l = k_{zz}^l$, $c_{yy}^l = c_{zz}^l$, $k_{yz}^l = -k_{zy}^l$ and $c_{yz}^l = -c_{zy}^l$, thus $k_b^l = c_b^l = 0$. In this case, one has $\bar{k}_f(x) = \bar{k}_m(x)$ and $\bar{c}_f(x) = \bar{c}_m(x)$, with $\bar{k}_m(x)$ and $\bar{c}_m(x)$ given by Eqs. (3.16). In addition, the system can have isotropic and anisotropic bearings at different locations x_b^l, for $l = 1, 2, ..., P$.

The boundary conditions remain the same as stated in Eqs. (3.17) and (3.18). Similarly to the isotropic case, the boundary-value problem is solved by means of the modal expansion method, which states

$$u(x,t) = \sum_{i=1}^{\infty}[\phi_{1i}^{F}(x)q_i^{F}(t) + \phi_{1i}^{B}(x)q_i^{B}(t)] \approx \sum_{i=1}^{N}[\phi_{1i}^{F}(x)q_i^{F}(t) + \phi_{1i}^{B}(x)q_i^{B}(t)] \tag{4.10}$$

$$\psi(x,t) = \sum_{i=1}^{\infty}[\eta_{1i}^{F}(x)q_i^{F}(t) + \eta_{1i}^{B}(x)q_i^{B}(t)] \approx \sum_{i=1}^{N}[\eta_{1i}^{F}(x)q_i^{F}(t) + \eta_{1i}^{B}(x)q_{1i}^{B}(t)] \tag{4.11}$$

where $\phi_{1i}(x)$ and $\eta_{1i}(x)$ are the eigenfunctions of mode i. The subscript 1 denotes that the functions are evaluated with the rotation at the specified direction. This is explained in the next section.

4.2 Eigenfunctions and eigenvalues

The free vibration of the multi-stepped rotor is obtained as,

$$\bar{m}(x)\frac{\partial^2 u}{\partial t^2} + \frac{\partial}{\partial x}\left[\kappa G\bar{A}(x)\left(\psi - \frac{\partial u}{\partial x}\right)\right] + \bar{k}_f(x)u + \bar{c}_f(x)\frac{\partial u}{\partial t} + \bar{k}_b(x)u^* + \bar{c}_b(x)\frac{\partial u^*}{\partial t} = 0 \tag{4.12}$$

$$\begin{aligned}\bar{J}_d(x)\frac{\partial^2 \psi}{\partial t^2} - j\Omega\bar{J}_p(x)\frac{\partial \psi}{\partial t} - \frac{\partial}{\partial x}\left[E\bar{I}(x)\frac{\partial \psi}{\partial x}\right] + \kappa G\bar{A}(x)\left[\psi - \frac{\partial u}{\partial x}\right] \\ - \bar{k}_t(x)\psi - \bar{c}_t(x)\frac{\partial \psi}{\partial t} = 0\end{aligned} \tag{4.13}$$

Assuming a solution on the form,

$$u(x,t) = \phi_1(x)e^{\lambda t} + \phi_2^*(x)e^{\lambda^* t} \tag{4.14a}$$

$$\psi(x,t) = \eta_1(x)e^{\lambda t} + \eta_2^*(x)e^{\lambda^* t} \tag{4.14b}$$

being λ the eigenvalues and * denotes the complex conjugate. By substituting the solutions in the equations and gathering the terms with $e^{\lambda t}$ and $e^{\lambda^* t}$, one may have,

$$\begin{aligned}\lambda^2\bar{m}(x)\phi_1(x) + \frac{d}{dx}\left[\kappa G\bar{A}(x)\left(\eta_1(x) - \frac{d\phi_1(x)}{dx}\right)\right] + \left[\bar{k}_f(x) + \lambda\bar{c}_f(x)\right]\phi_1(x) \\ + \left[\bar{k}_b(x) + \lambda\bar{c}_b(x)\right]\phi_2(x) = 0\end{aligned} \tag{4.15a}$$

$$\begin{aligned}\lambda^2\bar{m}(x)\phi_2(x) + \frac{d}{dx}\left[\kappa G\bar{A}(x)\left(\eta_2(x) - \frac{d\phi_2(x)}{dx}\right)\right] + \left[\bar{k}_f^*(x) + \lambda\bar{c}_f^*(x)\right]\phi_2(x) \\ + \left[\bar{k}_b^*(x) + \lambda\bar{c}_b^*(x)\right]\phi_1(x) = 0\end{aligned} \tag{4.15b}$$

$$\lambda^2 \bar{J}_d(x)\eta_1(x) - j\lambda\Omega\bar{J}_p(x)\eta_1(x) - \frac{d}{dx}\left[E\bar{I}(x)\frac{d\eta_1(x)}{dx}\right] + \kappa G\bar{A}(x)\left(\eta_1(x) - \frac{d\phi_1(x)}{dx}\right) - \left[\bar{k}_t(x) + \lambda\bar{c}_t(x)\right]\eta_1(x) = 0 \tag{4.15c}$$

$$\lambda^2 \bar{J}_d(x)\eta_2(x) + j\lambda\Omega\bar{J}_p(x)\eta_2(x) - \frac{d}{dx}\left[E\bar{I}(x)\frac{d\eta_2(x)}{dx}\right] + \kappa G\bar{A}(x)\left(\eta_2(x) - \frac{d\phi_2(x)}{dx}\right) - \left[\bar{k}_t(x) + \lambda\bar{c}_t(x)\right]\eta_2(x) = 0 \tag{4.15d}$$

By analyzing the above equations, one may note that they are not complex conjugate equations due to the anisotropic bearings coefficients $\bar{k}_b(x)$ and $\bar{c}_b(x)$. One may also note that the rotor rotates at the specified direction for the functions ϕ_1 and η_1, and at the opposite direction for ϕ_2 and η_2. Thus, the overall mode shape of the rotor will be non-planar and non-circular. Since the equations for the functions ϕ_1 and η_1 are coupled with the ones of ϕ_2 and η_2, they must be solved simultaneously; thus increasing by twofold the number of equations needed to be solved when compared to the isotropic case presented in Chapter 3. It is worth mentioning that when the rotor becomes isotropic, one has $\bar{k}_b(x) = \bar{c}_b(x) = 0$, and the equations for ϕ_1 and η_1 become complex conjugate of ϕ_2 and η_2; and thus one only needs to solve one of them.

As shown in the previous chapter for the isotropic rotor, the eigenvalue problem can be solved by dividing the domain and solving individually for each segment i. This gives the local mode shapes, and the global mode shape will be a combination of the latter. For an arbitrary segment i located at $x_i < x < x_{i+1}$ with eigenfunctions $\phi_{1i}(\xi_i)$, $\phi_{2i}(\xi_i)$, $\eta_{1i}(\xi_i)$ and $\eta_{2i}(\xi_i)$, being $\xi_i \in [0,\ L_i]$ the local coordinate of the segment. The segment is considered to have a lth bearing and a kth rigid disk. The local eigenvalue problem can be obtained as,

$$\lambda^2\Big(\rho A_i + M^k\delta_d(\xi_i - a_k)\Big)\phi_{1i}(\xi_i) + \kappa G A_i\Big(\eta'_{1i}(\xi_i) - \phi''_{1i}(\xi_i)\Big) + \left(k_f^l + \lambda c_f^l\right)\phi_{1i}(\xi_i)\delta_d(\xi_i - b_l) + \left(k_b^l + \lambda c_b^l\right)\phi_{2i}(\xi_i)\delta_d(\xi_i - b_l) = 0 \tag{4.16a}$$

$$\lambda^2\Big(\rho A_i + M^k\delta_d(\xi_i - a_k)\Big)\phi_{2i}(\xi_i) + \kappa G A_i\Big(\eta'_{2i}(\xi_i) - \phi''_{2i}(\xi_i)\Big) + \left(k_f^{l*} + \lambda c_f^{l*}\right)\phi_{2i}(\xi_i)\delta_d(\xi_i - b_l) + \left(k_b^{l*} + \lambda c_b^{l*}\right)\phi_{2i}(\xi_i)\delta_d(\xi_i - b_l) = 0 \tag{4.16b}$$

$$\lambda^2\Big(\rho A_i r_i^2 + J_d^k\delta_d(\xi_i - a_k)\Big)\eta_{1i}(\xi_i) - j\lambda\Omega\Big(2\rho A_i r_i^2 + J_p^k\delta_d(\xi_i - a_k)\Big)\eta_{1i}(\xi_i) - EI_i\eta''_{1i}(\xi_i) + \kappa G A_i\Big(\eta_{1i}(\xi_i) - \phi'_{1i}(\xi_i)\Big) - \left(k_t^l + \lambda c_t^l\right)\eta_{1i}(\xi_i)\delta_d(\xi_i - b_l) = 0 \tag{4.16c}$$

$$\lambda^2\Big(\rho A_i r_i^2 + J_d^k\delta_d(\xi_i - a_k)\Big)\eta_{2i}(\xi_i) + j\lambda\Omega\Big(2\rho A_i r_i^2 + J_p^k\delta_d(\xi_i - a_k)\Big)\eta_{2i}(\xi_i) - EI_i\eta''_{2i}(\xi_i) + \kappa G A_i\Big(\eta_{2i}(\xi_i) - \phi'_{2i}(\xi_i)\Big) - \left(k_t^l + \lambda c_t^l\right)\eta_{2i}(\xi_i)\delta_d(\xi_i - b_l) = 0 \tag{4.16d}$$

where $' = d/d\xi_i$. The above equations can be solved by means of the Laplace transform, which yields

$$\lambda^2\rho A_i\hat{\phi}_{1i}(s) + \kappa GA_i\Big[s\hat{\eta}_{1i}(s) - \eta_{1i}(0)\Big] - \kappa GA_i\left[s^2\hat{\phi}_{1i}(s) - \phi'_{1i}(0) - s\phi_{1i}(0)\right]$$
$$+\lambda^2 M^k\phi_{1i}(a_k)e^{-sa_k} + \Big(\left(k_f^l + \lambda c_f^l\right)\phi_{1i}(b_l) + \left(k_b^l + \lambda c_b^l\right)\phi_{2i}(b_l)\Big)e^{-sb_l} = 0 \tag{4.17a}$$

$$\lambda^2\rho A_i\hat{\phi}_{2i}(s) + \kappa GA_i\Big[s\hat{\eta}_{2i}(s) - \eta_{2i}(0)\Big] - \kappa GA_i\left[s^2\hat{\phi}_{2i}(s) - \phi'_{2i}(0) - s\phi_{2i}(0)\right]$$
$$+\lambda^2 M^k\phi_{2i}(a_k)e^{-sa_k} + \Big(\left(k_f^{l*} + \lambda c_f^{l*}\right)\phi_{2i}(b_l) + \left(k_b^{l*} + \lambda c_b^{l*}\right)\phi_{1i}(b_l)\Big)e^{-sb_l} = 0 \tag{4.17b}$$

$$\left(\lambda^2 - 2j\lambda\Omega\right)\rho A_i r_i^2\hat{\eta}_{1i}(s) - EI_i\left[s^2\hat{\eta}_{1i}(s) - \eta'_{1i}(0) - s\eta_{1i}(0)\right] - \kappa GA_i\left[s\hat{\phi}_{1i}(s) - \phi_{1i}(0)\right]$$
$$+\kappa GA_i\hat{\eta}_{1i}(s) + \left(\lambda^2 J_d^k - j\lambda\Omega J_p^k\right)\eta_{1i}(a_k)e^{-sa_k} + \left(k_t^l + \lambda c_t^l\right)\eta_{1i}(b_l)e^{-sb_l} = 0 \tag{4.17c}$$

$$\left(\lambda^2 + 2j\lambda\Omega\right)\rho A_i r_i^2\hat{\eta}_{2i}(s) - EI_i\left[s^2\hat{\eta}_{2i}(s) - \eta'_{2i}(0) - s\eta_{2i}(0)\right] - \kappa GA_i\left[s\hat{\phi}_{2i}(s) - \phi_{2i}(0)\right]$$
$$+\kappa GA_i\hat{\eta}_{2i}(s) + \left(\lambda^2 J_d^k + j\lambda\Omega J_p^k\right)\eta_{2i}(a_k)e^{-sa_k} + \left(k_t^l + \lambda c_t^l\right)\eta_{2i}(b_l)e^{-sb_l} = 0 \tag{4.17d}$$

where $\hat{\phi}_{1i}(s)$, $\hat{\phi}_{2i}(s)$, $\hat{\eta}_{1i}(s)$ and $\hat{\eta}_{2i}(s)$ are the Laplace transform of $\phi_{1i}(\xi_i)$, $\phi_{2i}(\xi_i)$, $\eta_{1i}(\xi_i)$ and $\eta_i(\xi_i)$, respectively. The equations in the s domain can be written in matrix form as,

$$[L]\{\hat{\Phi}(s)\} = \{b\} \tag{4.18}$$

where the terms are now given as,

$$[L] = \begin{bmatrix}[L_1] & [0]_{4\times4}\\ [0]_{4\times4} & [L_2]\end{bmatrix}, \quad [L_1] = \begin{bmatrix}\rho A_i\lambda^2 - \kappa GA_i s^2 & \kappa GA_i s\\ -\kappa GA_i s & \left(\lambda^2 - 2j\lambda\Omega\right)\rho A_i r_i^2 - EI_i s^2 + \kappa GA_i\end{bmatrix},$$

$$[L_2] = \begin{bmatrix}\rho A_i\lambda^2 - \kappa GA_i s^2 & \kappa GA_i s\\ -\kappa GA_i s & \left(\lambda^2 + 2j\lambda\Omega\right)\rho A_i r_i^2 - EI_i s^2 + \kappa GA_i\end{bmatrix} \tag{4.19}$$

$$\{\hat{\Phi}(s)\} = \begin{Bmatrix}\hat{\phi}_{1i}(s) & \hat{\eta}_{1i}(s) & \hat{\phi}_{2i}(s) & \hat{\eta}_{2i}(s)\end{Bmatrix}^T \tag{4.20}$$

$$\{b\} = \left\{ \begin{array}{c} \kappa G A_i \left[\eta_i(0) - \phi_i'(0) - s\phi(0)\right] - \lambda^2 M^k \phi_i(a_k) e^{-sa_k} \\ -\left(\left(k_f^l + \lambda c_f^l\right)\phi_{1i}(b_l) + \left(k_b^l + \lambda c_b^l\right)\phi_{2i}(b_l) \right) e^{-sb_l} \\ \\ -\kappa G A_i \phi_i(0) - EI_i \left[\eta_i'(0) + s\eta_i(0)\right] - \left(\lambda^2 J_d^k - j\lambda\Omega J_p^k\right)\eta_i(a_k) e^{-sa_k} \\ + \left(k_t^l + \lambda c_t^l\right)\eta_i(b_l) e^{-sb_l} \\ \\ \kappa G A_i \left[\eta_i(0) - \phi_i'(0) - s\phi(0)\right] - \lambda^2 M^k \phi_i(a_k) e^{-sa_k} \\ -\left(\left(k_f^{l*} + \lambda c_f^{l*}\right)\phi_{2i}(b_l) + \left(k_b^{l*} + \lambda c_b^{l*}\right)\phi_{1i}(b_l) \right) e^{-sb_l} \\ \\ -\kappa G A_i \phi_i(0) - EI_i \left[\eta_i'(0) + s\eta_i(0)\right] - \left(\lambda^2 J_d^k + j\lambda\Omega J_p^k\right)\eta_i(a_k) e^{-sa_k} \\ + \left(k_t^l + \lambda c_t^l\right)\eta_i(b_l) e^{-sb_l} \end{array} \right\} \tag{4.21}$$

Note that the problem in the s domain, Equation (4.18), now have twice the size as in the isotropic case, but the equations are uncoupled. Here it is important to point out that this would not be the case if cartesian coordinates were used, where the matrix $[L]$ would be a full block matrix. The approach to obtain the functions in the space domain is similar to the isotropic case, and the mode shape parameters are obtained from the determinants $det([L_1])$ and $det([L_2])$, which leads to, respectively,

$$s^4 + \left(\frac{\rho A_i r_i^2}{EI_i}\left(2j\lambda\Omega - \lambda^2\right) - \frac{\rho A_i \lambda^2}{\kappa G A_i} \right) s^2 + \frac{\rho A_i \lambda_i^2}{EI_i}\left(1 - \frac{\rho r_i^2}{\kappa G}\left(2j\lambda\Omega - \lambda^2\right) \right) = 0 \tag{4.22}$$

$$s^4 + \left(-\frac{\rho A_i r_i^2}{EI_i}\left(2j\lambda\Omega + \lambda^2\right) - \frac{\rho A_i \lambda^2}{\kappa G A_i} \right) s^2 + \frac{\rho A_i \lambda_i^2}{EI_i}\left(1 + \frac{\rho r_i^2}{\kappa G}\left(2j\lambda\Omega + \lambda^2\right) \right) = 0 \tag{4.23}$$

The roots of the first equation are δ_{1i}^2 and $-\varepsilon_{1i}^2$, while for the second one they are δ_{2i}^2 and $-\varepsilon_{2i}^2$. These roots have the same form as shown in Eqs. (3.34) and (3.35). However, note that for δ_{2i}^2 and $-\varepsilon_{2i}^2$ the rotation is reversed; thus one should apply $\Omega \to -\Omega$. Using the fact that $det([L_1]) = (s^2 - \delta_{1i}^2)(s^2 + \varepsilon_{1i}^2)$ and $det([L_2]) = (s^2 - \delta_{2i}^2)(s^2 + \varepsilon_{2i}^2)$, the inverse Laplace transform can be applied in Eq. (4.18), leading to,

$$\begin{aligned} \phi_{1i}(\xi_i) = {} & \eta_{1i}(0) f_1(\xi_i) + \eta_{1i}'(0) f_2(\xi_i) + \phi_{1i}(0) f_3(\xi_i) + \phi_{1i}'(0) f_4(\xi_i) \\ & + \left[p_1^{a_k}(\xi_i)\phi_{1i}(a_k) + h_1^{a_k}(\xi_i)\eta_{1i}(a_k) \right] H(x - a_k) \\ & + \left[p_{1f}^{b_l}(\xi_i)\phi_{1i}(b_l) + p_{1b}^{b_l}(\xi_i)\phi_{2i}(b_l) + h_1^{b_l}(\xi_i)\eta_{1i}(b_l) \right] H(x - b_l) \end{aligned} \tag{4.24}$$

$$\begin{aligned} \eta_{1i}(\xi_i) = {} & \eta_{1i}(0) g_1(\xi_i) + \eta_{1i}'(0) g_2(\xi_i) + \phi_{1i}(0) g_3(\xi_i) + \phi_{1i}'(0) g_4(\xi_i) \\ & + \left[p_2^{a_k}(\xi_i)\phi_{1i}(a_k) + h_2^{a_k}(\xi_i)\eta_{1i}(a_k) \right] H(x - a_k) \\ & + \left[p_{2f}^{b_l}(\xi_i)\phi_{1i}(b_l) + p_{2b}^{b_l}(\xi_i)\phi_{2i}(b_l) + h_2^{b_l}(\xi_i)\eta_{1i}(b_l) \right] H(x - b_l) \end{aligned} \tag{4.25}$$

$$\begin{aligned} \phi_{2i}(\xi_i) = {} & \eta_{2i}(0) f_5(\xi_i) + \eta_{2i}'(0) f_6(\xi_i) + \phi_{2i}(0) f_7(\xi_i) + \phi_{2i}'(0) f_8(\xi_i) \\ & + \left[p_3^{a_k}(\xi_i)\phi_{2i}(a_k) + h_3^{a_k}(\xi_i)\eta_{2i}(a_k) \right] H(x - a_k) \\ & + \left[p_{3f}^{b_l}(\xi_i)\phi_{2i}(b_l) + p_{3b}^{b_l}(\xi_i)\phi_{1i}(b_l) + h_3^{b_l}(\xi_i)\eta_{2i}(b_l) \right] H(x - b_l) \end{aligned} \tag{4.26}$$

$$\begin{aligned}\eta_{2i}(\xi_i) = {} & \eta_{2i}(0)g_5(\xi_i) + \eta'_{2i}(0)g_6(\xi_i) + \phi_{2i}(0)g_7(\xi_i) + \phi'_{2i}(0)g_8(\xi_i) \\ & + \Big[p_4^{a_k}(\xi_i)\phi_{2i}(a_k) + h_4^{a_k}(\xi_i)\eta_{3i}(a_k)\Big]H(x-a_k) \\ & + \Big[p_{4f}^{b_l}(\xi_i)\phi_{2i}(b_l) + p_{4b}^{b_l}(\xi_i)\phi_{1i}(b_l) + h_4^{b_l}(\xi_i)\eta_{2i}(b_l)\Big]H(x-b_l)\end{aligned} \tag{4.27}$$

the functions f, g, p and h above are shown in Appendix B. They are actually very similar to the isotropic case, with the exception of additional functions due to ϕ_{2i} and η_{2i}. As mentioned earlier, the functions ϕ_{1i} and η_{1i} rotate at the specified direction $+\Omega$, while ϕ_{2i} and η_{2i} rotate in the opposite direction $-\Omega$. This means that one only needs to obtain the functions f_1 through f_4 and g_1 through g_4, since f_5 through f_8 and g_5 through g_8 will be the same expression but with the reversed rotation direction.

The unknowns in Equations (4.24)-(4.27) are obtained from the boundary conditions together with the continuity conditions. The terms $\eta_{1i}(a_k)$, $\eta_{1i}(b_l)$, $\phi_{1i}(a_k)$, $\phi_{1i}(b_l)$, $\eta_{2i}(a_k)$, $\eta_{2i}(b_l)$, $\phi_{2i}(a_k)$ and $\phi_{2i}(b_l)$ can be obtained directly from Equations (4.24)-(4.27) by the continuity of the functions ϕ_{1i}, η_{1i}, ϕ_{2i} and η_{2i} at the coordinates $\xi_i = a_k$ and $\xi_i = b_l$. The procedure needed to obtain these term was shown in Sec. 3.2, and is simply the evaluation of the functions at the coordinates a_k or b_l, and the process is simplified if one considers the segment to have only a disk or a bearing. By performing the evaluations indicated by $\eta_{1i}(a_k)$, $\eta_{1i}(b_l)$ and so on, and substituting back in Eqs. (4.24)-(4.27) one arrives at,

$$\phi_{1i}(\xi_i) = [C_i(\xi)]\{X_i(0)\} \tag{4.28}$$

$$\eta_{1i}(\xi_i) = [D_i(\xi)]\{X_i(0)\} \tag{4.29}$$

$$\phi_{2i}(\xi_i) = [E_i(\xi)]\{X_i(0)\} \tag{4.30}$$

$$\eta_{2i}(\xi_i) = [F_i(\xi)]\{X_i(0)\} \tag{4.31}$$

where,

$$[C_i(\xi)] = [C_{1i}(\xi)\ C_{2i}(\xi)\ \cdots\ C_{8i}(\xi)], \quad [D_i(\xi)] = [D_{1i}(\xi)\ D_{2i}(\xi)\ \cdots\ D_{8i}(\xi)], \tag{4.32a}$$

$$[E_i(\xi)] = [E_{1i}(\xi)\ E_{2i}(\xi)\ \cdots\ E_{8i}(\xi)], \quad [F_i(\xi)] = [F_{1i}(\xi)\ F_{2i}(\xi)\ \cdots\ F_{8i}(\xi)], \tag{4.32b}$$

$$\{X_i(\xi_i)\} = \{\eta_{1i}(\xi_i)\ \eta'_{1i}(\xi_i)\ \phi_{1i}(\xi_i)\ \phi'_{1i}(\xi_i)\ \eta_{2i}(\xi_i)\ \eta'_{2i}(\xi_i)\ \phi_{2i}(\xi_i)\ \phi'_{2i}(\xi_i)\}^T \tag{4.32c}$$

The functions C_{ji}, D_{ji}, E_{ji} and F_{ji} ($j = 1, 2, ..., 8$) depend if segment i has a disk or a bearing. If segment i has a disk, the terms C_{1i} through C_{4i} and D_{1i} through D_{4i} have the same expression shown in Eq. (3.42) for the isotropic case, and the terms C_{5i} through C_{8i} and D_{5i} through D_{8i} will be zero. Also, the terms F_{ji} and E_{ji} will be the same as C_{ji} and D_{ji}, for $j = 1, 2, ..., 8$, but with the rotation reversed, that is, $\Omega \to -\Omega$. In case segment

i has a bearing, one has,

$$\begin{cases} C_{ij}(\xi_i) = f_j(\xi_i) + \Big[f_j(b_l)p_{1f}^{b_l}(\xi_i) + g_j(b_l)h_1^{b_l}(\xi_i)\Big]\, H(\xi_i - b_l) \quad \text{for } j = 1,2,3,4; \\ C_{ij}(\xi_i) = f_j(b_l)p_{1b}^{b_l}(\xi_i)H(\xi_i - b_l) \quad \text{for } j = 5,6,7,8; \end{cases} \tag{4.33}$$

$$\begin{cases} D_{ij}(\xi_i) = g_j(\xi_i) + \Big[f_j(b_l)p_{2f}^{b_l}(\xi_i) + g_j(b_l)h_2^{b_l}(\xi_i)\Big]\, H(\xi_i - b_l) \quad \text{for } j = 1,2,3,4; \\ D_{ij}(\xi_i) = f_j(b_l)p_{2b}^{b_l}(\xi_i)H(\xi_i - b_l) \quad \text{for } j = 5,6,7,8; \end{cases} \tag{4.34}$$

$$\begin{cases} E_{ij}(\xi_i) = f_j(\xi_i) + \Big[f_j(b_l)p_{3f}^{b_l}(\xi_i) + g_j(b_l)h_3^{b_l}(\xi_i)\Big]\, H(\xi_i - b_l) \quad \text{for } j = 1,2,3,4; \\ E_{ij}(\xi_i) = f_j(b_l)p_{3b}^{b_l}(\xi_i)H(\xi_i - b_l) \quad \text{for } j = 5,6,7,8; \end{cases} \tag{4.35}$$

$$\begin{cases} F_{ij}(\xi_i) = f_j(\xi_i) + \Big[f_j(b_l)p_{4f}^{b_l}(\xi_i) + g_j(b_l)h_4^{b_l}(\xi_i)\Big]\, H(\xi_i - b_l) \quad \text{for } j = 1,2,3,4; \\ F_{ij}(\xi_i) = f_j(b_l)p_{4b}^{b_l}(\xi_i)H(\xi_i - b_l) \quad \text{for } j = 5,6,7,8; \end{cases} \tag{4.36}$$

Although the functions above appear complicated, they are distinguished only by the terms $p_{jf}^{b_l}$, $p_{jb}^{b_l}$ and $h_j^{b_l}$, for $j = 1,2,3,4$. In case the bearings are isotropic, the functions $p_{jb}^{b_l}$ vanish, and the terms C_{ji} and D_{ji} become exactly as in the isotropic case, while F_{ji} and E_{ji} are equal to the latter but with $\Omega \to -\Omega$. In the anisotropic case, however, the terms F_{ji} and E_{ji} are not the same as C_{ji} and D_{ji} with the rotation reversed, but they are proportional by a complex constant. This constant is found solving the eigenvalue problem.

The eigenvalue problem now consist in finding the constants $\{X_i(0)\}$, for each segment $i = 1,2,...,n$, as well as the eigenvalue λ. Since the vector of constants has now eight components, one needs additional continuity conditions than the ones shown in Eq. (3.45). Since the conditions are isotropic, they will be exactly the same for both functions with subscript 1 and 2. Therefore, one can write,

$$\{X_{i+1}(0)\} = \begin{bmatrix} [h_i] & [0]_{4\times4} \\ [0]_{4\times4} & [h_i] \end{bmatrix} \{X_i(L_i)\} = [H_{1i}]\{X_i(L_i)\} \tag{4.37}$$

where $[h_i]$ was defined in Eq. (3.46) and $[0]_{4\times4}$ is a 4×4 matrix of zeros. Now, one can use Eqs. (4.28)-(4.31), and relate the constants $\{X_{i+1}(0)\}$ and $\{X_i(0)\}$, that is,

$$\{X_{i+1}(0)\} = [H_{1i}] \Big[[D_i(L)] \quad [D_i'(L)] \quad \cdots \quad [F_i'(L)]\Big]^T \{X_i(0)\} = [H_i]\{X_i(0)\} \tag{4.38}$$

where $[H_i]$ is now a 8×8 matrix. With Eq. (4.38), the eigenvalue problem can be solved in a similar way as in the isotropic case. By applying the continuity conditions from segment 1 up to n, the following equation is obtained,

$$[A]\Big([H_{n-1}] \times [H_{n-2}] \times \cdots \times [H_2]\Big)[B]\{X\} = [G(\lambda)]\{X\} = 0 \tag{4.39}$$

which has the same form as Eq. (3.48), but now the matrices have double the size. The way to obtain the matrices $[A]$ and $[B]$ is similar to the isotropic case. Consider again the free-free boundary conditions, which, from the isotropic rotor shown in Eq. (3.49), can be written for the anisotropic case as,

$$\begin{cases} \eta'_{11}(0) = \eta'_{21}(0) = \eta'_{1n}(L_n) = \eta'_{2n}(L_n) = 0 \\ \kappa G A_1 \Big(\eta_{11}(0) - \phi_{11}(0)\Big) = \kappa G A_1 \Big(\eta_{21}(0) - \phi_{21}(0)\Big) = 0 \\ \kappa G A_n \Big(\eta_{1n}(L_n) - \phi_{1n}(L_n)\Big) = \kappa G A_n \Big(\eta_{2n}(L_n) - \phi_{2n}(L_n)\Big) = 0 \end{cases} \tag{4.40}$$

Using Eq. (4.38), the functions for segment n can be written as,

$$\phi_{1n}(\xi_n) = [C_n(\xi_n)]\{X_n(0)\} = [C_n(\xi_n)]\Big([H_{n-1}] \times [H_{n-2}] \times \cdots \times [H_1]\Big)\{X_1(0)\}$$

$$\eta_{1n}(\xi_n) = [D_n(\xi_n)]\{X_n(0)\} = [D_n(\xi_n)]\Big([H_{n-1}] \times [H_{n-2}] \times \cdots \times [H_1]\Big)\{X_1(0)\}$$

$$\phi_{2n}(\xi_n) = [E_n(\xi_n)]\{X_n(0)\} = [E_n(\xi_n)]\Big([H_{n-1}] \times [H_{n-2}] \times \cdots \times [H_1]\Big)\{X_1(0)\}$$

$$\eta_{2n}(\xi_n) = [F_n(\xi_n)]\{X_n(0)\} = [F_n(\xi_n)]\Big([H_{n-1}] \times [H_{n-2}] \times \cdots \times [H_1]\Big)\{X_1(0)\}$$

By applying the boundary conditions for segment n, one may have,

$$\begin{bmatrix} [D'_n(L_n)] \\ [D_n(L_n)] - [C'_n(L_n)] \\ [F'_n(L_n)] \\ [F_n(L_n)] - [E'_n(L_n)] \end{bmatrix} \Big([H_{n-1}] \times [H_{n-2}] \times \cdots \times [H_1]\Big)\{X_1(0)\} = 0$$

where the first matrix on the left-hand side correspond to $[A]$ when the boundary at $x = L$ is free. To apply the boundary condition at $x = 0$, the terms $[H_1]$ and $\{X_1(0)\}$ must be modified. Similar to the isotropic case, this can be done as,

$$[H_1]\{X_1(0)\} = [H_1] \begin{Bmatrix} \eta_{11}(0) \\ \eta'_{11}(0) \\ \phi_{11}(0) \\ \phi'_{11}(0) \\ \eta_{21}(0) \\ \eta'_{21}(0) \\ \phi_{21}(0) \\ \phi'_{21}(0) \end{Bmatrix} = [H_1] \begin{Bmatrix} \phi'_{11}(0) \\ 0 \\ \phi_{11}(0) \\ \phi'_{11}(0) \\ \phi'_{21}(0) \\ 0 \\ \phi_{21}(0) \\ \phi'_{21}(0) \end{Bmatrix} = [H_1] \begin{bmatrix} 0 & 1 & 0 & 0 \\ 0 & 0 & 0 & 0 \\ 1 & 0 & 0 & 0 \\ 0 & 1 & 0 & 0 \\ 0 & 0 & 0 & 1 \\ 0 & 0 & 0 & 0 \\ 0 & 0 & 1 & 0 \\ 0 & 0 & 0 & 1 \end{bmatrix} \begin{Bmatrix} \phi_{11}(0) \\ \phi'_{11}(0) \\ \phi_{21}(0) \\ \phi'_{21}(0) \end{Bmatrix} = [B]\{X\}$$

Substituting the above expression in the previous one, Equation (4.39) is obtained. From the steps above, the application of other boundary conditions is straightforward. Here, it is worth mentioning that the bearings and disks are encoded in the matrices $[C_i(\xi_i)]$,

$[D_i(\xi_i)]$, $[E_i(\xi_i)]$ and $[F_i(\xi_i)]$, for an arbitrary segment i. They can be placed anywhere along the segment, including at the boundaries $\xi_i = 0, L_i$, by setting the local coordinates a_i or b_i as such. Thus, if segment 1 or n has a disk or bearing, it can be placed at the boundary. This in effect changes the boundary conditions, and it is equivalent to imposing the disk and bearings in the matrices $[A]$ and $[B]$, while removing them from the matrices $[C_i(\xi_i)]$, $[D_i(\xi_i)]$, $[E_i(\xi_i)]$ and $[F_i(\xi_i)]$. Both approaches are equivalent and they both give the same outcome.

The characteristic equation is obtained from the determinant of the coefficient matrix $[G(\lambda)]$ in Equation (4.39), which must be zero for non-trivial solutions. The eigenvalues will have the form

$$\lambda_i^k = \sigma_i^k \pm j\omega_i^k \quad \text{for } i = 1, 2, ..., N;\ k = F, B \tag{4.41}$$

where ω_i^k are the damped natural frequencies, σ_i^k are the damping parameters and F and B denote the forward and backward modes, respectively. Due to the anisotropy of the bearings, the backward and forward modes will have a positive $+j\omega_i^k$ and negative $-j\omega_i^k$ component, with $k = F, B$. This is different from the isotropic case, where the use of the complex notation leads to forward modes having only positive frequency and backward modes only negative ones. The reason for that is because in the isotropic case the functions ϕ_{2i} and η_{2i} do not contribute to the response as explained by Lee and Jei (1988). In fact, when the bearings are isotropic, the equations to obtain ϕ_{2i} and η_{2i} becomes decoupled from the ones leading to ϕ_{1i} and η_{1i}. Thus only one of these must be solved.

After obtaining the eigenvalues, the constants $\{X\}$ for mode i can be obtained by substituting λ_i in Eq. (4.39). This gives the ratio between the modal constants of segment 1, leaving an arbitrary constant that is obtained from the orthogonality conditions (MEIROVITCH, 1975). Thus the amplitudes of the eigenfunctions are not defined, but solely their shape. In case damping is considered, not only the shape, but the phase of the eigenfunctions is also arbitrary (ADHIKARI et al., 2007; GARVEY et al., 1998). Moreover, the global mode shape of the system is obtained as a combination of the mode shapes of each segment. The global function will thus be a piece-wise continuous function, which can be written as,

$$\phi_1(x) = \begin{cases} \phi_{11}(x) & \text{for } x_1 < x < x_2 \\ \phi_{12}(x) & \text{for } x_2 < x < x_3 \\ \vdots & \\ \phi_{1n}(x) & \text{for } x_n < x < x_{n+1} \end{cases} \tag{4.42}$$

and the same form is true for $\phi_2(x)$, $\eta_1(x)$ and $\eta_2(x)$. Since the system is anisotropic, the mode shapes in the horizontal ϕ_y and vertical ϕ_z directions will be different, and they can

be obtained from (LEE; JEI, 1988),

$$\phi_y^k(x) = \phi_1^k(x) + \phi_2^k(x), \quad \phi_z^k(x) = j\big(\phi_1^k(x) - \phi_2^k(x)\big) \text{ for } k = F, B \tag{4.43}$$

and a similar form is true for $\eta_y(x)$ and $\eta_z(x)$, using $\eta_1(x)$ and $\eta_2(x)$.

4.3 Modal analysis

With the eigenfunctions at hand, the modal analysis method can be used to discretize the partial differential equations given by Eqs. (4.7) and (4.8). Due to the anisotropic bearings of the system, the complex conjugate of the differential equations need to be used for the application of the modal analysis. Moreover, the equations of motion and its complex conjugate can be written as,

$$[m]\begin{Bmatrix}\{\ddot{w}(x,t)\}\\ \{\ddot{w}^*(x,t)\}\end{Bmatrix} + [c]\begin{Bmatrix}\{\dot{w}(x,t)\}\\ \{\dot{w}^*(x,t)\}\end{Bmatrix} + [k]\begin{Bmatrix}\{w(x,t)\}\\ \{w^*(x,t)\}\end{Bmatrix} = \begin{Bmatrix}\{g(x,t)\}\\ \{g^*(x,t)\}\end{Bmatrix} \tag{4.44}$$

where,

$$[m] = \begin{bmatrix}\bar{m}(x) & 0 & 0 & 0\\ 0 & \bar{J}_d(x) & 0 & 0\\ 0 & 0 & \bar{m}(x) & 0\\ 0 & 0 & 0 & \bar{J}_d(x)\end{bmatrix} \tag{4.45}$$

$$[c] = \begin{bmatrix}[c_1] & [c_2]\\ [c_2^*] & [c_1^*]\end{bmatrix}, \quad [c_1] = \begin{bmatrix}\bar{c}_f(x) & 0\\ 0 & -j\Omega\bar{J}_p(x) - \bar{c}_t(x)\end{bmatrix}, \quad [c_2] = \begin{bmatrix}\bar{c}_b(x) & 0\\ 0 & 0\end{bmatrix} \tag{4.46}$$

$$[k] = \begin{bmatrix}[k_1] & [k_2]\\ [k_2^*] & [k_1^*]\end{bmatrix}, \quad [k_1] = \begin{bmatrix}-\frac{\partial}{\partial x}\left(\kappa G\bar{A}(x)\frac{\partial}{\partial x}\right) + \bar{k}_f(x) & \frac{\partial}{\partial x}\left(\kappa G\bar{A}(x)\right)\\ -\kappa G\bar{A}(x)\frac{\partial}{\partial x} & -\frac{\partial}{\partial x}\left(E\bar{I}(x)\frac{\partial}{\partial x}\right) + \kappa G\bar{A}(x) - \bar{k}_t(x)\end{bmatrix}$$

$$[k_2] = \begin{bmatrix}\bar{k}_b(x) & 0\\ 0 & 0\end{bmatrix} \tag{4.47}$$

being $\{w(x,t)\}$ and $\{g(x,t)\}$ defined in Eqs. (3.55) and (3.56), respectively. Here one can clearly see that the equations of motion for $\{w(x,t)\}$ and $\{w^*(x,t)\}$ get coupled due to the bearing coefficients $\bar{c}_b(x)$ and $\bar{k}_b(x)$; and, therefore, they must be solved simultaneously. In the isotropic case, one only needs to solve one of them, since the equations are decoupled. Next, Equation (4.44) is written in the state space form, which gives,

$$[M]\{\dot{W}(x,t)\} = [K]\{W(x,t)\} + \{F(x,t)\} \tag{4.48}$$

where,

$$\{W(x,t)\} = \Big\{\{\dot{w}(x,t)\}\ \{\dot{w}^*(x,t)\}\ \{w(x,t)\}\ \{w^*(x,t)\}\Big\}^T \tag{4.49}$$

$$\{F(x,t)\} = \Big\{0 \;\; 0 \;\; 0 \;\; 0 \;\; \{g(x,t)\} \;\; \{g^*(x,t)\}\Big\}^T \tag{4.50}$$

and the matrices $[M]$ and $[K]$ have the same form as shown in Eqs. (3.60) and (3.61), but with the matrices $[m]$, $[c]$ and $[k]$ given above. In the same way shown for the isotropic case, one can show that the operator matrices $[M]$ and $[K]$ are positive-definite, and the former is non-self-adjoint and the latter self-adjoint. This property arises due to the gyroscopic effect and the anisotropic bearings. In order to decouple the equations of non-self-adjoint systems, one also needs to solve the adjoint eigenvalue problem to obtain the adjoint eigenfunctions, since the eigenfunctions of the regular problem are not orthogonal. Similar to the isotropic case, the state vector is expanded as,

$$\{W(x,t)\} = \sum_{i=0}^{\infty} \{\Phi_i(x)\} q_i(t) \tag{4.51}$$

where the mode shapes are now given by,

$$\{\Phi_i(x)\} = \Big\{\lambda_i\phi_{1i}(x) \quad \lambda_i\eta_{1i}(x) \quad \lambda_i\phi_{2i}(x) \quad \lambda_i\eta_{2i}(x) \quad \phi_{1i}(x) \quad \eta_{1i}(x) \quad \phi_{2i}(x) \quad \eta_{2i}(x)\Big\}^T \tag{4.52}$$

The eigenvalue problem related to Eq. (4.48) and its adjoint are given as,

$$\lambda_i[M]\{\Phi_i(x)\} = [K]\{\Phi_i(x)\} \quad \text{for} \quad i = 1, 2, ... \tag{4.53}$$

$$\lambda_i^*[\tilde{M}]\{\tilde{\Phi}_i(x)\} = [\tilde{K}]\{\tilde{\Phi}_i(x)\} \quad \text{for} \quad i = 1, 2, ... \tag{4.54}$$

where one can prove that the eigenvalue problem shown in Eq. (4.53) is the same as the one given by Eqs. (4.15a)-(4.15d). Similar to the isotropic case, the adjoints of the operators are $[\tilde{M}] = [M]^H$ and $[\tilde{K}] = [K]^H$, being H the complex conjugate transpose, also known as hermitian transpose. The adjoint mode shapes are now given as,

$$\{\tilde{\Phi}_i(x)\} = \Big\{\lambda_i^*\tilde{\phi}_{1i}(x) \quad \lambda_i^*\tilde{\eta}_{1i}(x) \quad \lambda_i^*\tilde{\phi}_{2i}(x) \quad \lambda_i^*\tilde{\eta}_{2i}(x) \quad \tilde{\phi}_{1i}(x) \quad \tilde{\eta}_{1i}(x) \quad \tilde{\phi}_{2i}(x) \quad \tilde{\eta}_{2i}(x)\Big\}^T \tag{4.55}$$

where $\tilde{\phi}_{1i}(x)$ is the adjoint of $\phi_{1i}(x)$, $\tilde{\eta}_{1i}(x)$ is the adjoint of $\eta_{1i}(x)$, and so on. Recall that the vectors $\{\Phi_i(x)\}$ and $\{\tilde{\Phi}_j(x)\}$ are biorthogonal and satisfy the conditions shown in Eqs. (3.70a) and (3.70b). After substituting $\{W(x,t)\}$ given by (4.51) in the state-space equation of motion, Equation (4.48), taking the internal product in both sides by $\{\tilde{\Phi}_i(x)\}$, and taking into account the orthogonality conditions, one may have,

$$\dot{q}_i(t) = \lambda_i q_i(t) + \int_0^L \tilde{\phi}_{1i}^*(x) f(x,t) dx + \int_0^L \tilde{\phi}_{2i}^*(x) f^*(x,t) dx \quad \text{for} \quad i = 1, 2, ... \tag{4.56}$$

Equation (4.56) consist of infinite first order complex modal equations, which are in reality truncated at N modes. In this case, each mode has a forward and backward case with

positive and negative frequency, each with a unique equation. Hence, for $4N$ modes, there is N forward modes with positive natural frequency $+j\omega_i^F$, N forward modes with negative natural frequency $-j\omega_i^F$, N backward modes with positive natural frequency $+j\omega_i^B$ and N backward modes with negative natural frequency $-j\omega_i^B$, where $i = 1, 2, ...N$. In every case one has $|\omega_i^F| > |\omega_i^B|$, which can be used to distinguish between forward and backward frequencies for mode i. The physical displacement and slopes are obtained from Eq. (4.51), which gives,

$$u(x,t) = \sum_{i=0}^{\infty} \phi_{1i}(x) q_i(t) \tag{4.57}$$

$$\psi(x,t) = \sum_{i=0}^{\infty} \eta_{1i}(x) q_i(t) \tag{4.58}$$

and the horizontal and vertical components are simply the real and imaginary parts of $u(x,t)$ and $\psi(x,t)$, respectively.

Here one can note that for anisotropic rotors, the complex conjugate of the external force also needs to be taken into account. For a synchronous unbalance excitation, which is the most common external source of excitation in rotors, Equation (4.56) shows that an excitation rotating in the opposite direction also affects the response, and thus it excites the backward modes. This is a well known result of rotors on anisotropic bearings, and leads the response to have backward critical speeds. As mentioned earlier, for isotropic bearings the functions $\phi_2(x)$ and $\eta_2(x)$ do not affect the result, and thus the term containing $f^*(x,t)$ vanish in Eq. (4.56); thus leading to the isotropic equation given by Eq. (3.71).

The vectors $\{\Phi_i(x)\}$ and $\{\tilde{\Phi}_i^*(x)\}$ are the result of the same eigenvalue problem, and thus they are the same within a constant; therefore, one can write (LEE, 1993),

$$\{\Phi_i(x)\} = \frac{1}{K_i}\{\tilde{\Phi}_i^*(x)\} \tag{4.59}$$

where again K_i is a complex normalizing constant and it is obtained from Eqs. (3.70a) or (3.70b). These equations will not be expanded here due to their length, but one gets a similar form as shown in the isotropic case by Eqs (3.75) and (3.76), with additional terms due the the ansiotropic bearings.

The response due to initial conditions can be obtained by multiplying Equation (4.51) by $[M]$ and taking the internal product with $\{\tilde{\Phi}_j(x)\}$ in both sides, which leads to,

$$q_i(0) = \langle\, [M]\{W(x,0)\}, \{\tilde{\Phi}_i(x)\}\,\rangle \tag{4.60}$$

where the orthogonality property (3.70a) was used.

The modal analysis presented here is more suitable for rotor systems than the

cartesian or physical approach, since the interpretation of the responses as rotating complex vectors can be applied. The solution of Equation (4.56) for each mode i will be a combination of two co- and counter-rotating complex vectors representing the forward and backward modes. In addition, the present approach does not limit the bearings to be orthotropic (where the cross-coupled bearing coefficients are the same, i.e. $k_{yz} = k_{zy}$) as the approach presented by Lee and Jei (1988), since the bearing coefficients, which are encoded in the functions $\bar{k}_f(x)$, $\bar{k}_b(x)$, $\bar{c}_f(x)$ and $\bar{c}_b(x)$, can be arbitrary. This allows the modeling of oil-film bearings, which are one of the most common bearings used in rotating machines and have generally different direct and cross-coupled coefficients.

This chapter presented the CSM applied to rotors on anisotropic bearings. The form of the bearings can be very general, and the approach is not limited to orthotropic cases. With the modal analysis, the response of a multi-stepped anisotropic rotor is possible in close form, depending on the external force $f(x,t)$ considered. The next step is shown in Chapter 5, and deals with rotors with asymmetric shafts and disks.

5 Modeling of asymmetric rotor systems

In the last two chapters, the CSM was established for isotropic and anisotropic rotors systems. In both cases, the shaft was considered axisymmetric, that is, it has the same moment of inertia in the two orthogonal axes. This chapter present the CSM for asymmetric shafts on isotropic bearings. Some examples of such shafts are the rotors of generators in steam power plants (Figure 5). This rotors have slots machined along their longitudinal length, to place the electrical windings. The machined slots alters the distribution of mass along the cross section, breaking the cylindrical symmetry of the shaft.

Due to rotation, the different properties in the orthogonal axes of asymmetric rotors generate a parametrically excited system, with coefficients dependent on time (KANG et al., 1992). Such systems cannot be solved by means of separation of variables as in previous chapters. However, the time-dependent coefficients can be transformed in constant coefficients if the equations of motion are written in the frame of reference rotating with the shaft, rather than the stationary inertial one. If one considers the bearings isotropic, the separation of variables is applicable, and the eigenfunctions can be used to discretize the system by means of modal analysis. For asymmetric shafts on anisotropic bearings one cannot apply separation of variables, and the solution of the equations are only possible by means of Floquet theory or similar approaches (GENTA, 2007).

The procedure for asymmetric rotors is similar in many ways to the method shown in Chapter 4. The main difference is that now the anisotropy is distributed along the shaft instead of located only at the bearings. Similar to the the rotor on anisotropic bearings, the asymmetric rotor also posses backward critical speeds, since the direction of the displacement is not collinear to the applied force, and a synchronous rotating force excites the backward modes. The phase of the synchronous force also has great impact in the response of the system. At a rotating speed between the backward and forward critical speed, asymmetric rotors have unstable regions where the displacements become very large. In addition to the instabilities unique to asymmetric rotors, these systems also present resonances at half the major critical speed caused by the action of gravity on the rotating asymmetric shaft (ISHIDA; YAMAMOTO, 2012).

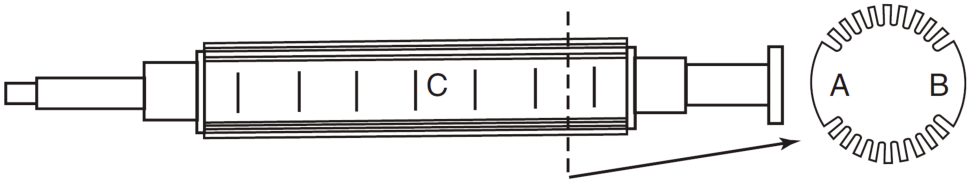

Figure 5: Two-pole generator rotor adapted from (ISHIDA; YAMAMOTO, 2012).

This chapter follows the same structure as the previous ones: the equations of motion are obtained in Section 5.1, where the asymmetry is introduced. The procedure followed to obtain the eigenfunctions is outlined in Section 5.2, while Section 5.3 shows the modal analysis method applied to the asymmetric rotor.

5.1 Equations of motion

The asymmetric rotor system is still divided as the depiction shown in Fig. 2, with the division of n segments with length L_i and constant cross-section area A_i. The difference now is that each segment has distinct area moments of inertia in the two orthogonal directions, which are denoted as I_{zi} and I_{yi}, with $I_{zi} > I_{yi}$. These orthogonal directions are considered to be the principal axes of the cross section, so that the products of inertia are null. The disks are also considered asymmetric, with transverse moments of inertia J_y^k and J_z^k, and polar moment of inertia J_p^k, for $k = 1, 2, ..., P$. The principal axes of the disks are considered to be aligned to that of the shaft.

Due to the rotation of the rotor, the asymmetry of the inertia becomes time-dependent in the stationary frame of reference, which was the frame used to developed the equations of motion in the previous chapters. On the other hand, if the equations are written in the rotating frame, the inertia becomes constant and the boundary-value problem solvable. Hence, the coordinate system used to describe the motion, namely z_1 and y_1, rotates at a velocity Ω, and are aligned to the principal axes of the cross-section (Figure 6). The relation between the displacements and bending angles in the stationary and rotating references are given as,

$$\begin{Bmatrix} u_y \\ u_z \end{Bmatrix} = \begin{bmatrix} \cos\Omega t & -\sin\Omega t \\ \sin\Omega t & \cos\Omega t \end{bmatrix} \begin{Bmatrix} u_{y_1} \\ u_{z_1} \end{Bmatrix}, \quad \begin{Bmatrix} \psi_y \\ \psi_z \end{Bmatrix} = \begin{bmatrix} \cos\Omega t & -\sin\Omega t \\ \sin\Omega t & \cos\Omega t \end{bmatrix} \begin{Bmatrix} \psi_{y_1} \\ \psi_{z_1} \end{Bmatrix} \tag{5.1}$$

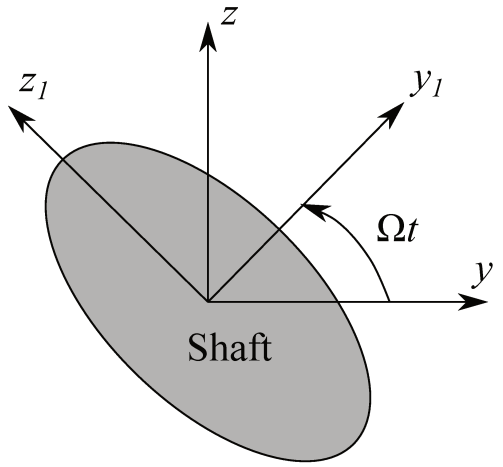

Figure 6: Asymmetric rotor coordinates

where $u_{y_1} = u_{y_1}(x,t)$, $u_{z_1} = u_{z_1}(x,t)$, $\psi_{y_1} = \psi_{y_1}(x,t)$ and $\psi_{z_1} = \psi_{z_1}(x,t)$ are the displacements and bending angles in the rotating coordinate system $y_1 z_1$. To obtain the equations of motion in the rotating frame, the EHP presented in Eq. (3.1) can be used, with the terms written in the rotating frame. The kinetic energy can be written in the rotating frame as (RAFFA; VATTA, 2001; KANG et al., 1992),

$$\begin{aligned} T = \frac{1}{2}\int_0^L \bar{m}(x)\left[\left(\frac{\partial u_{y_1}}{\partial t} - \Omega u_{z_1}\right)^2 + \left(\frac{\partial u_{z_1}}{\partial t} + \Omega u_{y_1}\right)^2\right] dx \\ + \frac{1}{2}\int_0^L \bar{J}_1(x)\left[\left(\frac{\partial \psi_{y_1}}{\partial t} - \Omega \psi_{z_1}\right)^2 + \left(\frac{\partial \psi_{z_1}}{\partial t} + \Omega \psi_{y_1}\right)^2\right] dx + \frac{1}{2}\int_0^L \bar{J}_p(x)\Omega^2 dx \\ + \frac{1}{2}\int_0^L \bar{J}_2(x)\left[\left(\frac{\partial \psi_{y_1}}{\partial t} - \Omega \psi_{z_1}\right)^2 - \left(\frac{\partial \psi_{z_1}}{\partial t} + \Omega \psi_{y_1}\right)^2\right] dx \\ + \int_0^L \bar{J}_p(x)\Omega\left[\frac{\partial \psi_{z_1}}{\partial t}\psi_{y_1} - \psi_{z_1}\frac{\partial \psi_{y_1}}{\partial t} - \Omega(\psi_{z_1}^2 + \psi_{y_1}^2)\right] dx \end{aligned} \tag{5.2}$$

where $\bar{m}(x)$ is the mass per unit length, $\bar{J}_1(x) = 1/2(\bar{J}_y(x) + \bar{J}_z(x))$ is the mean moment of inertia, $\bar{J}_2(x) = 1/2(\bar{J}_z(x) - \bar{J}_y(x))$ the deviatoric moment of inertia and $\bar{J}_p(x) = \bar{J}_y(x) + \bar{J}_z(x)$ the polar moment of inertia; all of these properties are given per unit length. As before, the disks are encoded in these distributed properties, as shown in Eq. (5.12). The potential energy of the shaft is given as,

$$\begin{aligned} V_s = \frac{1}{2}\int_0^L E\left[\bar{I}_y(x)\left(\frac{\partial \psi_{y_1}}{\partial x}\right)^2 + \bar{I}_z(x)\left(\frac{\partial \psi_{z_1}}{\partial x}\right)^2\right] dx + \frac{1}{2}\int_0^L \kappa G\bar{A}(x)\left(\frac{\partial u_{y_1}}{\partial x} - \psi_{z_1}\right)^2 dx \\ + \frac{1}{2}\int_0^L \kappa G\bar{A}(x)\left(\frac{\partial u_{z_1}}{\partial x} + \psi_{y_1}\right)^2 dx \end{aligned} \tag{5.3}$$

and the contribution of the bearings in the potential energy can be obtained from Eq. (3.4) and (5.1), which gives,

$$V_b = \frac{1}{2}\int_0^L \left(\bar{k}_m(x)u_{y_1}^2 + \bar{k}_m(x)u_{z_1}^2 + \bar{k}_t(x)\psi_{y_1}^2 + \bar{k}_t(x)\psi_{z_1}^2\right) dx \tag{5.4}$$

The total potential energy is $V = V_s + V_b$. The bearing coefficients are the same as shown in Eq. (3.16). The work of the non-conservative forces in the rotating frame is,

$$\begin{aligned} W_{nc} = \frac{1}{2}\int_0^L \left[\bar{c}_m\left(\frac{\partial u_{y_1}}{\partial t} - \Omega u_{z_1}\right)^2 + \bar{c}_m\left(\frac{\partial u_{z_1}}{\partial t} + \Omega u_{y_1}\right)^2\right] dx \\ + \frac{1}{2}\int_0^L \left[\bar{c}_t\left(\frac{\partial \psi_{y_1}}{\partial t} + \Omega \psi_{z_1}\right)^2 + \bar{c}_t\left(\frac{\partial \psi_{z_1}}{\partial t} - \Omega \psi_{y_1}\right)^2\right] dx \\ + \int_0^L \left(f_{y_1}u_{y_1} + f_{z_1}u_{z_1}\right) dx \end{aligned} \tag{5.5}$$

where f_{y_1} and f_{z_1} are the components of the distributed force in the rotating frame. The equations of motion can be obtained by substituting Eqs. (5.2)-(5.5) into the EHP, leading to,

$$\bar{m}(x)\frac{\partial^2 u_{y_1}}{\partial t^2} + 2\Omega\bar{m}(x)\frac{\partial u_{z_1}}{\partial t} - \bar{m}(x)\Omega^2 u_{y_1} + \frac{\partial}{\partial x}\left[\kappa G\bar{A}(x)\left(\psi_{z_1} - \frac{\partial u_{y_1}}{\partial x}\right)\right] + \Big(\bar{k}_m(x) + \Omega\bar{c}_m(x)\Big)u_{y_1} + \bar{c}_m(x)\frac{\partial u_{y_1}}{\partial t} = f_{y_1}(x,t) \tag{5.6}$$

$$\bar{m}(x)\frac{\partial^2 u_{z_1}}{\partial t^2} - 2\Omega\bar{m}(x)\frac{\partial u_{y_1}}{\partial t} - \bar{m}(x)\Omega^2 u_{z_1} - \frac{\partial}{\partial x}\left[\kappa G\bar{A}(x)\left(\psi_{y_1} + \frac{\partial u_{z_1}}{\partial x}\right)\right] + \Big(\bar{k}_m(x) - \Omega\bar{c}_m(x)\Big)u_{z_1} - \bar{c}_m(x)\frac{\partial u_{z_1}}{\partial t} = f_{z_1}(x,t) \tag{5.7}$$

$$\bar{J}_y(x)\frac{\partial^2 \psi_{y_1}}{\partial t^2} + \bar{J}_y(x)\Omega^2\psi_{y_1} - \frac{\partial}{\partial x}\left[E\bar{I}_y(x)\frac{\partial \psi_{y_1}}{\partial x}\right] + \kappa G\bar{A}(x)\left[\psi_{y_1} + \frac{\partial u_{z_1}}{\partial x}\right] - \Big(\bar{k}_t(x) + \Omega\bar{c}_t(x)\Big)\psi_{y_1} - \bar{c}_t(x)\frac{\partial \psi_{y_1}}{\partial t} = 0 \tag{5.8}$$

$$\bar{J}_z(x)\frac{\partial^2 \psi_{z_1}}{\partial t^2} + \bar{J}_z(x)\Omega^2\psi_{z_1} - \frac{\partial}{\partial x}\left[E\bar{I}_z(x)\frac{\partial \psi_{z_1}}{\partial x}\right] + \kappa G\bar{A}(x)\left[\psi_{z_1} - \frac{\partial u_{y_1}}{\partial x}\right] - \Big(\bar{k}_t(x) - \Omega\bar{c}_t(x)\Big)\psi_{z_1} - \bar{c}_t(x)\frac{\partial \psi_{z_1}}{\partial t} = 0 \tag{5.9}$$

Note that the gyroscopic effect now couples the equations of the displacements instead of the bending angles. Equations (5.6)-(5.9) can be transformed in complex form using the relations given by Eqs. (3.10) and (3.11), which leads to,

$$\bar{m}(x)\frac{\partial^2 u}{\partial t^2} + 2j\Omega\bar{m}(x)\frac{\partial u}{\partial t} - \bar{m}(x)\Omega^2 u + \frac{\partial}{\partial x}\left[\kappa G\bar{A}(x)\left(\psi - \frac{\partial u}{\partial x}\right)\right] + \Big(\bar{k}_m(x) + j\Omega\bar{c}_m(x)\Big)u + \bar{c}_m(x)\frac{\partial u}{\partial t} = f(x,t) \tag{5.10}$$

$$\bar{J}_1(x)\frac{\partial^2 \psi}{\partial t^2} + \bar{J}_1(x)\Omega^2\psi - \frac{\partial}{\partial x}\left[E\bar{I}_1(x)\frac{\partial \psi}{\partial x}\right] + \bar{J}_2(x)\frac{\partial^2 \psi^*}{\partial t^2} - \frac{\partial}{\partial x}\left[E\bar{I}_2(x)\frac{\partial \psi^*}{\partial x}\right] + \kappa G\bar{A}(x)\left[\psi - \frac{\partial u}{\partial x}\right] - \Big(\bar{k}_t(x) + j\Omega\bar{c}_t(x)\Big)\psi - \bar{c}_t(x)\frac{\partial \psi}{\partial t} = 0 \tag{5.11}$$

where * is the complex conjugate, $\bar{I}_1(x) = 1/2(\bar{I}_y(x) + \bar{I}_z(x))$ is the mean area moments of inertia and $\bar{I}_2(x) = 1/2(\bar{I}_z(x) - \bar{I}_y(x))$ the deviatoric area moment of inertia. The

following functions are assumed for the distributed properties,

$$\bar{A}(x) = \sum_{i=1}^{n} A_i H_i(x), \quad \bar{I}_1(x) = \sum_{i=1}^{n} I_{1i} H_i(x), \quad \bar{I}_2(x) = \sum_{i=1}^{n} I_{2i} H_i(x)$$

$$\bar{m}(x) = \sum_{i=1}^{n} \rho A_i H_i(x) + \sum_{j=1}^{P} M^j \delta_d(x - x_a^j), \quad \bar{J}_1(x) = \sum_{i=1}^{n} \rho I_{1i} H_i(x) + \sum_{j=1}^{P} J_1^j \delta_d(x - x_a^j)$$

$$\bar{J}_2(x) = \sum_{i=1}^{n} \rho I_{2i} H_i(x) + \sum_{j=1}^{P} J_2^j \delta_d(x - x_a^j) \tag{5.12}$$

being $J_1^j = 1/2(J_z^j + J_y^j)$ and $J_2^j = 1/2(J_z^j - J_y^j)$; δ_d the Dirac's delta function and x_a^j the coordinates of the disks. The function $H_i(x)$ is shown in Eq. (3.15). The boundary conditions can be stated in complex form as,

$$\left[\left(E\bar{I}_1(x) \frac{\partial \psi(x,t)}{\partial x} + E\bar{I}_2(x) \frac{\partial \psi^*(x,t)}{\partial x} \right) \delta\psi(x,t) \right]_{x=0,L} = 0 \tag{5.13}$$

$$\left[\kappa G \bar{A}(x) \left(\psi(x,t) - \frac{\partial u(x,t)}{\partial x} \right) \delta u(x,t) \right]_{x=0,L} = 0 \tag{5.14}$$

Equations (5.10), (5.11), (5.13) and (5.14) denote the boundary-value problem of the asymmetric rotor system. This problem can be solved in a similar way as shown in the isotropic and anisotropic rotor. First, one needs to find the eigenfunctions through separation of variables, which is done in Section 5.2, then the modal analysis is applied to obtain the responses, as shown in Section 5.3.

5.2 Eigenfunctions and eigenvalues

The free vibration of the asymmetric rotor can be obtained as,

$$\bar{m}(x) \frac{\partial^2 u}{\partial t^2} + 2j\Omega \bar{m}(x) \frac{\partial u}{\partial t} - \bar{m}(x)\Omega^2 u + \frac{\partial}{\partial x} \left[\kappa G \bar{A}(x) \left(\psi - \frac{\partial u}{\partial x} \right) \right] + \left(\bar{k}_m(x) + j\Omega \bar{c}_m(x) \right) u + \bar{c}_m(x) \frac{\partial u}{\partial t} = 0 \tag{5.15}$$

$$\bar{J}_1(x) \frac{\partial^2 \psi}{\partial t^2} + \bar{J}_1(x)\Omega^2 \psi - \frac{\partial}{\partial x} \left[E\bar{I}_1(x) \frac{\partial \psi}{\partial x} \right] + \bar{J}_2(x) \frac{\partial^2 \psi^*}{\partial t^2} - \frac{\partial}{\partial x} \left[E\bar{I}_2(x) \frac{\partial \psi^*}{\partial x} \right] + \kappa G \bar{A}(x) \left[\psi - \frac{\partial u}{\partial x} \right] - \left(\bar{k}_t(x) + j\Omega \bar{c}_t(x) \right) \psi - \bar{c}_t(x) \frac{\partial \psi}{\partial t} = 0 \tag{5.16}$$

Similar to the anisotropic rotor, the solutions are assumed as,

$$u(x,t) = \phi_1(x) e^{\lambda t} + \phi_2^*(x) e^{\lambda^* t} \tag{5.17a}$$

$$\psi(x,t) = \eta_1(x)e^{\lambda t} + \eta_2^*(x)e^{\lambda^* t} \tag{5.17b}$$

Upon substituting these solutions in the free equations of motion, and gathering the terms containing $e^{\lambda t}$ and $e^{\lambda^* t}$, one may have,

$$\bar{m}(x)\Big(\lambda^2 - \Omega^2 + 2j\Omega\lambda\Big)\phi_1(x) + \frac{d}{dx}\left[\kappa G\bar{A}(x)\left(\eta_1(x) - \frac{d\phi_1(x)}{dx}\right)\right] + \left[\bar{k}_m(x) + (\lambda + j\Omega)\bar{c}_m(x)\right]\phi_1(x) = 0 \tag{5.18a}$$

$$\bar{m}(x)\Big(\lambda^2 - \Omega^2 - 2j\Omega\lambda\Big)\phi_2(x) + \frac{d}{dx}\left[\kappa G\bar{A}(x)\left(\eta_2(x) - \frac{d\phi_2(x)}{dx}\right)\right] + \left[\bar{k}_m(x) + (\lambda - j\Omega)\bar{c}_m(x)\right]\phi_2(x) = 0 \tag{5.18b}$$

$$\bar{J}_1(x)\left(\lambda^2 + \Omega^2\right)\eta_1(x) - \frac{d}{dx}\left[E\bar{I}_1(x)\frac{d\eta_1(x)}{dx}\right] + \kappa G\bar{A}(x)\left(\eta_1(x) - \frac{d\phi_1(x)}{dx}\right) + \bar{J}_2(x)\left(\lambda^2 + \Omega^2\right)\eta_2(x) - \frac{d}{dx}\left[E\bar{I}_2(x)\frac{d\eta_2(x)}{dx}\right] - \left[\bar{k}_t(x) + (\lambda + j\Omega)\bar{c}_t(x)\right]\eta_1(x) = 0 \tag{5.18c}$$

$$\bar{J}_2(x)\left(\lambda^2 + \Omega^2\right)\eta_2(x) - \frac{d}{dx}\left[E\bar{I}_2(x)\frac{d\eta_2(x)}{dx}\right] + \kappa G\bar{A}(x)\left(\eta_2(x) - \frac{d\phi_2(x)}{dx}\right) + \bar{J}_1(x)\left(\lambda^2 + \Omega^2\right)\eta_1(x) - \frac{d}{dx}\left[E\bar{I}_1(x)\frac{d\eta_1(x)}{dx}\right] - \left[\bar{k}_t(x) + (\lambda - j\Omega)\bar{c}_t(x)\right]\eta_2(x) = 0 \tag{5.18d}$$

The above equations are not complex conjugate due to the deviatoric moments of inertia. Also, similar to the anisotropic rotor, the rotation is at the specified direction for the functions ϕ_1 and η_1, and at the opposite direction for ϕ_2 and η_2. Therefore, one should expect the mode shapes to be non-planar and the orbits non-circular.

As the reader is familiarized by now, the eigenfunctions are obtained by solving the eigenvalue problem for each segment of constant cross-section individually. Then the global eigenfunctions are obtained as a combination of those, as illustrated in Fig. 3. Consider an arbitrary segment i located at $x_i < x < x_{i+1}$ with eigenfunctions $\phi_{1i}(\xi_i)$, $\phi_{2i}(\xi_i)$, $\eta_{1i}(\xi_i)$ and $\eta_{2i}(\xi_i)$, being $\xi_i \in [0,\ L_i]$ the local coordinate of the segment. The segment is considered to have a lth bearing and a kth rigid disk. The local eigenvalue problem can be obtained as,

$$\Big(\rho A_i + M^k\delta_d(\xi_i - a_k)\Big)\Big(\lambda + j\Omega\Big)^2\phi_{1i}(\xi_i) + \kappa G A_i\Big(\eta_{1i}'(\xi_i) - \phi_{1i}''(\xi_i)\Big) + \left[k_m^l + (\lambda + j\Omega)c_m^l\right]\phi_{1i}(\xi_i)\delta_d(\xi_i - b_l) = 0 \tag{5.19a}$$

$$\Big(\rho A_i + M^k\delta_d(\xi_i - a_k)\Big)\Big(\lambda - j\Omega\Big)^2\phi_{2i}(\xi_i) + \kappa G A_i\Big(\eta_{2i}'(\xi_i) - \phi_{2i}''(\xi_i)\Big) + \left[k_m^l + (\lambda - j\Omega)c_m^l\right]\phi_{2i}(\xi_i)\delta_d(\xi_i - b_l) = 0 \tag{5.19b}$$

$$\Big(\rho I_{1i} + J_1^k \delta_d(\xi_i - a_k)\Big)\left(\lambda^2 + \Omega^2\right)\eta_{1i}(\xi_i) - EI_{1i}\eta_{1i}''(\xi_i) + \kappa GA_i\Big(\eta_{1i}(\xi_i) - \phi_{1i}'(\xi_i)\Big)$$
$$\Big(\rho I_{2i} + J_2^k \delta_d(\xi_i - a_k)\Big)\left(\lambda^2 + \Omega^2\right)\eta_{2i}(\xi_i) - EI_{2i}\eta_{2i}''(\xi_i) - \left[k_t^l + (\lambda + j\Omega)c_t^l\right]\eta_{1i}(\xi_i)\delta_d(\xi_i - b_l) = 0 \tag{5.19c}$$

$$\Big(\rho I_{2i} + J_2^k \delta_d(\xi_i - a_k)\Big)\left(\lambda^2 + \Omega^2\right)\eta_{2i}(\xi_i) - EI_{2i}\eta_{2i}''(\xi_i) + \kappa GA_i\Big(\eta_{2i}(\xi_i) - \phi_{2i}'(\xi_i)\Big)$$
$$\Big(\rho I_{1i} + J_1^k \delta_d(\xi_i - a_k)\Big)\left(\lambda^2 + \Omega^2\right)\eta_{1i}(\xi_i) - EI_{1i}\eta_{1i}''(\xi_i) - \left[k_t^l + (\lambda - j\Omega)c_t^l\right]\eta_{2i}(\xi_i)\delta_d(\xi_i - b_l) = 0 \tag{5.19d}$$

Just as in the previous chapters, the local eigenvalue problem above can be solved by means of the Laplace transform, which gives,

$$\begin{aligned}(\lambda + j\Omega)^2 \rho A_i \hat{\phi}_{1i}(s) + \kappa GA_i\Big[s\hat{\eta}_{1i}(s) - \eta_{1i}(0)\Big] - \kappa GA_i\left[s^2\hat{\phi}_{1i}(s) - \phi_{1i}'(0) - s\phi_{1i}(0)\right] \\ + (\lambda + j\Omega)^2 M^k \phi_{1i}(a_k)e^{-sa_k} + \left(k_m^l + (\lambda + j\Omega)c_m^l\right)\phi_{1i}(b_l)e^{-sb_l} = 0\end{aligned} \tag{5.20a}$$

$$\begin{aligned}(\lambda - j\Omega)^2 \rho A_i \hat{\phi}_{2i}(s) + \kappa GA_i\Big[s\hat{\eta}_{2i}(s) - \eta_{2i}(0)\Big] - \kappa GA_i\left[s^2\hat{\phi}_{2i}(s) - \phi_{2i}'(0) - s\phi_{2i}(0)\right] \\ + (\lambda - j\Omega)^2 M^k \phi_{2i}(a_k)e^{-sa_k} + \left(k_m^l + (\lambda - j\Omega)c_m^l\right)\phi_{2i}(b_l)e^{-sb_l} = 0\end{aligned} \tag{5.20b}$$

$$\begin{aligned}\left(\lambda^2 + \Omega^2\right)\rho I_{1i}\hat{\eta}_{1i}(s) - EI_{2i}\left[s^2\hat{\eta}_{1i}(s) - \eta_{1i}'(0) - s\eta_{1i}(0)\right] - \kappa GA_i\left[s\hat{\phi}_{1i}(s) - \phi_{1i}(0)\right] \\ +\kappa GA_i\hat{\eta}_{1i}(s) + \left(\lambda^2 + \Omega^2\right)\rho I_{2i}\hat{\eta}_{2i}(s) - EI_{1i}\left[s^2\hat{\eta}_{2i}(s) - \eta_{2i}'(0) - s\eta_{2i}(0)\right] \\ + \left(J_1^k\eta_{1i}(a_k) + J_2^k\eta_{2i}(a_k)\right)\left(\lambda^2 + \Omega^2\right)e^{-sa_k} + \left(k_t^l + (\lambda + j\Omega)c_t^l\right)\eta_{1i}(b_l)e^{-sb_l} = 0\end{aligned} \tag{5.20c}$$

$$\begin{aligned}\left(\lambda^2 + \Omega^2\right)\rho I_{2i}\hat{\eta}_{2i}(s) - EI_{2i}\left[s^2\hat{\eta}_{2i}(s) - \eta_{2i}'(0) - s\eta_{2i}(0)\right] - \kappa GA_i\left[s\hat{\phi}_{2i}(s) - \phi_{2i}(0)\right] \\ +\kappa GA_i\hat{\eta}_{2i}(s) + \left(\lambda^2 + \Omega^2\right)\rho I_{1i}\hat{\eta}_{1i}(s) - EI_{1i}\left[s^2\hat{\eta}_{1i}(s) - \eta_{1i}'(0) - s\eta_{1i}(0)\right] \\ + \left(J_1^k\eta_{1i}(a_k) + J_2^k\eta_{2i}(a_k)\right)\left(\lambda^2 + \Omega^2\right)e^{-sa_k} + \left(k_t^l + (\lambda - j\Omega)c_t^l\right)\eta_{2i}(b_l)e^{-sb_l} = 0\end{aligned} \tag{5.20d}$$

where $\hat{\phi}_{1i}(s)$, $\hat{\phi}_{2i}(s)$, $\hat{\eta}_{1i}(s)$ and $\hat{\eta}_{2i}(s)$ are the Laplace transform of $\phi_{1i}(\xi_i)$, $\phi_{2i}(\xi_i)$, $\eta_{1i}(\xi_i)$ and $\eta_{2i}(\xi_i)$, respectively. The above equations can be written in matrix form as,

$$[L]\{\hat{\Phi}(s)\} = \{b\} \tag{5.21}$$

where the terms are now given as,

$$[L] = \begin{bmatrix}[L_1] & [L_3] \\ [L_3] & [L_2]\end{bmatrix}, \quad [L_1] = \begin{bmatrix}\rho A_i(\lambda + j\Omega)^2 - \kappa GA_i s^2 & \kappa GA_i s \\ -\kappa GA_i s & \rho I_{1i}\left(\lambda^2 + \Omega^2\right) - EI_{1i}s^2 + \kappa GA_i\end{bmatrix},$$

$$[L_2] = \begin{bmatrix}\rho A_i(\lambda - j\Omega)^2 - \kappa GA_i s^2 & \kappa GA_i s \\ -\kappa GA_i s & \rho I_{1i}\left(\lambda^2 + \Omega^2\right) - EI_{1i}s^2 + \kappa GA_i\end{bmatrix}$$

$$[L_3] = \begin{bmatrix} 0 & 0 \\ 0 & \rho I_{2i}\left(\lambda^2 + \Omega^2\right) - EI_{2i}s^2 \end{bmatrix} \tag{5.22}$$

$$\{\hat{\Phi}(s)\} = \left\{ \hat{\phi}_{1i}(s) \quad \hat{\eta}_{1i}(s) \quad \hat{\phi}_{2i}(s) \quad \hat{\eta}_{2i}(s) \right\}^T \tag{5.23}$$

The vector $\{b\}$ can be obtained from Eqs. (5.20) and its omitted here due to its excessive length. The procedure to obtain the functions in the space domain is now considerably more complicated than the previous cases. First, the matrix $[L]$ is now a full block matrix due the the deviatoric term I_{2i}. Then the solution of $\hat{\phi}_{1i}(s)$ and $\hat{\eta}_{1i}(s)$ are no longer decoupled with $\hat{\phi}_{2i}(s)$ and $\hat{\eta}_{2i}(s)$ as in the anisotropic case shown in Eq. (4.18). This means that one needs to find the determinant of $[L]$ in its full form, which leads to the following polynomial,

$$as^8 + bs^6 + cs^4 + ds^2 + e = 0 \tag{5.24}$$

where,

$$a = 1 - \gamma_i^2, \quad b = (a_1 + a_2)\left(1 - \gamma_i^2\right), \quad c = b_1 + b_2 + a_1a_2 - \gamma_i^2(b_3 + b_4 + a_1a_2)$$

$$d = a_1b_2 + a_2b_1 - \gamma_i^2(a_1b_4 + a_2b_3), \quad e = b_1b_2 - \gamma_i^2 b_3b_4 \tag{5.25}$$

with,

$$a_{1,2} = -\frac{\rho}{\kappa G}\left(\lambda \pm j\Omega\right)^2 - \frac{\rho}{E}\left(\lambda^2 + \Omega^2\right) \tag{5.26}$$

$$b_{1,2} = \left(\frac{\rho^2}{\kappa GE}\left(\lambda^2 + \Omega^2\right) + \frac{\rho A_i}{EI_{1i}}\right)\left(\lambda \pm j\Omega\right)^2, \quad b_{3,4} = \frac{\rho^2}{\kappa GE}\left(\lambda^2 + \Omega^2\right)\left(\lambda \pm j\Omega\right)^2 \tag{5.27}$$

being $\gamma_i = I_{2i}/I_{1i}$. The polynomial given by Eq. (5.24) is of fourth order on s^2. Although there is close form solutions for quartic polynomials (See Abramowitz et al. (1988) for example), their expressions are so complicated that it its advisable to solve them numerically. Similar to the anisotropic rotor, the polynomial of Eq. (5.24) will have two positive solutions, denoted δ_{1i}^2 and δ_{2i}^2, and two negative solutions, denoted $-\varepsilon_{1i}^2$ and $-\varepsilon_{2i}^2$. Therefore, one can write $det([L_1]) = (s^2 - \delta_{1i}^2)(s^2 + \varepsilon_{1i}^2)(s^2 - \delta_{2i}^2)(s^2 + \varepsilon_{2i}^2)$ and the application of the inverse Laplace becomes possible. After solving for $\hat{\phi}_{1i}(s)$, $\hat{\phi}_{2i}(s)$, $\hat{\eta}_{1i}(s)$ and $\hat{\eta}_{2i}(s)$ in Eq. (5.21), and applying the inverse Laplace transformation, one may have

$$\begin{aligned} \phi_{1i}(\xi_i) &= \eta_{1i}(0)f_1(\xi_i) + \eta'_{1i}(0)f_2(\xi_i) + \phi_{1i}(0)f_3(\xi_i) + \phi'_{1i}(0)f_4(\xi_i) \\ &+\eta_{2i}(0)f_5(\xi_i) + \eta'_{2i}(0)f_6(\xi_i) + \phi_{2i}(0)f_7(\xi_i) + \phi'_{2i}(0)f_8(\xi_i) \\ &+\left[p_{1f}^{b_l}(\xi_i)\phi_{1i}(b_l) + h_{1f}^{b_l}(\xi_i)\eta_{1i}(b_l) + p_{1b}^{b_l}(\xi_i)\phi_{2i}(b_l) + h_{1b}^{b_l}(\xi_i)\eta_{2i}(b_l)\right]H(x - b_l) \\ &+\left[p_{1f}^{a_k}(\xi_i)\phi_{1i}(a_k) + h_{1f}^{a_k}(\xi_i)\eta_{1i}(a_k) + p_{1b}^{a_k}(\xi_i)\phi_{2i}(a_k) + h_{1b}^{a_k}(\xi_i)\eta_{2i}(a_k)\right]H(x - a_k) \end{aligned} \tag{5.28}$$

$$\begin{aligned}\eta_{1i}(\xi_i) &= \eta_{1i}(0)g_1(\xi_i) + \eta'_{1i}(0)g_2(\xi_i) + \cdots + \phi'_{2i}(0)g_8(\xi_i) \\ &+\Big[p^{b_l}_{2f}(\xi_i)\phi_{1i}(b_l) + h^{b_l}_{2f}(\xi_i)\eta_{1i}(b_l) + p^{b_l}_{2b}(\xi_i)\phi_{2i}(b_l) + h^{b_l}_{2b}(\xi_i)\eta_{2i}(b_l)\Big]H(x-b_l) \\ &+\Big[p^{a_k}_{2f}(\xi_i)\phi_{1i}(a_k) + h^{a_k}_{2f}(\xi_i)\eta_{1i}(a_k) + p^{a_k}_{2b}(\xi_i)\phi_{2i}(a_k) + h^{a_k}_{2b}(\xi_i)\eta_{2i}(a_k)\Big]H(x-a_k)\end{aligned} \tag{5.29}$$

$$\begin{aligned}\phi_{2i}(\xi_i) &= \eta_{1i}(0)f_9(\xi_i) + \eta'_{1i}(0)f_{10}(\xi_i) + \cdots + \phi'_{2i}(0)f_{16}(\xi_i) \\ &+\Big[p^{b_l}_{3f}(\xi_i)\phi_{1i}(b_l) + h^{b_l}_{3f}(\xi_i)\eta_{1i}(b_l) + p^{b_l}_{3b}(\xi_i)\phi_{2i}(b_l) + h^{b_l}_{3b}(\xi_i)\eta_{2i}(b_l)\Big]H(x-b_l) \\ &+\Big[p^{a_k}_{3f}(\xi_i)\phi_{1i}(a_k) + h^{a_k}_{3f}(\xi_i)\eta_{1i}(a_k) + p^{a_k}_{3b}(\xi_i)\phi_{2i}(a_k) + h^{a_k}_{3b}(\xi_i)\eta_{2i}(a_k)\Big]H(x-a_k)\end{aligned} \tag{5.30}$$

$$\begin{aligned}\eta_{2i}(\xi_i) &= \eta_{1i}(0)g_9(\xi_i) + \eta'_{1i}(0)g_{10}(\xi_i) + \cdots + \phi'_{2i}(0)g_{16}(\xi_i) \\ &+\Big[p^{b_l}_{4f}(\xi_i)\phi_{1i}(b_l) + h^{b_l}_{4f}(\xi_i)\eta_{1i}(b_l) + p^{b_l}_{4b}(\xi_i)\phi_{2i}(b_l) + h^{b_l}_{4b}(\xi_i)\eta_{2i}(b_l)\Big]H(x-b_l) \\ &+\Big[p^{a_k}_{4f}(\xi_i)\phi_{1i}(a_k) + h^{a_k}_{4f}(\xi_i)\eta_{1i}(a_k) + p^{a_k}_{4b}(\xi_i)\phi_{2i}(a_k) + h^{a_k}_{4b}(\xi_i)\eta_{2i}(a_k)\Big]H(x-a_k)\end{aligned} \tag{5.31}$$

the functions f, g, p and h above are shown in Appendix C. The introduction of the asymmetry of the shaft require additional functions to describe the local mode shapes. However, similar to the anisotropic rotor, one only needs to obtain the functions f_1 through f_8 and g_1 through g_8, since f_9 through f_{16} and g_9 through g_{16} will have the exact same form, but with Ω interchanged with $-\Omega$ (see Appendix C for a better clarification).

The number of unknowns in Eqs. (5.28)-(5.31) is eight; the same as in the anisotropic case. The terms $\eta_{1i}(a_k)$, $\eta_{1i}(b_l)$, $\phi_{1i}(a_k)$, $\phi_{1i}(b_l)$, $\eta_{2i}(a_k)$, $\eta_{2i}(b_l)$, $\phi_{2i}(a_k)$ and $\phi_{2i}(b_l)$ can be obtained directly from Equations (5.28)-(5.31) by the continuity of the functions ϕ_{1i}, η_{1i}, ϕ_{2i} and η_{2i} at the coordinates $\xi_i = a_k$ and $\xi_i = b_l$. As explained in previous chapters, this means evaluating the functions at these points. After performing such evaluations, the standard form of the eigenfunctions for segment i will be,

$$\phi_{1i}(\xi_i) = [C_i(\xi)]\{X_i(0)\} \tag{5.32}$$

$$\eta_{1i}(\xi_i) = [D_i(\xi)]\{X_i(0)\} \tag{5.33}$$

$$\phi_{2i}(\xi_i) = [E_i(\xi)]\{X_i(0)\} \tag{5.34}$$

$$\eta_{2i}(\xi_i) = [F_i(\xi)]\{X_i(0)\} \tag{5.35}$$

being the terms above the same as defined in Eq. (4.32). The specific form of the functions C_{ji}, D_{ji}, E_{ji} and F_{ji} ($j = 1, 2, ..., 8$) depend if segment i has a disk or a bearing. For segment i with a kth disk, they have the general form,

$$\begin{cases} C_{ji}(\xi_i) = f_j(\xi_i) + \left[f_j(a_k)p^{a_k}_{1f}(\xi_i) + g_j(a_k)h^{a_k}_{1f}(\xi_i)\right]H(\xi_i - a_k) \\ \qquad + \left[f_{j+4}(a_k)p^{a_k}_{1b}(\xi_i) + g_{j+4}(a_k)h^{a_k}_{1b}(\xi_i)\right]H(\xi_i - a_k) \end{cases} \quad \text{for } j = 1, 2, 3, 4 \tag{5.36a}$$

$$\begin{cases} C_{ji}(\xi_i) = f_j(\xi_i) + \left[f_j(a_k)p^{a_k}_{1f}(\xi_i) + g_j(a_k)h^{a_k}_{1f}(\xi_i)\right]H(\xi_i - a_k) \\ \qquad + \left[f_{j-4}(a_k)p^{a_k}_{1b}(\xi_i) + g_{j-4}(a_k)h^{a_k}_{1b}(\xi_i)\right]H(\xi_i - a_k) \end{cases} \quad \text{for } j = 5, 6, 7, 8 \tag{5.36b}$$

$$\begin{cases} D_{ji}(\xi_i) = g_j(\xi_i) + \left[f_j(a_k)p_{2f}^{a_k}(\xi_i) + g_j(a_k)h_{2f}^{a_k}(\xi_i)\right] H(\xi_i - a_k) \\ \qquad + \left[f_{j+4}(a_k)p_{2b}^{a_k}(\xi_i) + g_{j+4}(a_k)h_{2b}^{a_k}(\xi_i)\right] H(\xi_i - a_k) \end{cases} \quad \text{for } j = 1,2,3,4 \tag{5.36c}$$

$$\begin{cases} D_{ji}(\xi_i) = g_j(\xi_i) + \left[f_j(a_k)p_{2f}^{a_k}(\xi_i) + g_j(a_k)h_{2f}^{a_k}(\xi_i)\right] H(\xi_i - a_k) \\ \qquad + \left[f_{j-4}(a_k)p_{2b}^{a_k}(\xi_i) + g_{j-4}(a_k)h_{2b}^{a_k}(\xi_i)\right] H(\xi_i - a_k) \end{cases} \quad \text{for } j = 5,6,7,8 \tag{5.36d}$$

$$\begin{cases} E_{ij}(\xi_i) = C^{-}_{ij+4}(\xi_i) & \text{for } j = 1,2,3,4 \\ E_{ij}(\xi_i) = C^{-}_{ij-4}(\xi_i) & \text{for } j = 5,6,7,8 \end{cases} \tag{5.36e}$$

$$\begin{cases} F_{ij}(\xi_i) = D^{-}_{ij+4}(\xi_i) & \text{for } j = 1,2,3,4 \\ F_{ij}(\xi_i) = D^{-}_{ij-4}(\xi_i) & \text{for } j = 5,6,7,8 \end{cases} \tag{5.36f}$$

where $^{-}$ means Ω interchanged with $-\Omega$. In case the segment is symmetric, the functions $p_{1b}^{a_k}$ and $h_{1b}^{a_k}$ vanish. If segment i has a lth bearing, one simply changes $p_{1f}^{a_k}$ to $p_{1f}^{b_l}$, $h_{1f}^{a_k}$ to $h_{1f}^{b_l}$, and so on.

The next step now is to find the continuity conditions that relate the constants of two neighbor segments, namely $\{X_{i+1}(0)\}$ and $\{X_i(0)\}$. The continuity conditions are a bit different than the isotropic case shown in Eq. (3.45) due to the asymmetry. The conditions of displacement, slope and shear force will be unchanged, but the bending moment continuity is given as,

$$\begin{cases} EI_{1i+1}\eta'_{1i+1}(0) + EI_{2i+1}\eta'_{2i+1}(0) = EI_{1i}\eta'_{1i}(L_i) + EI_{2i}\eta'_{2i}(L_i) \\ EI_{1i+1}\eta'_{2i+1}(0) + EI_{2i+1}\eta'_{1i+1}(0) = EI_{2i}\eta'_{1i}(L_i) + EI_{1i}\eta'_{2i}(L_i) \end{cases} \tag{5.37}$$

these equations are obtained from the complex bending moment condition and assuming the solutions shown in Eq. (5.17). After some algebraic manipulations, Equation (5.37) can be written as,

$$\begin{Bmatrix} \eta'_{1i+1}(0) \\ \eta'_{2i+1}(0) \end{Bmatrix} = \frac{\beta_i}{1-\gamma_i^2} \begin{bmatrix} (1-\gamma_i\gamma_{i+1}) & (\gamma_{i+1}-\gamma_i) \\ (\gamma_{i+1}-\gamma_i) & (1-\gamma_i\gamma_{i+1}) \end{bmatrix} \begin{Bmatrix} \eta'_{1i}(L_i) \\ \eta'_{2i}(L_i) \end{Bmatrix} \tag{5.38}$$

where $\beta_i = I_{1i}/I_{1i+1}$ and $\gamma_i = I_{2i}/I_{1i}$. Note that the relation shown in Eq. (5.38) accounts the asymmetry in both segments. If both segments are symmetric, one has $\gamma_i = \gamma_{i+1} = 0$, and the Eq. (5.38) becomes exactly that of the symmetric rotor. Also, it is possible that segment i is symmetric, $\gamma_i = 0$, and segment $i+1$ is asymmetric, $\gamma_{i+1} \neq 0$, or vice-versa. Moreover, the relation between $\{X_{i+1}(0)\}$ and $\{X_i(L_i)\}$ is given as,

$$\{X_{i+1}(0)\} = \begin{bmatrix} [h_{1i}] & [h_{2i}] \\ [h_{2i}] & [h_{1i}] \end{bmatrix} \{X_i(L_i)\} = [H_{1i}]\{X_i(L_i)\} \tag{5.39}$$

being,

$$[h_{1i}] = \begin{bmatrix} 1 & 0 & 0 & 0 \\ 0 & \frac{\beta_i(1-\gamma_i\gamma_{i+1})}{(1-\gamma_i^2)} & 0 & 0 \\ 0 & 0 & 1 & 0 \\ 1-\alpha_i & 0 & 0 & \alpha_i \end{bmatrix}, \quad [h_{2i}] = \begin{bmatrix} 0 & 0 & 0 & 0 \\ 0 & \frac{\beta_i(\gamma_{i+1}-\gamma_i)}{(1-\gamma_i^2)} & 0 & 0 \\ 0 & 0 & 0 & 0 \\ 0 & 0 & 0 & 0 \end{bmatrix} \tag{5.40}$$

Note that in the symmetric case $[h_{1i}] = [h_i]$ and $[h_{2i}] = 0$, with $[h_i]$ defined in Eq. (3.46). The terms $\{X_{i+1}(0)\}$ and $\{X_i(0)\}$ can now be related using the relations shown in Eq. (5.32)-(5.35), leading to,

$$\{X_{i+1}(0)\} = [H_{1i}] \begin{bmatrix} [D_i(L)] & [D_i'(L)] & \cdots & [F_i'(L)] \end{bmatrix}^T \{X_i(0)\} = [H_i]\{X_i(0)\} \tag{5.41}$$

which has the same form as the anisotropic rotor. With the continuity condition above, one can relate the terms of all segments $i = 1, 2, ..., n$, and solve the eigenvalue problem. By using the conditions given in Eq. (5.41) for every segment, and applying the boundary conditions, one arrives at the now familiar equation,

$$[A]\Big([H_{n-1}] \times [H_{n-2}] \times \cdots \times [H_2]\Big)[B]\{X\} = [G(\lambda)]\{X\} = 0 \tag{5.42}$$

that has the same form as the previous cases (isotropic and anisotropic rotor). The boundary condition terms, $[A]$, $[B]$ and $\{X\}$, are obtained in the same way as before. The procedure for the case when both boundaries are free are now presented as an example.

The boundary conditions when both ends are free are given as,

$$\begin{cases} \kappa GA_1\Big(\eta_{11}(0) - \phi_{11}(0)\Big) = \kappa GA_1\Big(\eta_{21}(0) - \phi_{21}(0)\Big) = 0 \\ \kappa GA_n\Big(\eta_{1n}(L_n) - \phi_{1n}(L_n)\Big) = \kappa GA_n\Big(\eta_{2n}(L_n) - \phi_{2n}(L_n)\Big) = 0 \\ EI_{11}\eta_{11}'(0) + EI_{21}\eta_{21}'(0) = EI_{1n}\eta_{1n}'(L_n) + EI_{2n}\eta_{2n}'(L_n) = 0 \\ EI_{21}\eta_{11}'(0) + EI_{11}\eta_{21}'(0) = EI_{2n}\eta_{1n}'(L_n) + EI_{1n}\eta_{2n}'(L_n) = 0 \end{cases} \tag{5.43}$$

The last two equations can be written compactly as,

$$\begin{bmatrix} 1 & \gamma_1 \\ \gamma_1 & 1 \end{bmatrix} \begin{Bmatrix} \eta_{11}'(0) \\ \eta_{21}'(0) \end{Bmatrix} = \begin{Bmatrix} 0 \\ 0 \end{Bmatrix}, \quad \begin{bmatrix} 1 & \gamma_n \\ \gamma_n & 1 \end{bmatrix} \begin{Bmatrix} \eta_{1n}'(L_n) \\ \eta_{2n}'(L_n) \end{Bmatrix} = \begin{Bmatrix} 0 \\ 0 \end{Bmatrix},$$

One can readily note that these equations have only the trivial solutions $\eta_{11}'(0) = \eta_{21}'(0) = 0$ and $\eta_{1n}'(0) = \eta_{2n}'(0) = 0$, since, as can be easily checked, the determinant of the coefficient matrix is not zero. Recall that, by means of Eq. (5.41), the functions for the

nth segment can be written as,

$$\phi_{1n}(\xi_n) = [C_n(\xi_n)]\{X_n(0)\} = [C_n(\xi_n)]\Big([H_{n-1}] \times [H_{n-2}] \times \cdots \times [H_1]\Big)\{X_1(0)\}$$

$$\eta_{1n}(\xi_n) = [D_n(\xi_n)]\{X_n(0)\} = [D_n(\xi_n)]\Big([H_{n-1}] \times [H_{n-2}] \times \cdots \times [H_1]\Big)\{X_1(0)\}$$

$$\phi_{2n}(\xi_n) = [E_n(\xi_n)]\{X_n(0)\} = [E_n(\xi_n)]\Big([H_{n-1}] \times [H_{n-2}] \times \cdots \times [H_1]\Big)\{X_1(0)\}$$

$$\eta_{2n}(\xi_n) = [F_n(\xi_n)]\{X_n(0)\} = [F_n(\xi_n)]\Big([H_{n-1}] \times [H_{n-2}] \times \cdots \times [H_1]\Big)\{X_1(0)\}$$

By applying the boundary conditions for segment n, and using the fact that $\eta'_{1n}(0) = \eta'_{2n}(0) = 0$, one may have,

$$\begin{bmatrix} [D'_n(L_n)] \\ [D_n(L_n)] - [C'_n(L_n)] \\ [F'_n(L_n)] \\ [F_n(L_n)] - [E'_n(L_n)] \end{bmatrix} \Big([H_{n-1}] \times [H_{n-2}] \times \cdots \times [H_1]\Big)\{X_1(0)\} = 0$$

where the first matrix in the left-hand side correspond to the matrix $[A]$ for the case where the boundary is free at $x = L$. The terms $[B]$ and $\{X\}$ are obtained modifying $[H_1]$ and $\{X_1(0)\}$. Recall that the boundary conditions state that $\eta'_{11}(0) = \eta'_{21}(0) = 0$, thus one may have,

$$[H_1]\{X_1(0)\} = [H_1]\begin{Bmatrix} \eta_{11}(0) \\ \eta'_{11}(0) \\ \phi_{11}(0) \\ \phi'_{11}(0) \\ \eta_{21}(0) \\ \eta'_{21}(0) \\ \phi_{21}(0) \\ \phi'_{21}(0) \end{Bmatrix} = [H_1]\begin{Bmatrix} \phi'_{11}(0) \\ 0 \\ \phi_{11}(0) \\ \phi'_{11}(0) \\ \phi'_{21}(0) \\ 0 \\ \phi_{21}(0) \\ \phi'_{21}(0) \end{Bmatrix} = [H_1]\begin{bmatrix} 0 & 1 & 0 & 0 \\ 0 & 0 & 0 & 0 \\ 1 & 0 & 0 & 0 \\ 0 & 1 & 0 & 0 \\ 0 & 0 & 0 & 1 \\ 0 & 0 & 0 & 0 \\ 0 & 0 & 1 & 0 \\ 0 & 0 & 0 & 1 \end{bmatrix}\begin{Bmatrix} \phi_{11}(0) \\ \phi'_{11}(0) \\ \phi_{21}(0) \\ \phi'_{21}(0) \end{Bmatrix} = [B]\{X\}$$

which is the same procedure performed in the anisotropic rotor. With this result, Equation (5.42) is obtained. Any other combination of boundary conditions can be obtained following the same steps outlined above.

The characteristic equation is obtained from the determinant of the coefficient matrix $[G(\lambda)]$ in Eq. (5.42), which must be zero for non-trivial solutions. The eigenvalues will have the form

$$\lambda_i^k = \sigma_i^k \pm j\omega_i^k \quad \text{for } i = 1, 2, ..., N;\ k = F, B \tag{5.44}$$

where ω_i^k are the damped natural frequencies, σ_i^k are the damping parameters and F and B denote the forward and backward modes, respectively. In the asymmetric case, the forward and backward modes both have positive and negative frequencies, just as in the anisotropic rotor. After obtaining the eigenvalues, the constants $\{X\}$ for mode i can be obtained by substituting λ_i in Eq. (5.42). This gives the ratio between the modal constants of segment 1, leaving an arbitrary constant that is obtained from the orthogonality conditions. The global function will thus be a piece-wise continuous function, which can be written as,

$$\phi_1(x) = \begin{cases} \phi_{11}(x) & \text{for } x_1 < x < x_2 \\ \phi_{12}(x) & \text{for } x_2 < x < x_3 \\ \vdots & \\ \phi_{1n}(x) & \text{for } x_n < x < x_{n+1} \end{cases} \tag{5.45}$$

and the same form is true for $\phi_2(x)$, $\eta_1(x)$ and $\eta_2(x)$. As in the anisotropic case, the horizontal ϕ_y and vertical ϕ_z mode shapes of the asymmetric rotor are distinct, and they can be obtained in a similar way as (JEI; LEE, 1992b),

$$\phi_y^k(x) = \phi_1^k(x) + \phi_2^k(x), \quad \phi_z^k(x) = j\big(\phi_1^k(x) - \phi_2^k(x)\big) \text{ for } k = F, B \tag{5.46}$$

This form is also true for $\eta_y(x)$ and $\eta_z(x)$, using $\eta_1(x)$ and $\eta_2(x)$. As noted by Jei and Lee (1992b), the undamped mode shapes are real and planar when the boundary conditions are isotropic. In case one has a bearing or an asymmetric disk at the boundary, the mode shapes will become complex and non-planar.

5.3 Modal analysis

In the previous section, the eigenfunctions were obtained by means of separation of variables. These functions can now be used to solve the equations of motion, Eqs. (5.10) and (5.11), by means of modal analysis. The approach for the asymmetric rotor is very similar to the rotor on anisotropic bearings presented in Chapter 4. First, the equations of motion, and their complex conjugate, are rewritten as,

$$[m]\begin{Bmatrix} \{\ddot{w}(x,t)\} \\ \{\ddot{w}^*(x,t)\} \end{Bmatrix} + [c]\begin{Bmatrix} \{\dot{w}(x,t)\} \\ \{\dot{w}^*(x,t)\} \end{Bmatrix} + [k]\begin{Bmatrix} \{w(x,t)\} \\ \{w^*(x,t)\} \end{Bmatrix} = \begin{Bmatrix} \{g(x,t)\} \\ \{g^*(x,t)\} \end{Bmatrix} \tag{5.47}$$

where,

$$[m] = \begin{bmatrix} \bar{m}(x) & 0 & 0 & 0 \\ 0 & \bar{J}_1(x) & 0 & \bar{J}_2(x) \\ 0 & 0 & \bar{m}(x) & 0 \\ 0 & \bar{J}_2(x) & 0 & \bar{J}_1(x) \end{bmatrix} \tag{5.48}$$

$$[c] = \begin{bmatrix} [c_1] & [0]_{2\times 2} \\ [0]_{2\times 2} & [c_1^*] \end{bmatrix}, \quad [c_1] = \begin{bmatrix} \bar{c}_m(x) + 2j\Omega\bar{m}(x) & 0 \\ 0 & -\bar{c}_t(x) \end{bmatrix} \tag{5.49}$$

$$[k] = \begin{bmatrix} [k_1] & [k_2] \\ [k_2^*] & [k_1^*] \end{bmatrix},$$

$$[k_1] = \begin{bmatrix} -\frac{\partial}{\partial x}\left(\kappa G\bar{A}(x)\frac{\partial}{\partial x}\right) - \bar{m}(x)\Omega^2 & \frac{\partial}{\partial x}\left(\kappa G\bar{A}(x)\right) \\ \quad +\bar{k}_m(x) + j\Omega\bar{c}_m(x) & \\ -\kappa G\bar{A}(x)\frac{\partial}{\partial x} & -\frac{\partial}{\partial x}\left(E\bar{I}_1(x)\frac{\partial}{\partial x}\right) + \kappa G\bar{A}(x) - \bar{J}_1(x)\Omega^2 \\ & -\bar{k}_t(x) - j\Omega\bar{c}_t(x) \end{bmatrix},$$

$$[k_2] = \begin{bmatrix} 0 & 0 \\ 0 & -\frac{\partial}{\partial x}\left(E\bar{I}_2(x)\frac{\partial}{\partial x}\right) \end{bmatrix} \tag{5.50}$$

being $\{w(x,t)\}$ and $\{g(x,t)\}$ defined in Eqs. (3.55) and (3.56), respectively. The equations for $\{w(x,t)\}$ and $\{w^*(x,t)\}$ are now coupled due to the asymmetry in the inertia and stiffness of the shaft, given by the functions $\bar{J}_2(x)$ and $E\bar{I}_2(x)$. For $\bar{J}_2(x) = E\bar{I}_2(x) = 0$, the equations becomes decoupled and the problem becomes the same as the isotropic case, but in the rotating reference frame. Next, Equation (5.47) is written in the state space form, which gives,

$$[M]\{\dot{W}(x,t)\} = [K]\{W(x,t)\} + \{F(x,t)\} \tag{5.51}$$

where,

$$\{W(x,t)\} = \Big\{\{\dot{w}(x,t)\}\ \{\dot{w}^*(x,t)\}\ \{w(x,t)\}\ \{w^*(x,t)\}\Big\}^T \tag{5.52}$$

$$\{F(x,t)\} = \Big\{0\ 0\ 0\ 0\ \{g(x,t)\}\ \{g^*(x,t)\}\Big\}^T \tag{5.53}$$

and the matrices $[M]$ and $[K]$ have the same form as shown in Eqs. (3.60) and (3.61), with the matrices $[m]$, $[c]$ and $[k]$ being corrected as above. In the asymmetric rotor, both operator matrices $[M]$ and $[K]$ are non-self-adjoint and positive definite (see Sec. 3.3 for how to demonstrate that). The same procedure presented in the isotropic and anisotropic cases can be taken, where one solves the adjoint eigenvalue problem in addition to the regular problem. As usual, the state vector is expanded as,

$$\{W(x,t)\} = \sum_{i=0}^{\infty}\{\Phi_i(x)\}q_i(t) \tag{5.54}$$

where the mode shapes are similar to the anisotropic case, that is,

$$\{\Phi_i(x)\} = \Big\{\lambda_i\phi_{1i}(x)\quad \lambda_i\eta_{1i}(x)\quad \lambda_i\phi_{2i}(x)\quad \lambda_i\eta_{2i}(x)\quad \phi_{1i}(x)\quad \eta_{1i}(x)\quad \phi_{2i}(x)\quad \eta_{2i}(x)\Big\}^T \tag{5.55}$$

The eigenvalue problem related to Eq. (5.47) and its adjoint are given as,

$$\lambda_i[M]\{\Phi_i(x)\} = [K]\{\Phi_i(x)\} \quad \text{for} \quad i = 1, 2, ... \tag{5.56}$$

$$\lambda_i^*[\tilde{M}]\{\tilde{\Phi}_i(x)\} = [\tilde{K}]\{\tilde{\Phi}_i(x)\} \quad \text{for} \quad i = 1, 2, ... \tag{5.57}$$

where one can prove that the eigenvalue problem shown in Eq. (5.56) is the same as the one given by Eqs. (5.18a)-(5.18d). The adjoints of the operators are $[\tilde{M}] = [M]^H$ and $[\tilde{K}] = [K]^H$, being H the complex conjugate transpose. The vector $\{\tilde{\Phi}_i(x)\}$ is given as,

$$\{\tilde{\Phi}_i(x)\} = \left\{\lambda_i^*\tilde{\phi}_{1i}(x) \quad \lambda_i^*\tilde{\eta}_{1i}(x) \quad \lambda_i^*\tilde{\phi}_{2i}(x) \quad \lambda_i^*\tilde{\eta}_{2i}(x) \quad \tilde{\phi}_{1i}(x) \quad \tilde{\eta}_{1i}(x) \quad \tilde{\phi}_{2i}(x) \quad \tilde{\eta}_{2i}(x)\right\}^T \tag{5.58}$$

where $\tilde{\phi}_{1i}(x)$ is the adjoint of $\phi_{1i}(x)$, $\tilde{\eta}_{1i}(x)$ is the adjoint of $\eta_{1i}(x)$, and so on. As mentioned in the previous chapters, the vectors $\{\Phi_i(x)\}$ and $\{\tilde{\Phi}_j(x)\}$ are biorthogonal and satisfy the conditions shown in Eqs. (3.70a) and (3.70b). After substituting $\{W(x,t)\}$ given by Eq. (5.54) in the state-space equation of motion, Equation (5.51), taking the internal product in both sides by $\{\tilde{\Phi}_i(x)\}$, and taking into account the orthogonality conditions, one may have,

$$\dot{q}_i(t) = \lambda_i q_i(t) + \int_0^L \tilde{\phi}_{1i}^*(x) f(x,t) dx + \int_0^L \tilde{\phi}_{2i}^*(x) f^*(x,t) dx \quad \text{for} \quad i = 1, 2, ... \tag{5.59}$$

which is very similar to the result of the anisotropic rotor. Equation (5.59) consist of infinite first order complex modal equations, which are in reality truncated at N modes. In this case, each mode has a forward and backward case with positive and negative frequency, each with a unique equation. As noted in the anisotropic rotor, for $4N$ modes, there is N forward modes with positive natural frequency $+j\omega_i^F$, N forward modes with negative natural frequency $-j\omega_i^F$, N backward modes with positive natural frequency $+j\omega_i^B$ and N backward modes with negative natural frequency $-j\omega_i^B$, where $i = 1, 2, ...N$. The physical displacement and slopes are obtained from Equation (5.54), which gives,

$$u(x,t) = \sum_{i=0}^{\infty} \phi_{1i}(x) q_i(t) \tag{5.60}$$

$$\psi(x,t) = \sum_{i=0}^{\infty} \eta_{1i}(x) q_i(t) \tag{5.61}$$

The same comments made in Sec. 4.3 can be applied to Eq. (5.59). However, the asymmetric rotor has some particular phenomenon such as the instability between the forward and backward critical speeds and the gravity critical speed (LEE, 1993). Also, the initial conditions can be obtained using Eq. (4.60).

As in the isotropic and ansiotropic cases, the vectors $\{\Phi_i(x)\}$ and $\{\tilde{\Phi}_i^*(x)\}$ are the

result of the same eigenvalue problem, and they satisfy the relation

$$\{\Phi_i(x)\} = \frac{1}{K_i}\{\tilde{\Phi}_i^*(x)\} \tag{5.62}$$

where again K_i is a complex normalizing constant and it is obtained from Equations (3.70a) or (3.70b). These equations will not be expanded here due to their length, but one gets a similar form as shown in the isotropic case by Eqs (3.75) and (3.76), with additional terms due to the asymmetry of the shaft.

With the asymmetric rotor, the applicability of the CSM to the most known types of rotors are all covered. The case when the rotor is asymmetric and the bearings are anisotropic was not covered, since the eigenvalue problem becomes unsolvable by means of the methods used in this work.

6 Rotor-stator rubbing

This chapter present some background on the rubbing phenomenon in rotating machinery. The idea is to apply a model based on the CSM to study nonlinear applications. Section 6.1 presents a overview on the phenomenon in rotating machinery, while the nonlinear model of the contact force is presented in Sec. 6.2.

6.1 Overview

A special phenomenon seen recurrently in rotating machines is the rubbing between rotor and stator. Since the gap between rotating and stationary parts tend to decrease, mainly due to efficiency and power needs, this phenomenon becomes more and more inevitable and thus a understating of its effect on the overall dynamics of the machine is vital. This is specially true for turbomachines (JACQUET-RICHARDET et al., 2013). Also, the effect of rotor-stator contact affects greatly oil drilling applications (JANSEN, 1991; CHEN et al., 2019) as well as auxiliary bearings for magnetically levitated rotors (FONSECA et al., 2017; CHIBA et al., 2005; SUN, 2006).

The complexity of rubbing arises due to the several physical phenomena involved, such as friction, physical contacts, and stiffness changes (MUSZYNSKA, 2005). Depending on these parameters, the system can posses different dynamic characteristics that can be divided as: forward annular rub (FWAR), forward partial rub (FWPR) and backward whirl (JACQUET-RICHARDET et al., 2013). In the FWAR, the rotor whirls in continuous contact with the stator at a synchronous speed. This behavior is very common when friction at the contact interface is low. However, due to the continuous contact, the rub may generate considerable heat, leading to thermal bow, also known as the Newkirk effect (DIMAROGONAS, 1974). Some effects of the FWAR can be avoided by increasing the friction between the rotor and stator. On the other hand, this friction increase may lead the rotor to a bouncing state, or FWPR, which is characterized by discontinuous contacts along the whirling motion of the rotor. Depending on different parameters, this motion can lead to steady-state or transient motions. The FWPR is known to posses rich dynamics characteristics that range from periodic to chaotic (EHRICH, 1991; GOLDMAN; MUSZYNSKA, 1994). For this reason, many researches devoted their work in identifying regions of periodic solutions and routes to chaos (AZEEZ; VAKAKIS, 1999; POPPRATH; ECKER, 2007; VARNEY; GREEN, 2015), which is usually done by means of bifurcation diagrams, Poincaré sections and Lyapunov exponents (see Strogatz (2018) for an introduction on nonlinear systems). In addition, the FWPR motion rises different harmonics in the frequency spectrum such as multiple harmonics (2X, 3X,..), semi-harmonics (X/2, 3X/2,...) and third harmonics (X/3, 2X/3) (EHRICH, 1988; CHU; LU, 2005).

A distinct phenomenon that can appear in rotor-stator rub is the asynchronous partial contacts, where the rotor whirls in FWPR with frequencies unrelated to the rotating speed. According to Shaw et al. (2016), this phenomenon is due to internal resonance and can occur at multiple drive speeds even with no friction. The authors went further to experimentally study this phenomenon in a recent paper by Crespo et al. (2020), giving convincing evidence for their assumptions. The motions due to asynchronous bouncing appear to have quasi-periodic characteristics in a fixed-frame of reference but they may turn into periodic in a rotating frame (COLE; KEOGH, 2003). The asynchronous motion appears to occur because of transient energy that gets amplified due to internal resonance, as shown by Zilli et al. (2015), where a transient analysis showed that this phenomenon may be avoided with low acceleration rates.

The rubbing motion can turn into self-excited motion once the rotors starts to whirling in the backward direction, which can lead to very dangerous situations, including the complete failure of the machines as reported by Rosenblum (1995). Following the definitions from Childs and Bhattacharya (2007), the backward motion during rubbing can be divided as: dry-friction whirl (DWL) and dry-friction whip (DWP). In the former, the rotor rolls-without-slipping around the stator, whereas in the latter the motion occurs with continuous slipping between the rotor and stator. Both of these motions are characterized by their nonsynchronous nature, and the DWP is noted to be more violent. Several works focused on detecting the rotor frequency where DWP occurs (BLACK, 1968; CRANDALL, 1990; BARTHA, 2000; YU et al., 2002). Wilkes et al. (2010) and Wang et al. (2020) present numerical and experimental results for multi-mode systems, where different whip and whirl frequencies can be found. Despite the DWP phenomenon being seen extensively in test rigs, it is not seen much in practice on turbomachines. Bhattacharya and Childs (2009) suggested that this may be because real machines have enough cross coupled stiffness and damping to hinder DWP. Similar results were obtained by Shang et al. (2010). Moreover, the boundaries between different rubbing motions is the main topic in Jiang et al. (2010), Jiang (2009) and Jiang and Ulbrich (2005).

Given the importance of rotor-stator rub in rotating machinery, adequate models to represent this phenomenon are essential in the understanding of its effects on the machines. The simple 2-DOF Jeffcott rotor model seems to represent most of the rubbing characteristics described above, and it is the most used approach used by researchers in the analysis of rubbing (ALBER; MARKERT, 2014). As for the stator, some works consider a massless ring (CHIPATO et al., 2019; YU et al., 2000; JIANG; ULBRICH, 2000), others model the stator as a S-DOF system with stiffness and damping (POPPRATH; ECKER, 2007; CHILDS; BHATTACHARYA, 2007; JIANG et al., 2010). Despite the fact that the Jeffcott model presents several characteristics seen in real rotor machines, its use is mainly towards giving insights into the rubbing phenomenon, and its results are often not used in

the design of machines. Some researchers tried to overcome this issue and presented more detailed models using the FEM to model both the rotor and stator (WILKES et al., 2010; BEHZAD et al., 2013; BEHZAD; ALVANDI, 2018; ROQUES et al., 2010; MOKHTAR et al., 2018; AGRAPART et al., 2019). In this work, the CSM is proposed to model the rotor system and study the rubbing phenomenon.

In some cases, the use of FEM method results in a very large system of differential equations, which requires a great deal of computational time. This encouraged researchers to look for methods to reduce the order of the equations (WAGNER et al., 2010; MARTIN et al., 2020). Some of the most used methods for these reductions on rotor systems are Guyan Reduction (GUYAN, 1965; STEPHENSON; ROUCH, 1993), Modal analysis (CHATELET et al., 2002; KHULIEF; MOHIUDDIN, 1997) and Component Mode Synthesis (CHATELET et al., 2002; GLASGOW; NELSON, 1980).

6.2 Contact force model

The rubbing model consist in how the contact between the rotor and the stator is modeled. The common approach is to consider the indentation as a nonlinear spring-damping system. In this model, the contact force is zero initially after contact, and increases proportionally to the deformation and relative velocity of the bodies (VARANIS et al., 2019; VARANIS et al., 2017). The force considered is based on the model by Hunt e Crossley (1975), which is given as,

$$F_c(\chi, \dot{\chi}) = k_h \chi^m + c_h \chi^n \dot{\chi}^p \tag{6.1}$$

being χ and $\dot{\chi}$ the indentation and its rate of change, k_h the stiffness coefficient; and c_h the damping coefficient. The exponents are assumed as $n = p = 1$ and $m = 1$. The model given by Eq. (6.1) is more suitable to model the contact between elastic bodies than the commonly used linear spring-dashpot model, as the force at the end of the contact is zero (PUST; PETERKA, 2003). The indentation χ is the normal deformation in the rotor-stator contact, and is given as,

$$\chi(t) = |u(b,t)| - d_c = \sqrt{u_y(b,t)^2 + u_z(b,t)^2} - d_c \tag{6.2}$$

where u is the complex displacement field, b is the rubbing location and d_c the initial gap between the rotor and the stator. The rate of change is obtained by applying the derivative, thus,

$$\dot{\chi}(t) = |\dot{u}(b,t)| = \frac{u_y(b,t)\dot{u}_y(b,t) + u_z(b,t)\dot{u}_z(b,t)}{|u(b,t)|} \tag{6.3}$$

In order to model the rubbing, a model for the tangential force must also be given. The commonly used Coulomb model is assumed here, where the tangential force is proportional to the normal contact force, that is,

$$F_t = \mu(v_{rel})F_c \tag{6.4}$$

being μ the friction coefficient and it is a function of the relative velocity at the contact point v_{rel}. The sign of the tangential velocity must be taken into account, since the tangential force is always against the direction of movement. In this work the function $\mu(v_{rel})$ is assumed as (CHIPATO et al., 2019),

$$\mu = \mu(v_{rel}) = \mu_m \tanh(v_{rel}/v_0) \tag{6.5}$$

where v_0 is a curve-fitting parameter and μ_m is the maximum friction coefficient. It is worth mentioning that the $\tanh(\cdot)$ function, with a sufficient small v_0, approximates the function $\text{sign}(\cdot)$, and it is less computationally expensive. The relative velocity can be obtained as,

$$v_{rel}(t) = \dot{\theta}(t)|u(b,t)| + \Omega R \tag{6.6}$$

where R is the rotor's radius and $\dot{\theta}$ is the whirl speed, which is given as

$$\dot{\theta}(t) = \frac{d}{dt}\left[\tan^{-1}\left(\frac{u_z(b,t)}{u_y(b,t)}\right)\right] = \frac{u_y(b,t)\dot{u}_z(b,t) - u_z(b,t)\dot{u}_y(b,t)}{|u(b,t)|^2} \tag{6.7}$$

The complex form of the contact forces are expressed as,

$$f_{cont}(x,t) = -\Theta[F_c(t) + jF_t(t)]e^{j\theta}\delta_d(x-b) = -\Theta[1 + j\mu(v_{rel})]F_c(t)\frac{u(b,t)}{|u(b,t)|}\delta_d(x-b) \tag{6.8}$$

where Θ ensures that the force is only positive when there is contact and it is defined as,

$$\Theta = \begin{cases} 1 & \text{for } |u(b,t)| \geq d_c \\ 0 & \text{for } |u(b,t)| < d_c \end{cases} \tag{6.9}$$

Equation (6.8) can be applied in the equations of motion to study the rubbing effect.

7 Results and discussion

This chapter presents numerical examples of the proposed method. In the first example, shown in Section 7.1, a uniform rotor is presented. Different cases of the bearings, from isotropic to anisotropic, are considered and the Campbell diagrams, mode shapes and unbalance responses are shown. The approaches presented in Chapters 3 and 4 are used in this example. Section 7.2 presents another numerical example, where the rotor is asymmetric and the model shown in Chapter 5 is used. Section 7.3 shows an example of a rotor with complex geometry and anisotropic bearings. Lastly, Section 7.4 shows the application of the present method in nonlinear analysis, namely the rubbing between rotor and stator. In all cases, the results given by CSM are compared to models based on the FEM.

All the results are obtained by means of the software MATLAB. In the CSM, the eigenvalue problem is solved by means of the function *fsolve*, while in the FEM the function *eig* is used. The unbalance responses are obtained by solving the equations of motion analytically. In the rubbing results, the responses are obtained using the integrator *ode45*.

7.1 Uniform rotor

In this numerical example, the system shown in Figure 7a is studied. It consists of a three segment shaft with lengths l, a total length of L and a diameter d. A rigid thin disk is positioned at the second segment with local coordinate a and with width h_d, internal diameter d and external diameter D. Two identical bearings are positioned at the first and last segment, their local coordinates are b_1 and b_2, respectively. The fixed dimensions and material properties are listed in Table 1.

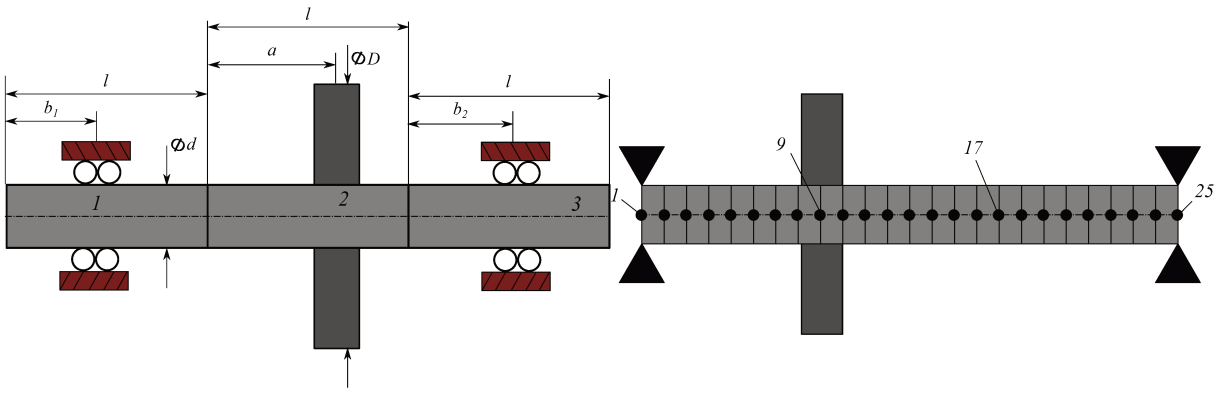

Figure 7: Dimensions of the uniform rotor: (a) rotor scheme for CSM and (b) rotor discretization for FEM.

Table 1: Parameters used for the uniform rotor.

Parameter	Symbol	Value
Shaft length	L	600 mm
Segment length	l	200 mm
Shaft diameter	d	24 mm
Density of the material	ρ	7850 kg/m^3
Young's modulus	E	200 GPa
Poisson's ratio	ν	0.3
Shear modulus	G	76.92 GPa
Shear factor	κ	0.8864
Disk length	h_d	15 mm
Disk external diameter	D	150 mm
Disk location	a	0 mm
Bearing locations	b_1	0 mm
	b_2	200 mm
Unbalance moment	$m_u e$	0.0213 kg·m

Table 2: Bearing parameters for the uniform rotor.

Case	Direct coefficients	Cross-coupled coefficients
Case 1 (Isotropic)	$k_{yy} = 10^6$ N/m, $k_{zz} = k_{yy}$	$k_{yz} = k_{zy} = 0$ N/m
	$c_{yy} = 10^2$ N/m, $c_{zz} = c_{yy}$	$c_{yz} = c_{zy} = 0$ N/m
Case 2 (Isotropic)	$k_{yy} = 10^6$ N/m, $k_{zz} = k_{yy}$	$k_{yz} = 4.2 \times 10^4$ N/m, $k_{zy} = -k_{zy}$
	$c_{yy} = 10^2$ N/m, $c_{zz} = c_{yy}$	$c_{yz} = c_{zy} = 0$ N/m
Case 3 (Anisotropic)	$k_{yy} = 10^6$ N/m, $k_{zz} = 0.8k_{yy}$	$k_{yz} = k_{zy} = 0$ N/m
	$c_{yy} = 10^2$ N/m, $c_{zz} = c_{yy}$	$c_{yz} = c_{zy} = 0$ N/m

In order to evaluate the present method, a model based on the FEM was also established with the same dimensions and with a mesh containing 24 finite elements. The mesh is shown in Fig. 7b. The elements considered were standard Timoshenko beams with gyroscopic effect; the matrices obtained after the discretization can be consulted in Friswell et al. (2010) or Tiwari (2017). In addition, the bearings were placed at the boundary nodes, and the rigid disk at node 9, which corresponds to the position set in the model based on the CSM.

Two types of bearings were considered: isotropic and anisotropic. The values of the stiffness and damping coefficients used are listed in Table 2. The analysis was separated in three cases: in cases 1 and 2 the bearings are isotropic and represent the cases with and without the cross-coupled coefficients in the stiffness, respectively. In case 3 the bearings are anisotropic.

7.1.1 Case 1

In case 1 the stiffness of the bearings are $k_{yy} = k_{zz} = k = 10^6$ N/m and $k_{zy} = k_{yz} = 0$, while the damping is $c_{yy} = c_{zz} = c = 10^2$ Ns/m. Figure 8 shows the Campbell diagram

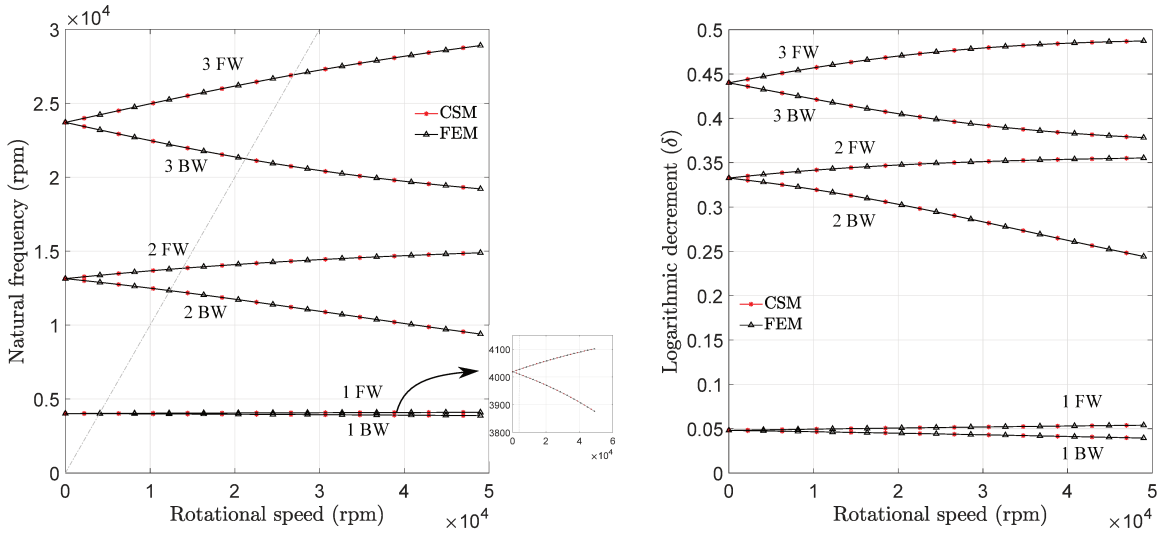

Figure 8: Case 1 results: (a) Campbell diagram and (b) logarithmic decrement

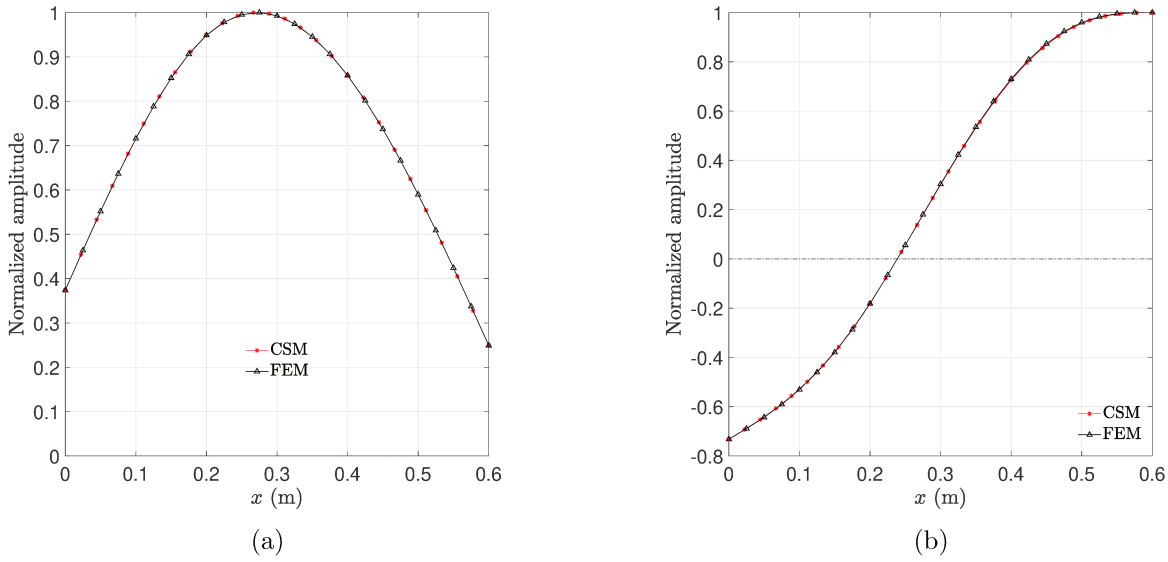

Figure 9: Forward mode shapes for case 1 with $\Omega = 2000$ rpm: (a) first and (b) second mode shape

and the logarithmic decrement up to the third mode obtained with the model based on the CSM and FEM. In this figure and the next ones, FW denotes the forward modes, BW the backward modes, and the gray dashed line is where $\omega = \Omega$. The results given by both methods are practically the same for the modes considered in the response. The first and second forward mode shapes are shown in Fig. 9, where again a great agreement is seen from both methods.

To investigate the forced response of the system, a unbalance moment of $m_u e = 0.0213$ kg·m was introduced at the disk. The unbalance is introduced as an external force

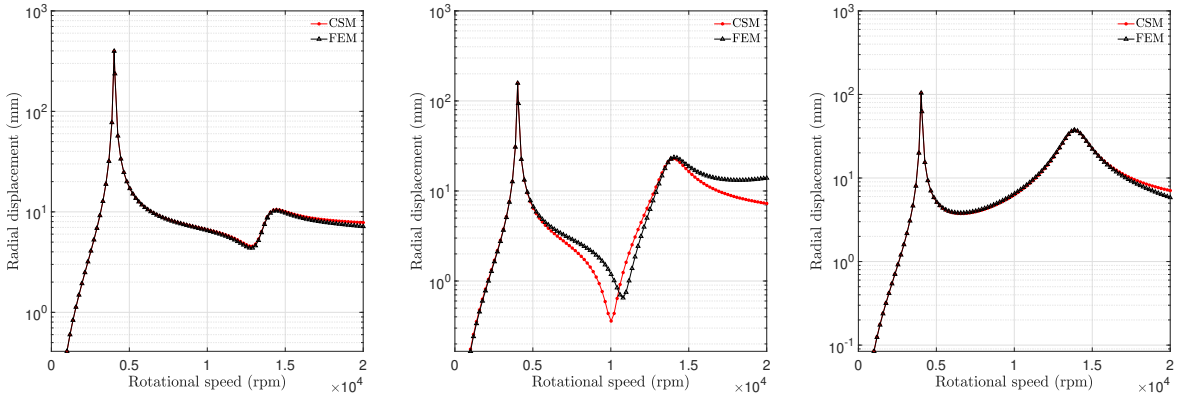

(a) (b) (c)

Figure 10: Unbalance responses for case 1 at: (a) disk, (b) bearing 1 and (c) bearing 2.

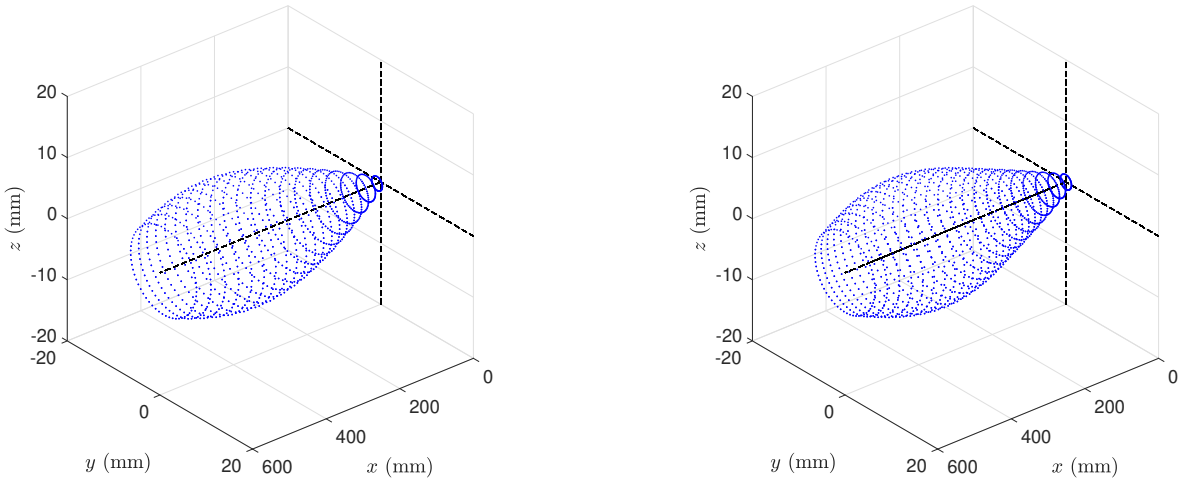

(a) (b)

Figure 11: Global unbalance responses for $\Omega = 10^4$ rpm: (a) CSM and (b) FEM.

in the modal equations and a closed form solution is easily obtained. To establish the number of modes to be used in the CSM, and thus the number of equations to be solved, the response was obtained considering $N = 1$ to $N = 5$ modes. This showed that three modes (that is three forward and three backward) were enough for good results. In the FEM, one needs to apply the force at the corresponding degrees of freedom of the disk. Figure 10 shows the steady-state amplitudes from $\Omega = 10^3$ rpm to $\Omega = 2 \times 10^4$ rpm at three different points along the rotor: at the unbalance location, which is where the disk is located; at bearing 1, which is the bearing at $x = 0$; and at bearing 2, that is the bearing at $x = L$. The amplitudes given by both methods were very close, and the main difference appeared mainly at the anti-resonance at the bearing 1, as Fig. 10b shows. This difference occurs because the bearings were placed exactly at the boundary nodes

in the FEM and at $x = 0$ and $x = L$ in the CSM. Although not physically possible, this was done to simplify the analysis, considering the bearing acting only at a point. When the bearing location is moved farther from the boundaries, the agreement between the methods is better at all locations along the rotor.

The global steady-state responses for $\Omega = 10^4$ rpm are shown in Fig. 11. Thus, the CSM was effective in modeling the system in this case when compared with the FEM, as the global responses were very close.

7.1.2 Case 2

In case 2, the bearings are still isotropic but the cross-coupled stiffness are non-zero. The system still isotropic since $k_{yz} = -k_{zy}$, and the direction of the displacement is collinear with an exciting force (LEE, 1993). In this case, two scenarios are possible: $k_{yz} > 0$ and $k_{yz} < 0$. In the former case, one has a follower force in the direction of the whirl, causing an instability for the forward modes. When $k_{yz} < 0$, the force is opposite to the whirl direction and thus a stable force; although it can be destabilizing if the rotor whirls backwardly. Here both scenarios are considered, and the idea is to see whether the CSM can predict the unstable regions when compared to the FEM.

Figure 12 shows the logarithmic decrements when $k_{yz} < 0$ and $k_{yz} > 0$. In these figures, it is also shown in detail the speed where the system becomes unstable, which is were the real part of the eigenvalue becomes positive. When $k_{yz} < 0$, the first backward mode becomes unstable after a certain speed (approximately 6×10^4 rpm). On the other hand, when $k_{yz} > 0$, the first forward mode is unstable until a certain speed (nearly

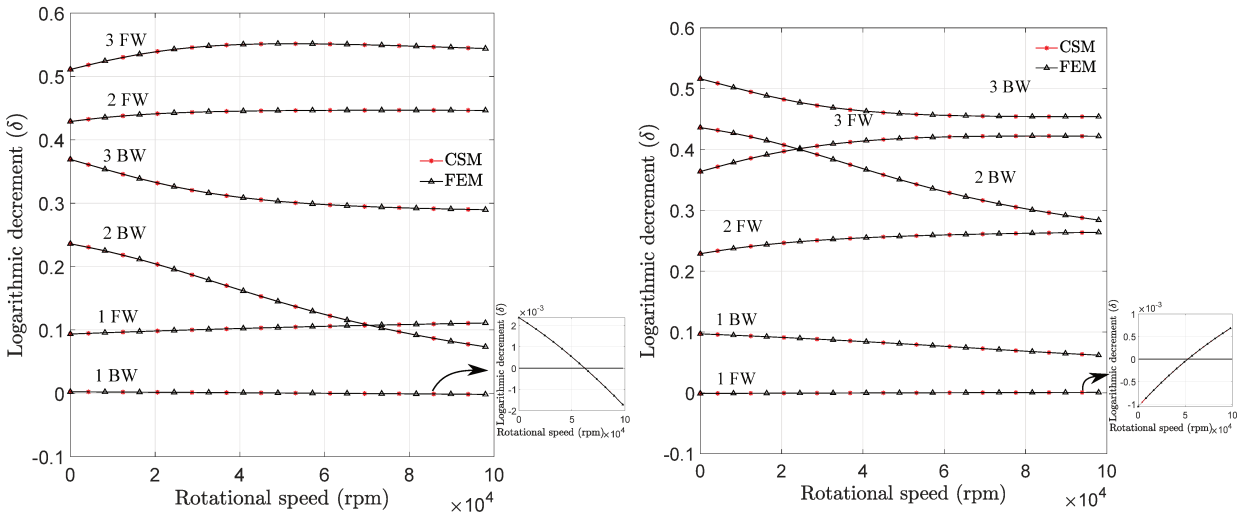

Figure 12: Logarithmic decrements for: (a) $k_{yz} < 0$ and (b) $k_{yz} > 0$.

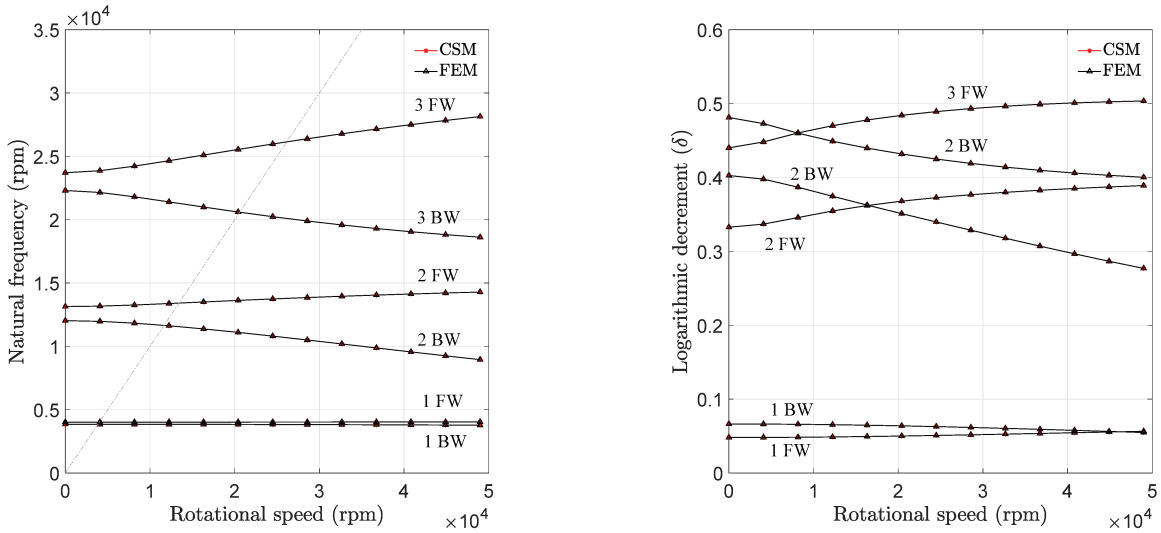

Figure 13: Case 3 results: (a) Campbell diagram and (b) logarithmic decrement

5×10^4 rpm), where a stable case is reached. By comparing Fig. 12 with 8b, one can note that for $k_{yz} < 0$ the damping is increased for the forward modes and decreased for the backward ones, while the opposite is true when $k_{yz} > 0$. The results of the CSM and FEM are practically indistinguishable, with a great agreement. This means that both methods can be used to detect instabilities in rotor systems with similar accuracies. Also, the Campbell diagram is not shown for case 2, as the cross-coupled coefficient affect less the natural frequencies then the damping.

7.1.3 Case 3

In the third and last case, the bearings were anisotropic with $k_{yy} = 10^6$ N/m and $k_{zz} = 0.8k_{yy}$. The cross-coupled coefficients were neglected and the damping is isotropic. The Campbell diagram and the logarithmic decrement are shown in Fig. 13. The CSM and FEM were again in very good agreement, as noticed from the results. In addition, Figure 14 shows the first and second forward mode shapes. Since the system is anisotropic, the shapes in the horizontal and vertical direction are different. The results shows that the CSM can give reliable results for anisotropic rotors.

Next, the response given by the models due to mass unbalance is investigated. The unbalance moment was the same as in case 1, namely $m_u e = 0.0213$ kg·m, and it was introduced at the disk. Another study was performed to determine the number of modes required, which showed that three was enough to represent the system at the speed range studied. Also, the same measurement points were considered: at the disk and at both bearings. The horizontal and vertical steady-state amplitudes obtained with

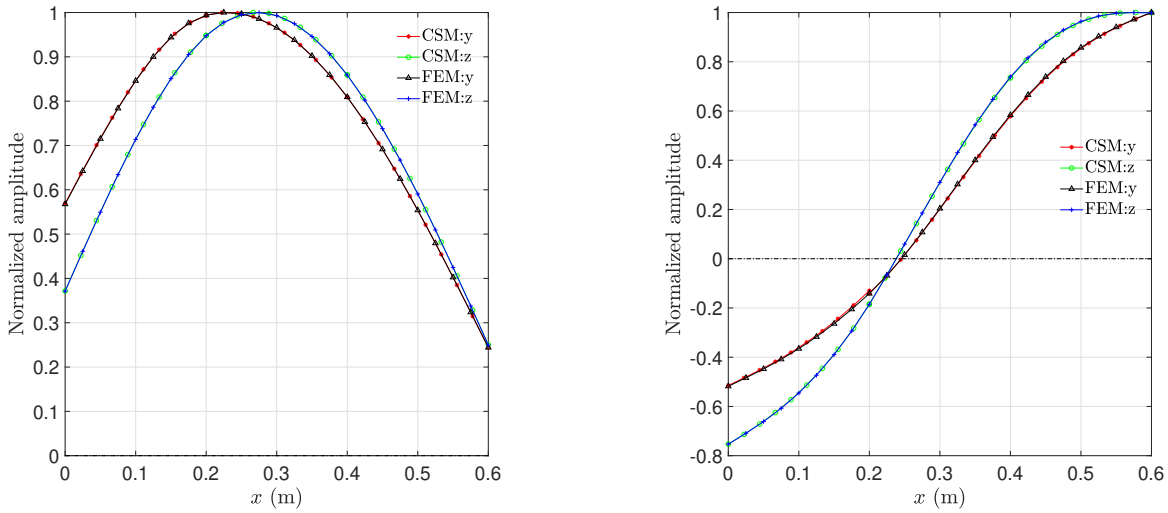

Figure 14: Horizontal and vertical forward mode shapes for case 3 with $\Omega = 2000$ rpm: (a) first and (b) second mode shape

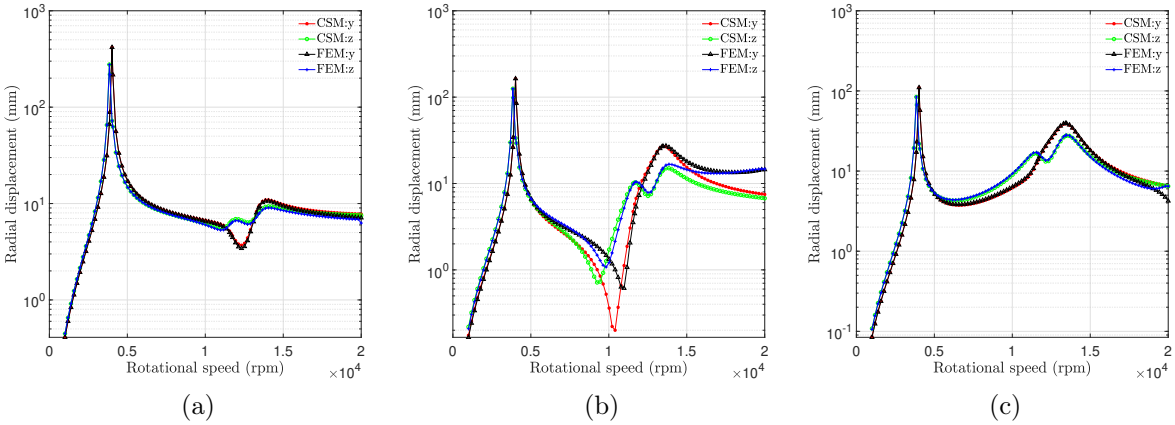

Figure 15: Unbalance responses for case 3 at: (a) disk, (b) bearing 1 and (c) bearing 2.

both methods are presented in Fig. 15. Comparing these results with the isotropic rotor, Figure 10, one can note that the vertical and horizontal displacements are different and additional critical speeds can be seen, which correspond to the backward critical speeds. The agreement between the CSM and FEM was very good; the responses were mostly different at bearing 1 near 10000 rpm, just as in case 1. The orbits of the rotor at this speed are shown in Fig. 16 in the same three locations. The orbits are in great agreement in most of the speed range, except at bearing 1 near the second backward critical speed, around 13000 rpm. The difference in the responses at bearing 1 may be due to the different modeling approaches of the CSM and FEM, as indicated in Fig. 15b, mainly in the y direction (without weight effect), causing a delay in the backward/forward transition rotation speed between the models. In this case, FEM appears slightly more conservative

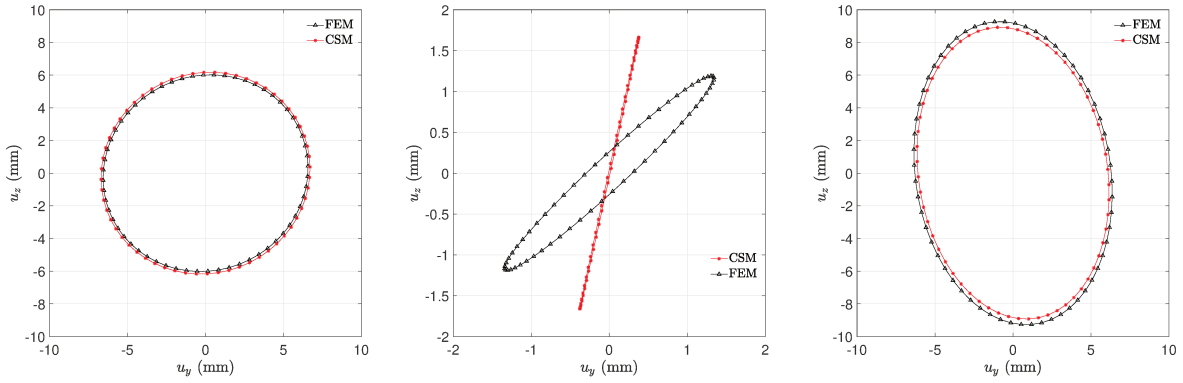

(a) (b) (c)

Figure 16: Rotor orbit for case 3 with $\Omega = 10^4$ rpm at: (a) disk, (b) bearing 1 and (c) bearing 2.

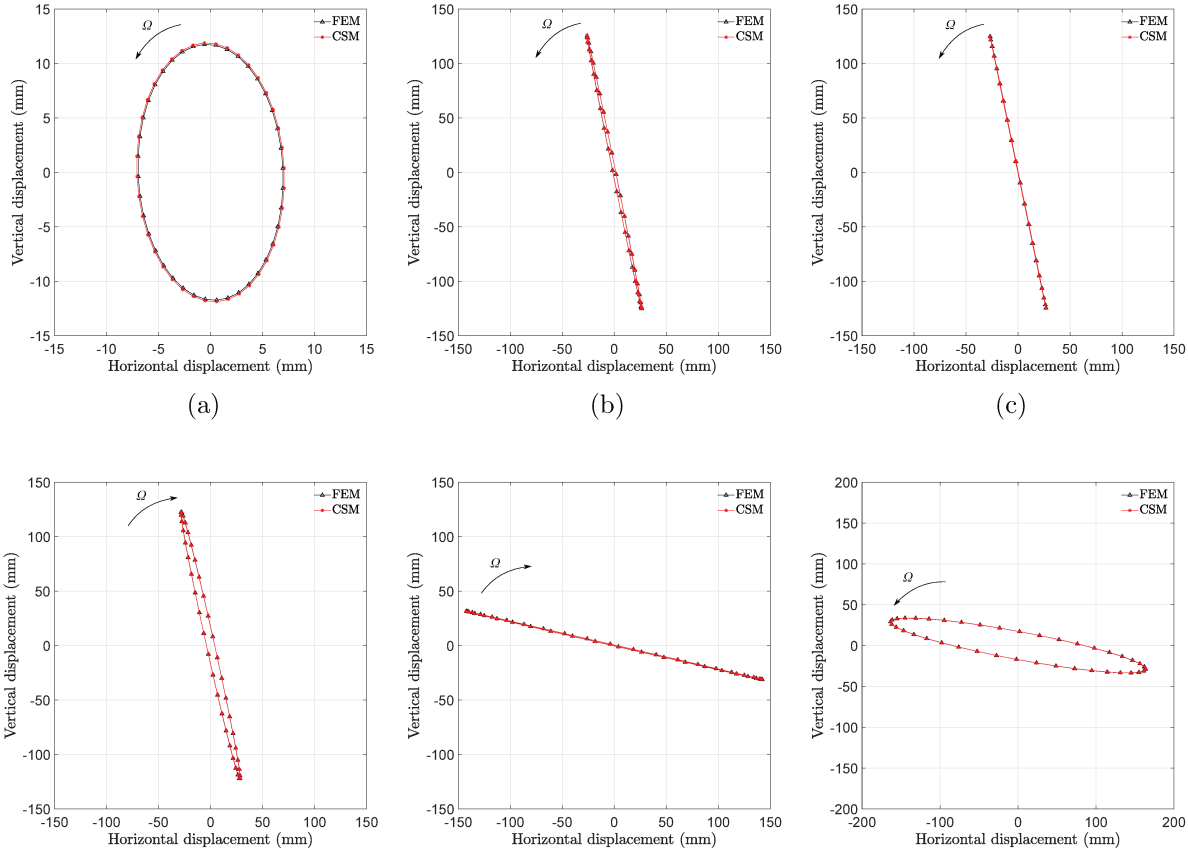

(a) (b) (c)

(d) (e) (f)

Figure 17: Rotor orbits for case 3 at bearing 1 showing the passage through the first two critical speeds ω_1 and ω_2: (a) $\Omega = 0.9\omega_1$ (FW whirl), (b) $\Omega = \omega_1$ (FW whirl), (c) $\Omega = 1.004\omega_1$ (FW whirl), (d) $\Omega = 1.0022\omega_1$ (BW whirl), (e) $\Omega = 0.996\omega_2$ (BW whirl) and (f) $\Omega = \omega_2$ (FW whirl) .

then CSM.

Figure 17 shows the orbits between the critical speeds. It is well known that a rotor on anisotropic supports present a transition from forward to backward whirl between the first two critical speeds (KRÄMER, 1993). The orbits on Fig. 17 illustrate the exact moments when this transition occurs. As the results points out, the CSM and FEM where very close in this analysis.

7.2 Asymmetric rotor

For the asymmetric rotor, the same rotor system depicted in Fig. 7 was considered, with the properties listed in Table 1. However, the moments of inertia of the shafts were distinct in the two orthogonal directions, thus the model presented in Chapter 5 was used. Similarly to the previous example, a FEM-based model was also established to evaluate the CSM for asymmetric rotors. The matrices for asymmetric rotors using FEM can be consulted in Friswell et al. (2010), Kang et al. (1992) or Jei and Lee (1988).

In this study three cases are considered. In the first case, the rotor is uniformly asymmetric, that is, the shaft has the same asymmetry along its length. The second case considers a general asymmetric rotor, where the three segments have different asymmetry in the moments of inertia. In both these cases the disks and bearings are not considered, and the shaft is simply supported. The disk and bearings are taken into account in the last case, where one has an asymmetric disk and shaft on isotropic bearings.

7.2.1 Uniformly asymmetric rotor

In the first case, the asymmetry of the rotor was considered the same for all three segments. The cross-section area was $A = 3.9815$ cm^2, and the moments of inertia considered were $I_y = 2 \times 10^{-4}$ and $I_z = 3/5 I_y$, which gives an asymmetry ratio of $\gamma = I_2/I_1 = 0.25$. The remaining parameters are the same as listed in Table 1. Figure 18 shows the Campbell diagram in the rotating and stationary frame obtained using the CSM and FEM. Since the models are in the rotating frame, the line $\omega = \Omega$ is on the x axis. The natural frequencies for mode i in the stationary frame can be obtained as $\omega_i^S = \omega_i^R \pm \Omega$, where S denotes stationary and R rotating frame. This transformation essentially rotates the diagram in the rotating frame, giving the results shown in Fig. 18b. Also, note that by performing the transformation $\omega_i^S = \omega_i^R \pm \Omega$ additional speeds appear from the negative y axis, which in reality correspond to the same mode of vibration i but with inverted speed (-Ω). The reader is referred to Jei and Lee (1992b) for more information.

The shaded area in the diagram of Fig. 18 represents the unstable range, which is between the first, ω_1, and second, ω_2, critical speeds. From Fig. 18, the agreement between the CSM and FEM can be clearly observed. The first and second forward mode

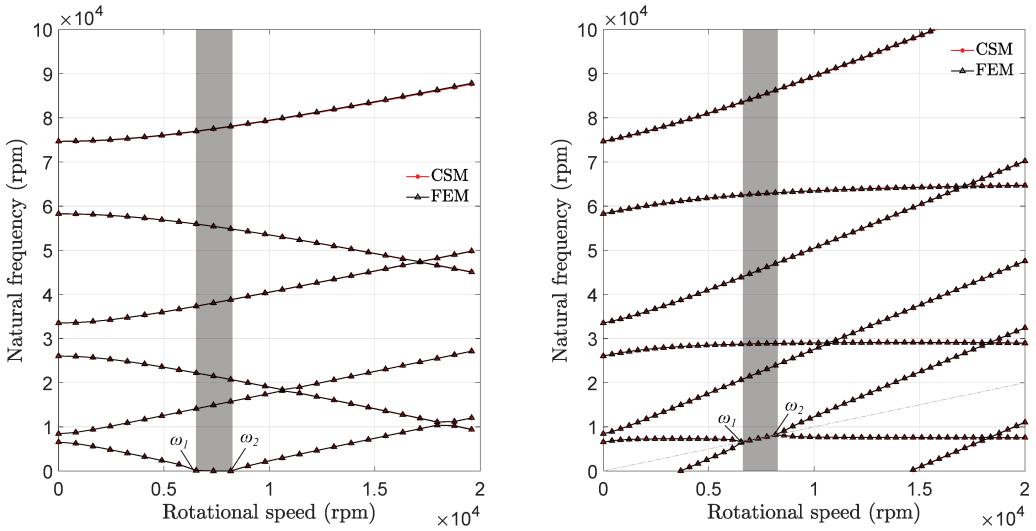

Figure 18: Campbell diagram for the uniformly asymmetric rotor: (a) rotating frame and (b) stationary frame.

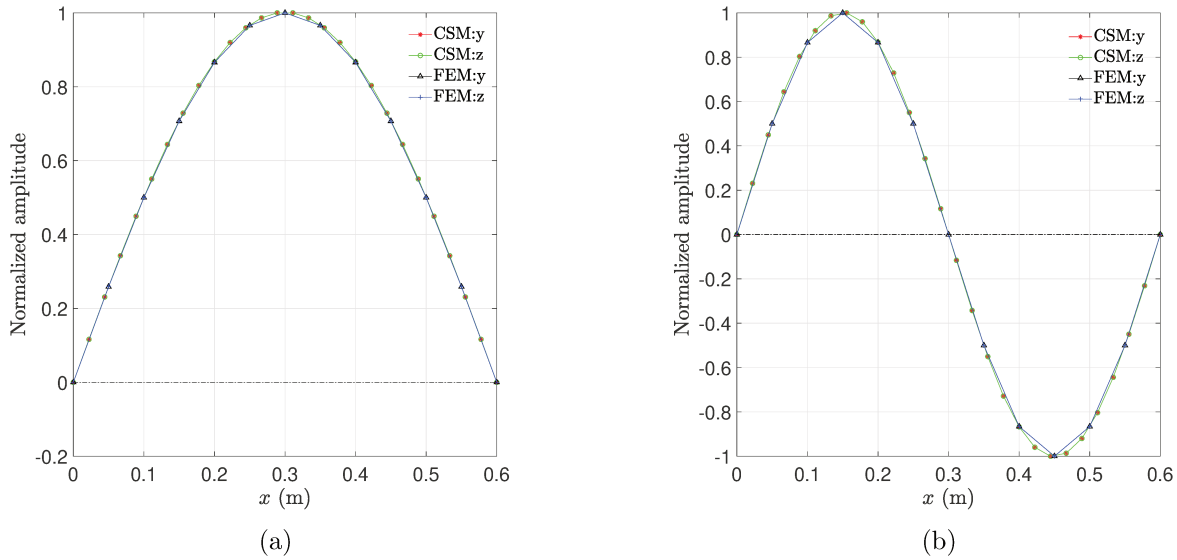

Figure 19: Horizontal and vertical forward mode shapes for the uniformly asymmetric rotor with $\Omega = 1000$ rpm: (a) first and (b) second mode shape

shapes are shown in Figure 19. Since the rotor is simply-supported, the mode shapes are simply sine functions and they are the same for both orthogonal directions.

7.2.2 General asymmetric rotor

The next step was to consider different asymmetries for the rotor segments. In this case, the cross-section areas were $A_1 = 4.3025\ \text{cm}^2$, $A_2 = 3.9815\ \text{cm}^2$ and $A_3 = 3.6603\ \text{cm}^2$;

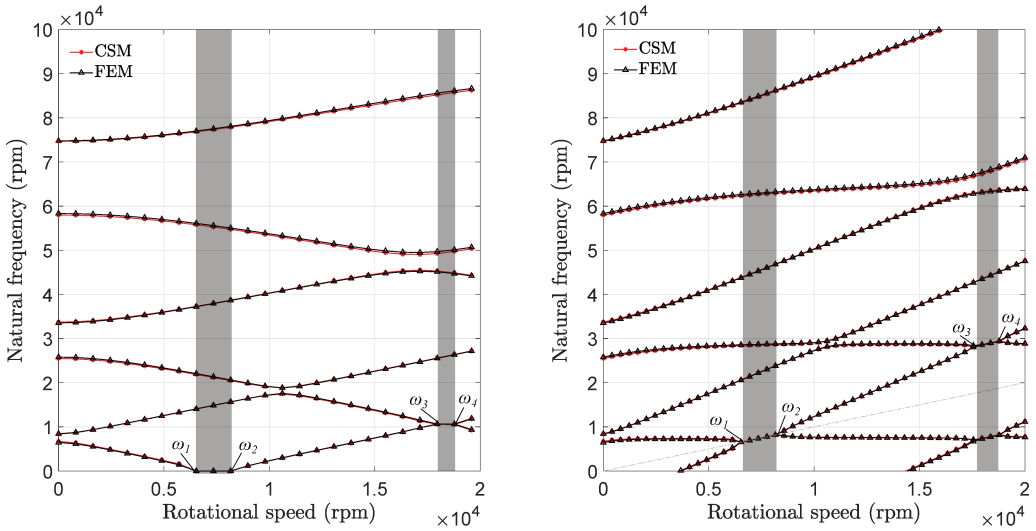

Figure 20: Campbell diagram for the general asymmetric rotor: (a) rotating frame and (b) stationary frame.

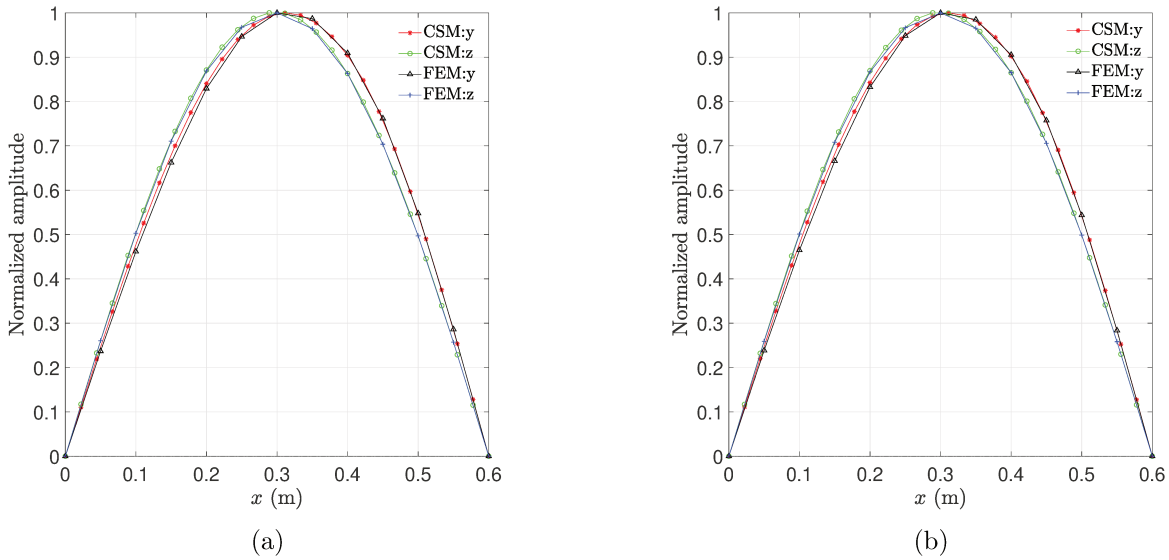

Figure 21: First horizontal and vertical mode shapes for the general asymmetric rotor at $\Omega = 1000$ rpm: (a) first forward and (b) first backward.

while the area moments of inertia were $I_{y1} = I_{y2} = I_{y3} = 1.6286$ cm^2, $I_{z1} = 9/11 I_{y1}$, $I_{z2} = 3/5 I_{y1}$ and $I_{z3} = 3/7 I_{y1}$; which gives the values for asymmetries as $\gamma_1 = 0.1$, $\gamma_2 = 0.25$ and $\gamma_3 = 0.4$. Table 1 lists the remaining parameter. The rotor was also simply-supported at both ends and the disk is not considered.

The Campbell diagram is shown in Fig. 20. Comparing the results with the previous case, Figure 18, one notes that the general asymmetric rotor shows an additional unstable region in the same speed range. This second region, however, is not between

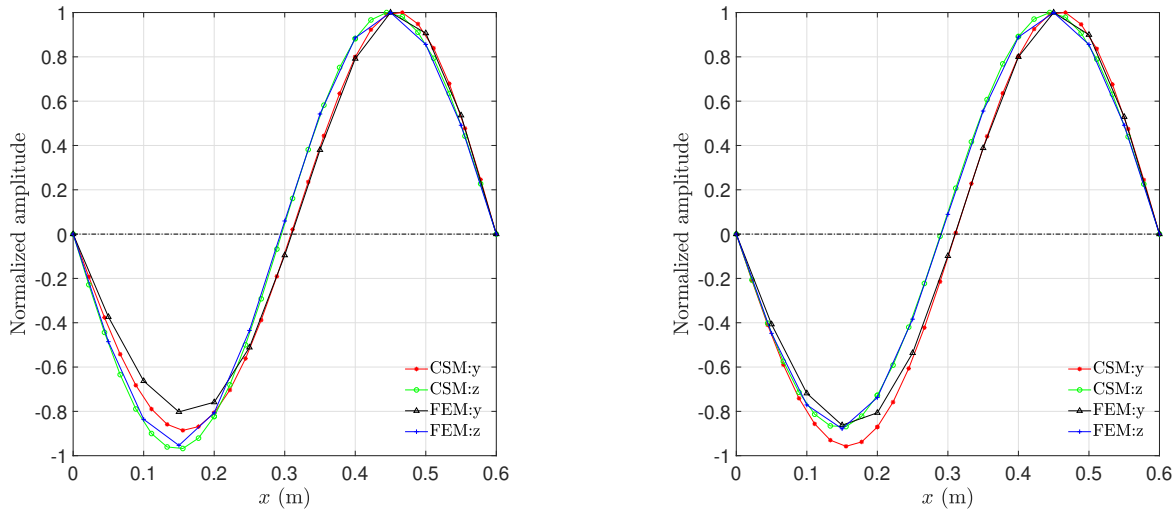

Figure 22: Second horizontal and vertical mode shapes for the general asymmetric rotor at $\Omega = 1000$ rpm: (a) second forward and (b) second backward.

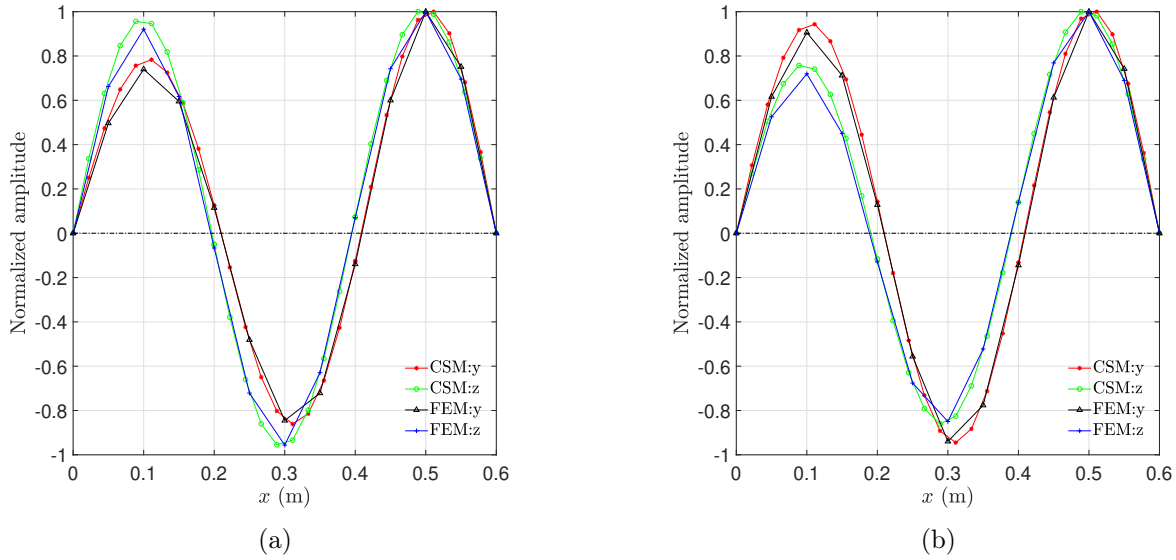

Figure 23: Third horizontal and vertical mode shapes for the general asymmetric rotor at $\Omega = 1000$ rpm: (a) third forward and (b) third backward.

critical speeds as the first one, since the natural frequencies do not become zero in the rotating frame nor cross the line $\omega = \Omega$ in the stationary frame. In addition to this, while in the uniformly asymmetric rotor the natural frequencies crossed each other, in this case they somewhat "repel" each other avoiding an intersection. This phenomenon is seen often in asymmetric rotors and it is known as *curve veering* (CRANDALL; YEH, 1989; JEI; LEE, 1992a).

The first three forward and backward mode shapes are shown in Figs. 21-23. Due

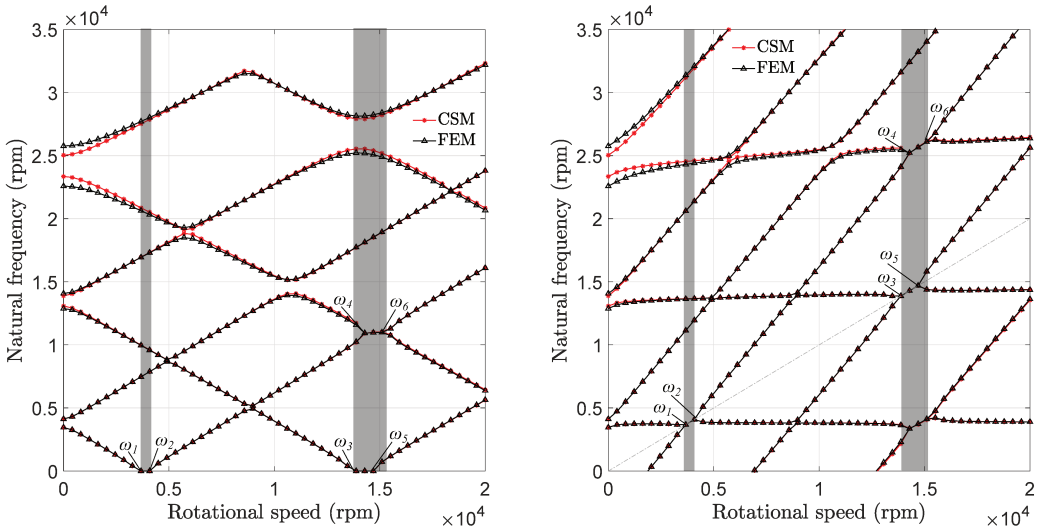

Figure 24: Campbell diagram for the asymmetric rotor with disks and bearings: (a) rotating frame and (b) stationary frame.

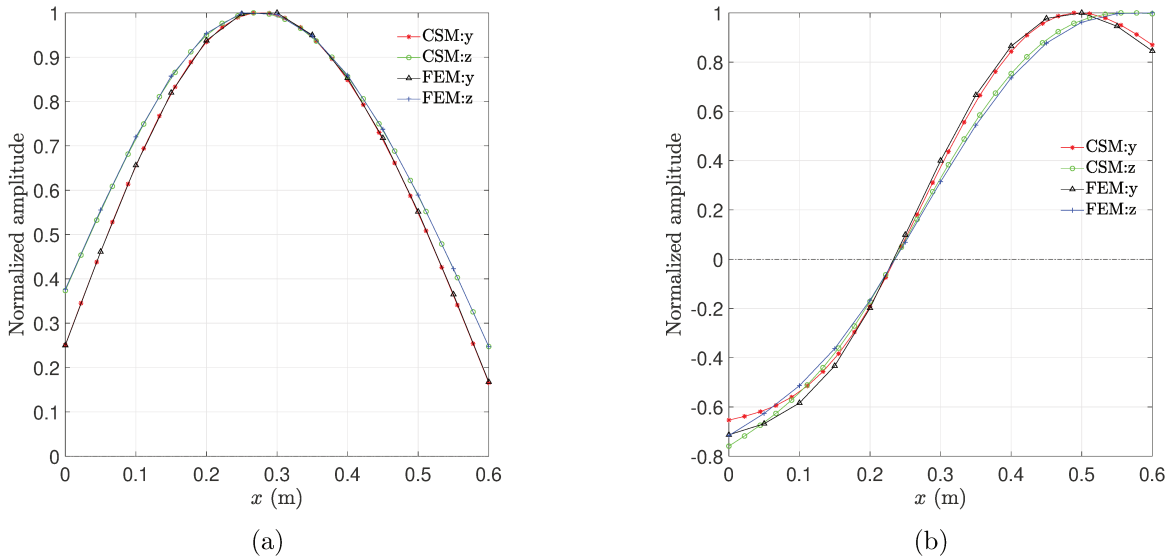

Figure 25: Horizontal and vertical forward mode shapes for the asymmetric rotor with disks and bearings with $\Omega = 1000$ rpm: (a) first and (b) second mode shape.

to the different asymmetry in the segments, the mode shapes are not sine functions, and are distinct in the horizontal and vertical directions. This case finally points a great agreement between the CSM and FEM.

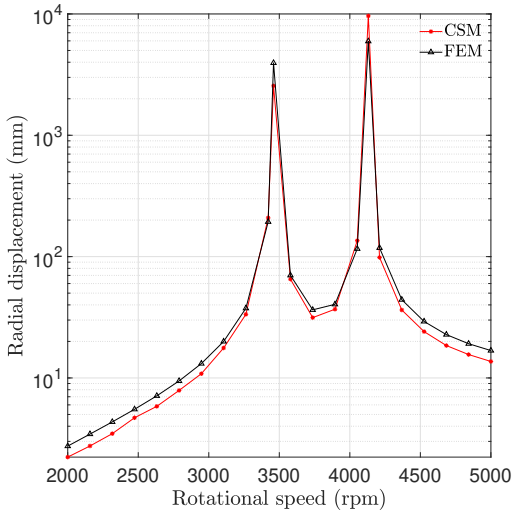

Figure 26: Unbalance response of the asymmetric rotor with disks and bearings at the disk.

7.2.3 Asymmetric rotor with disk and bearings

So far the rotor was considered simply-supported and with no disk. In this case, the disk and the elasticity of the bearings are also considered. The shaft has the same properties as in the uniformly asymmetric rotor: $A_1 = A_2 = A_3 = 3.9815$ cm^2, $I_{y1} = I_{y2} = I_{y3} = 1.6286$ cm^{4}and $I_{z1} = I_{z2} = I_{z3} = 3/5I_y$. The bearings are identical and isotropic with stiffness of $k = 10^6$ N/m and with no damping. The disk is asymmetric with mass $M = 2.0275$ kg, and mass moment of inertia of $J_y = 0.003$ kg·m^2 and $J_z = 3/5J_y$. The principal axis of the disk are considered to be aligned to that of the shaft, as discussed in Chapter 5.

Figure 24 shows the Campbell diagram of the asymmetric rotor with disk and bearings. Two unstable regions can be detected, as shown by the shaded areas. In the second unstable region, one has a combination of two unstable modes. Also, this diagram shows a combination of natural frequencies crossing and repelling each other, which was different from the previous cases. The CSM and FEM differ a little in their results, but the overall behavior of the natural frequencies was similar. Figure 25 shows the forward mode shapes. Due to the asymmetry, the horizontal and vertical mode shapes are different. The agreement was very good between the both methods for the mode shapes.

The unbalance response of the system at the disk location is shown in Fig. 26. The unbalance moment was set to $m_u e = 0.0213$ kg·m and it was introduced at the disk. The effect of gravity was neglected. Also, the phase of the unbalance, which makes a lot of difference in the asymmetric rotor, was set to $\theta = 45°$ and two modes (two forward and two backward) were used. Also, damping was introduced with a coefficient of $c = 10^2$ Ns/m. As one can note from the response, two peaks occur corresponding to two critical

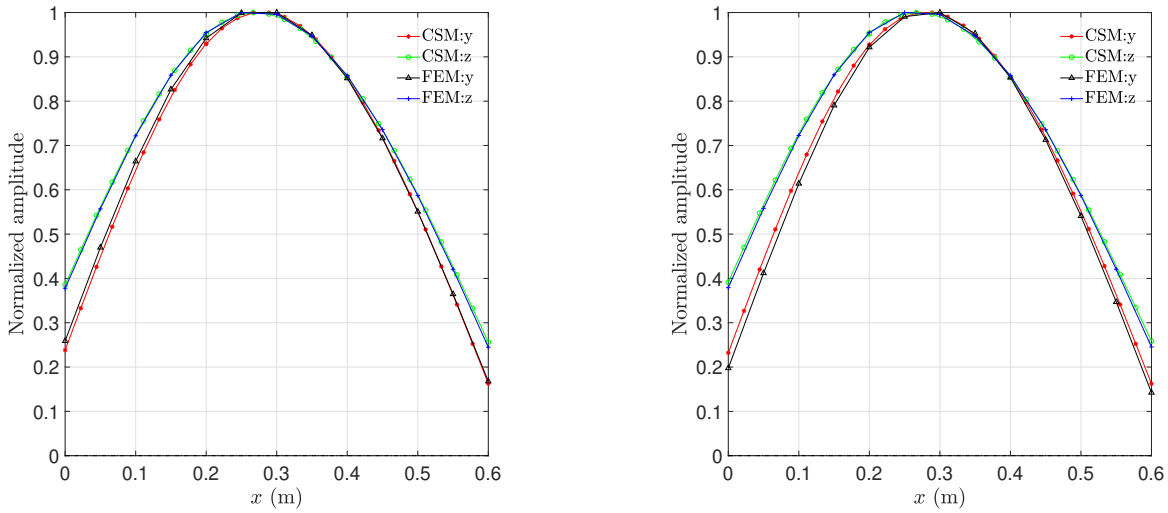

Figure 27: First horizontal and vertical forward mode shapes for the asymmetric rotor with disks and bearings at the critical speeds: (a) $\Omega = 3459$ rpm and (b) $\Omega = 4131$ rpm.

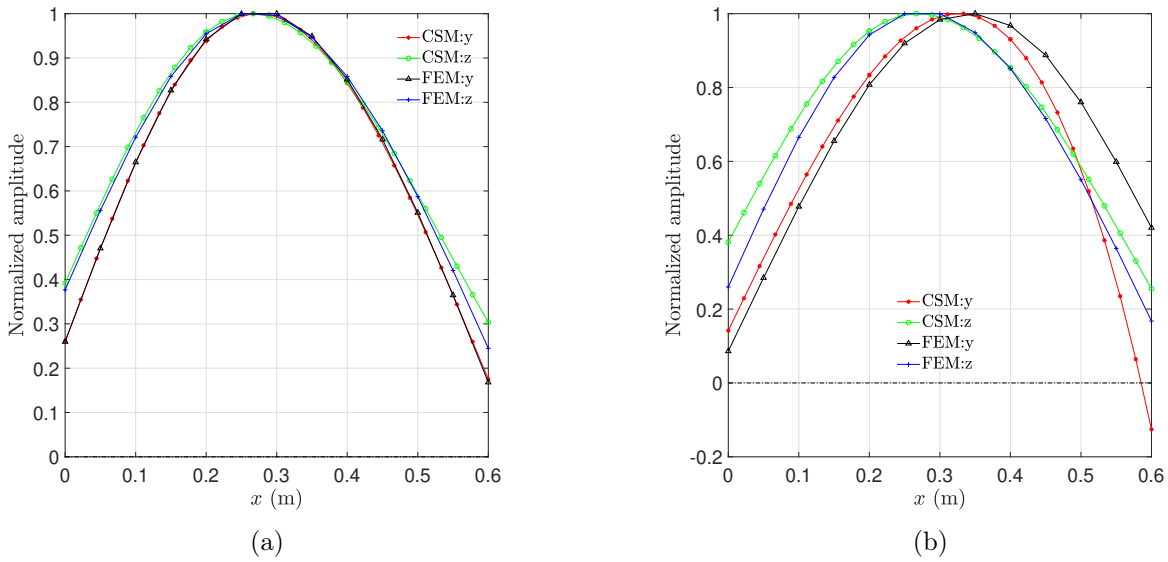

Figure 28: First horizontal and vertical backward mode shapes for the asymmetric rotor with disks and bearings at the critical speeds: (a) $\Omega = 3459$ rpm and (b) $\Omega = 4131$ rpm.

speeds, 3459 rpm and 4131 rpm. The response between these two speeds are unstable, as shown in Fig. 24, thus these solutions are not achievable and the response amplitude grows exponentially. This could be avoided by increasing the damping coefficient, making the rotor stable in all operating speeds.

Figures 27 and 28 shows the first and second mode shapes at the critical speeds. The first mode shapes suffers little difference between the two speeds, while for the second mode shape one can see a great difference. It is noted that for higher speeds the mode

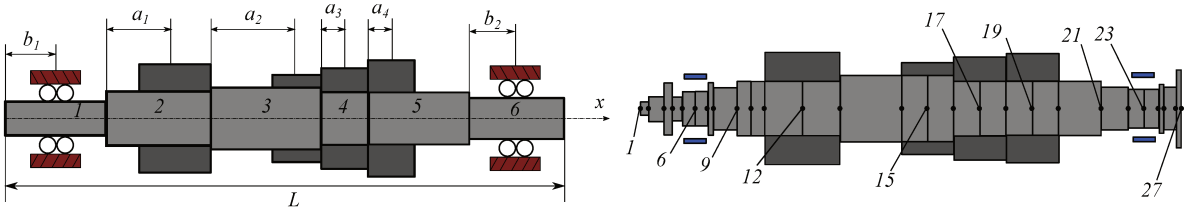

(a) (b)

Figure 29: Multi-stepped rotor: (a) CSM and (b) FEM mesh.

shapes given by the CSM and FEM start to differ more, as shown in Fig. 28. However, the unbalance response showed that the displacement was in good agreement, as Fig 26 shows. With the results presented, one can conclude that the CSM is a reliable alternative to model rotors with asymmetric shafts and disks.

7.3 Multi-stepped rotor

In this example, a multi-stepped rotor is studied. The FEM mesh is shown in Fig. 29b. This mesh was obtained by modeling a real turbomachine using the FEM. Table 3 shows the dimensions of the 26 Timoshenko beams elements used. The rotor has a total length of $L = 2.5$ m and four disks positioned at nodes 12, 15, 17 and 19, with the dimensions shown in Tab. 4. Additionally, two identical bearings are placed at nodes 6 and 25, with coefficients $k_{yy} = 10^9$ N/m, $k_{zz} = 6 \times 10^8$ N/m, $c_{yy} = 10^5$ Ns/m, $c_{zz} = 6 \times 10^4$ Ns/m and $k_{yz} = k_{zy} = c_{yz} = c_{zy} = 0$. Note that not only the stiffness, but also the damping is considered anisotropic.

The model based on the CSM is shown in Fig. 29a, and it has 6 segments. This

Table 3: FE mesh data.

Element	Length (mm)	Diameter (mm)	Element	Length (mm)	Diameter (mm)
1	37.5	60	14	122	300
2	73.5	111.8	15	122	300
3	37.7	242	16	122	248
4	53.3	108.8	17	122	248
5	61	159.76	18	122	248
6	61	159.76	19	122	248
7	23.1	237	20	195.9	248
8	113.9	199.6	21	125	199.6
9	62.5	248	22	72.5	179.73
10	62.5	248	23	72.5	179.73
11	175.5	248	24	20	220
12	175.5	248	25	50	199.7
13	284	300	26	11	354

Table 4: Disks and bearings dimensions.

Parameter		Symbol	Value (mm)
	Position	a_1	300.5
Disk 1	Diameter	D_1	550
	Length	h_1	351
	Position	a_2	406
Disk 2	Diameter	D_2	350
	Length	h_2	244
	Position	a_3	122
Disk 3	Diameter	D_3	400
	Length	h_3	244
	Position	a_4	122
Disk 4	Diameter	D_4	450
	Length	h_4	244
Bearing 1	Position	b_1	263
Bearing 2	Position	b_2	197.5

model is based directly on the FEM mesh. Segment 1 has a length of $L_1 = 461$ mm and models elements from 1 to 8 in the mesh, and the diameter adopted was the mean diameters of these elements, giving $d_1 = 170$ mm. Segments 2, 3, 4 and 5 represent elements from 9 to 12, 13 to 15, 16 to 17 and 18 to 20, respectively. The dimensions of the segments are the same as in the mesh, namely, $d_2 = d_4 = d_5 = 248$ mm, $d_3 = 300$ mm, $L_2 = 476$ mm, $L_3 = 528$ mm, $L_4 = 244$ mm, $L_5 = 439.9$ mm. Segment 6 has a length of $L_6 = 351.1$ mm and a diameter of $d_6 = 222$ mm, which was obtained as the mean diameter of elements from 21 to 26. The bearings and disks are located at the same coordinates as in the FEM mesh; the local coordinates are shown in Tab. 4. It is noted that, since simplifications has been adopted in the CSM model (utilizing mean diameters for instance), the results will no longer be exactly the same.

Figure 30 shows the Campbell diagram and logarithmic decrement obtained with the CSM and FEM. The anisotropy of the system is clearly seen, as the backward and forward natural frequencies are different even at zero rotational speed. The behavior of the natural frequencies given by both methods are not identical as in the previous examples, since the system is more complex now, but one can conclude that they are fairly similar. An interesting outcome is the third forward natural frequencies. Both CSM and FEM showed a curve veering similar to that seen in the asymmetric rotor. As for the logarithmic decrement, one notes that the CSM predicts in general higher damping than the FEM, but the behavior for different rotational speeds are similar nonetheless, since the errors do not increase with the speed. The first and second undamped forward mode shapes are presented in Fig. 31. As seen in previous cases, the anisotropy causes the horizontal and vertical mode shapes to be different. The mode shapes given by the CSM and FEM were not identical, but one notes great similarities. The amplitudes differed the most in segment 1 in the CSM or elements 1 to 8 in the FEM, due to the approach assumed for

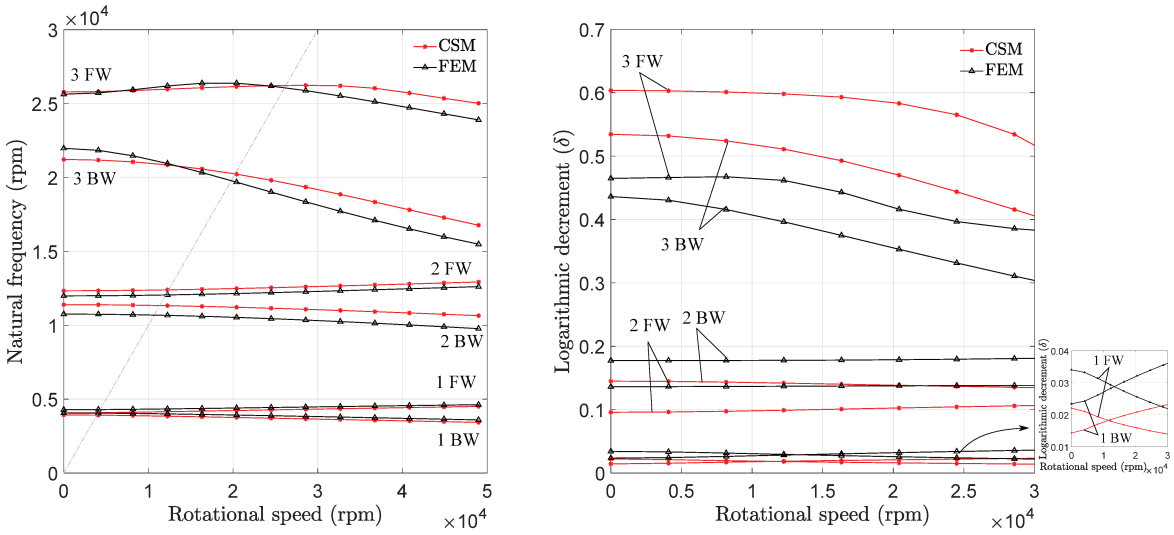

(a) (b)

Figure 30: Multi-stepped rotor results: (a) Campbell diagram and (b) logarithmic decrement.

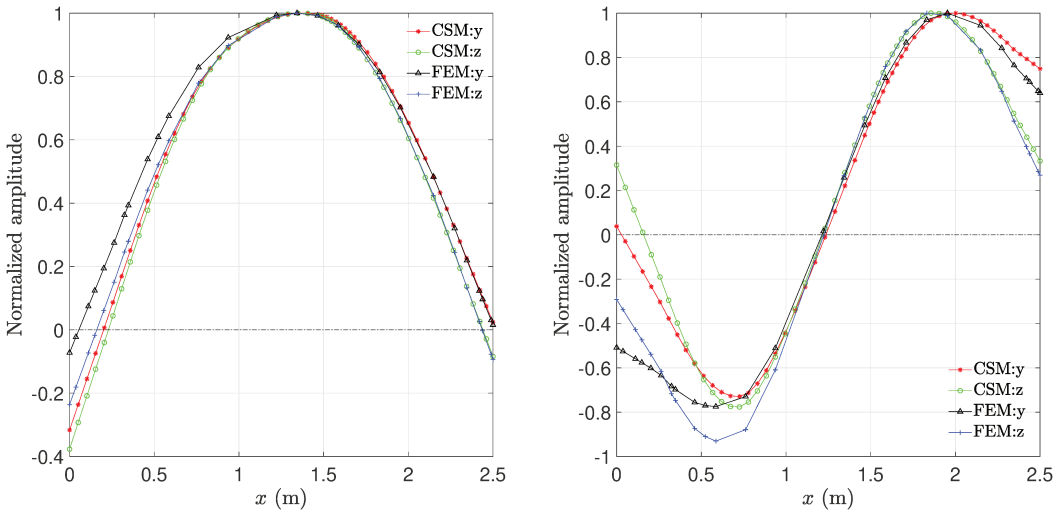

(a) (b)

Figure 31: Horizontal and vertical undamped forward mode shapes for the multi-stepped rotor with $\Omega = 2000$ rpm: (a) first and (b) second mode shape.

the diameter. Future investigation should improve these results searching for a better equivalent diameter at each section.

Sequentially, an unbalance moment of $m_u e = 0.0213$ kg·m was introduced at disk 2, which is located at $x_u = 1.343$ m from the left free end or node 15 in the FEM model mesh. The phase of the unbalance is considered zero. In the CSM, three modes were used to obtain the responses. Figure 32 shows the amplitudes of the rotor at the unbalance location, bearing 1 and bearing 2. Since the system is anisotropic, the horizontal and

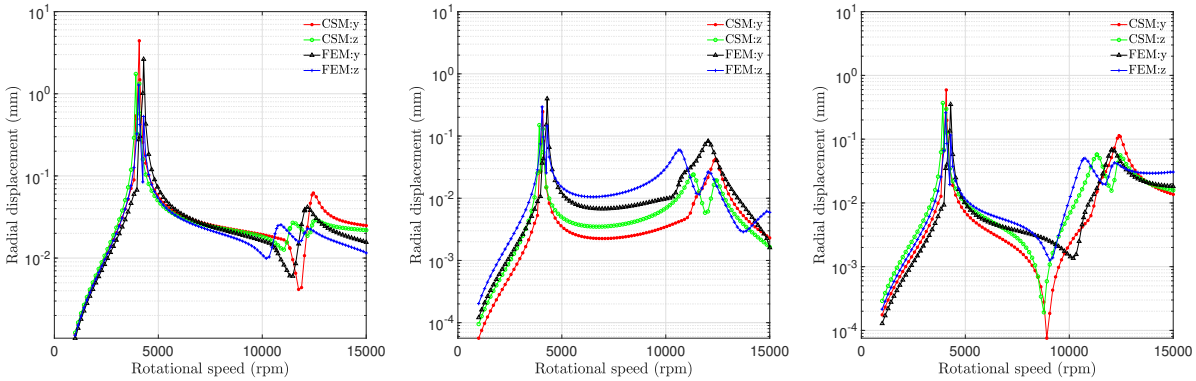

Figure 32: Unbalance responses for the multi-stepped rotor at: (a) unbalance location, (b) bearing 1 and (c) bearing 2.

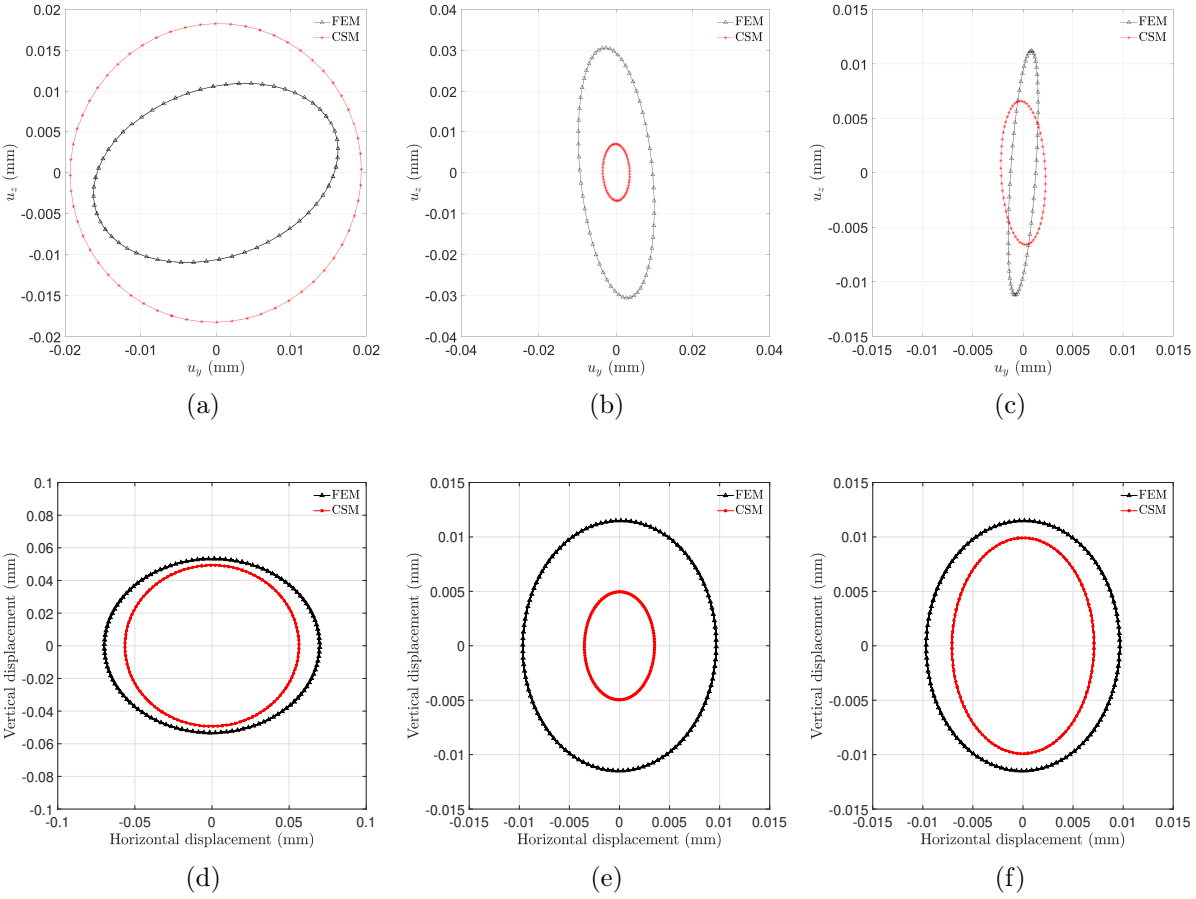

Figure 33: Multi-stepped rotor orbit at $\Omega = 10^4$ rpm (a) unbalance location, (b) bearing 1 and (c) bearing 2; and at $\Omega = 5000$ rpm (d) unbalance location, (e) bearing 1 and (f) bearing 2.

vertical amplitudes are different, and the orbit is an ellipse. As one can note from the results, the amplitudes predicted by both methods were satisfactory close. Since the

critical speeds were not the same, the peaks in the amplitudes occur at different rotational speeds. The major differences in the amplitudes predicted were at bearing 1, where the FEM model predicted higher amplitudes in general. Figure 33 shows the orbits at the same measurement points for $\Omega = 10^4$ rpm and $\Omega = 5000$ rpm. The differences in the response can be attributed to the equivalent diameters adopted in the CSM method, which become more relevant at higher speeds due to inertia effects.

7.4 Rubbing response

This section presents a rubbing analysis, for the purpose of evaluating the CSM for nonlinear studies in rotordynamics using the impact model presented in Chapter 6. In that matter, the same system used in the first example, depicted in Fig. 7, is used. The dimensions are the same as shown in Tab. 1. The bearings are considered isotropic with coefficients $k_{yy} = k_{zz} = k = 10^6$ N/m, $c_{yy} = c_{zz} = c = 50$ Ns/m, $k_{yz} = k_{zy} = c_{yz} = c_{zy} = 0$. The impact is considered to occur on the disk rather than on the shaft. When the impact is on the disk, less modes of vibration can be used since the lumped mass of the disk in general dominates the dynamics of the rotor system. This is done in order to simplify the analysis, as in real rotating machines rubbing can occur at any point of the rotor. The impact stiffness that it is used in the contact model is considered ten times the bearing stiffness, thus $k_h = 10^7$ N/m, and the impact damping is not considered. To define the stator clearance, a rotor's radius to clearance ratio of $R/d_c = 120$ was defined, giving $d_c = 0.1$ mm. Such radius to clearance ratio are common in real turbomachines (BHATTACHARYA; CHILDS, 2009). The speed is fixed at 60 % the first critical speed of the system, giving $\Omega = 6443.1$ rpm, and the unbalance moment is $m_u e = 0.111$ kg·mm. The parameters are also listed in Tab. 5.

In order to evaluate the CSM, a FEM based model was also established with 9 standard beam elements considering rotary inertia and shear deformation. The same dimensions, material properties and impact model were used in the FEM model. The rubbing responses were obtained by means of the integrator *ode45* of the software Matlab. For the CSM model, three modes (three forward and three backward) were used in the discretization of the equations of motion, while in the FEM model, all degrees of freedom

Table 5: Parameters used for the rubbing analysis.

Parameter	Symbol	Value
Impact stiffness	k_h	10^7 N/m
Impact damping	c_h	0 Ns/m^2
Rotational speed	Ω	6443.1 rpm
Radial clearance	d_c	0.1 mm
Unbalance moment	$m_u e$	0.111 kg·mm

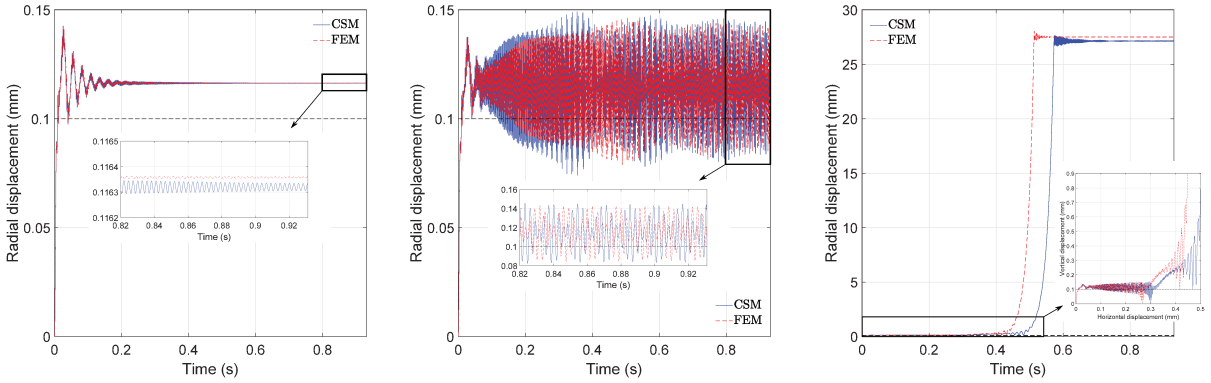

Figure 34: Radial displacement for: (a) $\mu_m = 0.05$, (b) $\mu_m = 0.1$ and (c) $\mu_m = 0.11$. The black dashed line represent the radial clearance.

were considered, that is, no reduction was applied in the equations.

Figure 34 shows the radial displacement under rub for the CSM and FEM considering different friction coefficients. The results of the first 100 cycles are shown. Three different rub cases are outlined: in Fig. 34a for $\mu_m = 0.05$, the rotor enters in Forward Annular Rub (FWAR), where the rotor enters in a state of continuous contact. For an increased friction coefficient of $\mu_m = 0.1$, the rotor enters in a Forward Partial Rub (FWPR) state, with successive contacts throughout the whirl motion, as shown in Fig. 34b. Increasing the friction a bit more to $\mu_m = 0.11$, Figure 34c shows that the rotor enters in a backward motion, also known as Dry-friction Whip (DWP), whirling far beyond the clearance. This motion can readily be identified as DWP due to the unstable nature of it, which leads to large displacements (JIANG; ULBRICH, 2005). When modeling rotors under rub, the detection of the onset of the DWP is very important, and the result showed that both CSM and FEM predicted this phenomenon at similar simulation times and friction coefficients. It's worth mentioning that the displacements well over the clearance seen in Fig. 34c occurs due to numerical errors, as in experiments the rotor whirls around the clearance as shown in Yu et al. (2000) and Ehehalt et al. (2019). The rub states FWAR, FWPR and DWP were explained in detail in Chapter 6.

The orbits of the rotor for the 100 cycles, the first 10 cycles and the last 10 cycles are presented in Figs. 35, 36 and 37, respectively. The first ten cycles shows almost no difference between the three friction cases. The last ten cycles, however, clearly depict the final states reached by the rotor, which were completely different. From the results, one notes significant agreement between the CSM and the FEM. However, the computational costs were far lower for the CSM. Using a personal computer with Windows 10 and an Intel i7-7500U processor, the times to obtain the 100 cycles shown in Fig. 34 were, respectively: 1.96 s, 1.28 s, and 366 s. For the FEM, using the same computer, the simulation times

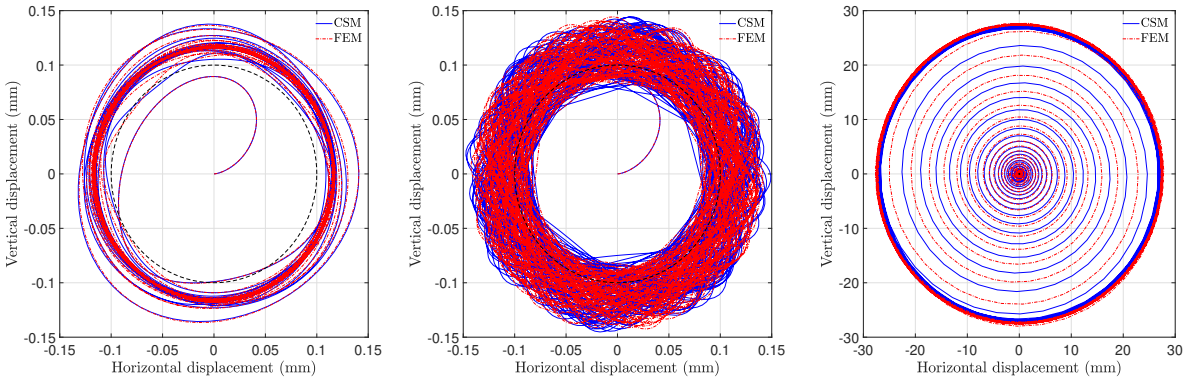

(a) (b) (c)

Figure 35: Rotor orbits for 100 cycles: (a) $\mu_m = 0.05$, (b) $\mu_m = 0.1$ and (c) $\mu_m = 0.11$. The black dashed line represent the radial clearance.

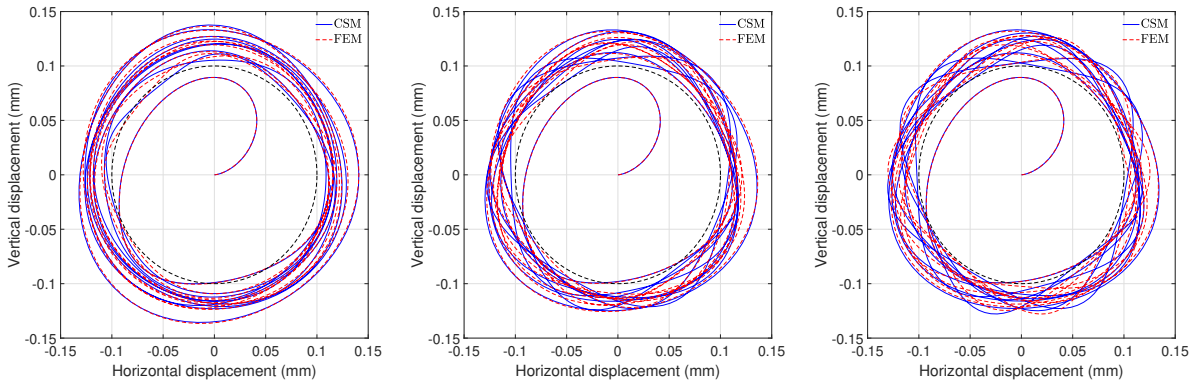

(a) (b) (c)

Figure 36: Rotor orbits for the first 10 cycles: (a) $\mu_m = 0.05$, (b) $\mu_m = 0.1$ and (c) $\mu_m = 0.11$. The black dashed line represent the radial clearance.

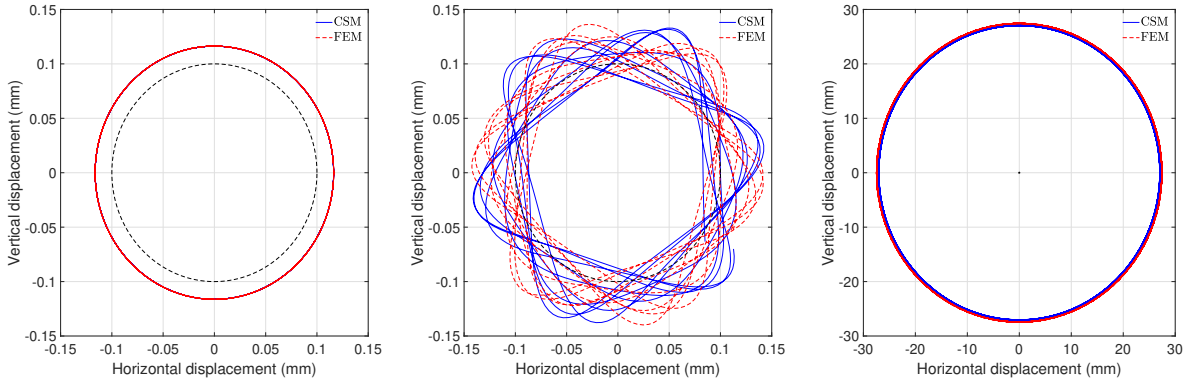

(a) (b) (c)

Figure 37: Rotor orbits for the last 10 cycles: (a) $\mu_m = 0.05$, (b) $\mu_m = 0.1$ and (c) $\mu_m = 0.11$. The black dashed line represent the radial clearance.

were: 186.8 s, 194.5 s and 251.6 s. It is worth noting that no reduction in the FEM equations were performed, thus leading to a large number of equations when compared with the CSM.

7.5 Additional comments

This chapter presented different applications of the CSM, which in every case were evaluated by comparing the results with the ones given by the FEM. The CSM provides exact solutions for rotors with stepped cross-sections, and it can be applied to a wide variety of systems, from isotropic to asymmetric rotors. Before reaching to some conclusions, it is worth mentioning some aspects of the numerical solutions. Firstly, the eigenvalue problem of the CSM consist of a transcendental equation, which is considerable more difficult to solve than the problem for the FEM, a polynomial equation. These equations have to be solved for a great number of rotational speeds to obtain the Campbell diagrams. In this regard, the FEM proves much faster than the CSM, specially in the asymmetric rotor, which, due to the size of the functions, showed a very slow solution. However, the Campbell diagram comparison was quite necessary to qualify the CSM accuracy and representativeness. The main application of CSM lays on applying reduced models to nonlinear analysis, uncertainties quantification and controller design for rotating machines. Meanwhile, since the results given by the CSM are exact, provided the segments have constant cross-sections, they can be used to evaluate different FEM procedures, comparing different elements sizes and different shape functions. In case one needs higher modes of vibration, for example to perform acoustic analysis, the CSM can be a better choice, since the discretization needed in the FEM would require a highly dense mesh.

8 Conclusions

This work aimed at presenting a method for the mathematical modeling of rotor systems with several segments, disks and bearings. Since the understanding and prediction of faults of the machines are highly dependent on models, ever accurate representations of them are always required in engineering applications. In this manner, the contribution of the present work is to offer an additional tool for designers and engineers to study rotating machines.

The main idea of the method, named Continuous Segment Method (CSM), is to use eigenfunctions, obtained directly from the partial differential equations that govern the system, written in complex form. The bending and shear deformation are taken into account in the model, but axial and torsional motions are neglected. The method is valid for rotor systems with several segments with constant cross-sections each and with any number of disks and bearings. By means of the CSM, the critical speeds, mode shapes and forced response can be obtained for very general rotor systems, including rotors with anisotropic bearings and asymmetric shafts.

The CSM allows one to solve the eigenvalue problem of the system by dividing the domain into subdomains or segments. Each segment is a beam with uniform cross-section with disks and bearings. The approach followed is to solve the local eigenvalue problems to obtain the local eigenfunctions, and then use continuity conditions to arrive at the global functions and the eigenvalues. With the eigenfunctions of the system at hand, modal analysis is applied to discretize the equations leading to uncoupled differential equations for the modal coordinates. The number of equations needed to be solved equals the number of modes required for the analysis. The solutions of the CSM are exact for rotors with stepped cross-sections, rigid disks and linear bearings.

The evaluation of the proposed model was done by means of numerical simulations, where the results were compared to the well known Finite Element Method (FEM). The results consisted of Campbell diagrams, logarithmic decrement and unbalance response for three rotor systems with different configurations. For the rotor systems with simpler geometries, the natural frequencies and mode shapes were closely coincident both CSM and FEM. When considering a more complex rotor discrete discrepancies can be observed, but the CSM proves to be a good alternative to model a wide range rotor systems, from isotropic rotors to rotors with asymmetric shafts and disks. In addition to that, the CSM can be used as a model reduction technique as it shows consistent results for a large range of rotational speeds; since most techniques present problems at high speeds, this is can be great advantage.

8.1 Future works

This section briefly mentions the improvements that can be done to the proposed method. Despite the wide applicability of the CSM, it is still limited to rotors with stepped geometries, homogeneous shafts, linear bearings and rigid disks. The method can be further expanded by considering segments with varying cross-sections or material property. Although it is not possible to solve the problems for shafts with arbitrary shapes, there are solutions for shafts with cross-sections varying linearly or exponentially as shown by Magrab (2012). The solutions of the local segment with varying cross-section can then be related to the remaining segments of the rotor system through the same continuity conditions presented for the CSM.

Elastic disks, or even blades modeled as beams, can also be incorporated in the equations of motion to generalize the CSM. In this case, the shaft model would need to account the axial and torsional movement, since the motion of the blades in general couples with the axial and torsional motion of the shaft. The approach presented by Lee and Chun (1998) can be combined with the CSM for rotors with stepped cross-sections and elastic disks.

Additionally, since real rotating machinery exhibits some kind of nonlinear behavior, the CSM can be expanded to account for nonlinearities of the shaft, in case of large deformations, or bearings. For that matter, the Nonlinear Normal Modes (NNMs) approach can be used (VAKAKIS, 1997; LEGRAND et al., 2004). To the author's knowledge, no works has been done regarding nonlinear multi-stepped rotor systems.

References

ABRAMOWITZ, M.; STEGUN, I. A.; ROMER, R. H. *Handbook of mathematical functions with formulas, graphs, and mathematical tables*. Mineola, NY: Dover Publications, Inc, 1988. 1046 p.

ADHIKARI, S.; FRISWELL, M. I.; LEI, Y. Modal analysis of nonviscously damped beams. *Journal of Applied Mechanics*, v. 74, n. 5, p. 1026–1030, 2007.

AFSHARI, H.; RAHAGHI, M. I. Whirling analysis of multi-span multi-stepped rotating shafts. *Journal of the Brazilian Society of Mechanical Sciences and Engineering*, Springer, v. 40, n. 9, p. 424, 2018.

AFSHARI, H.; TORABI, K.; JAZI, A. J. Exact closed form solution for whirling analysis of Timoshenko rotors with multiple concentrated masses. *Mechanics Based Design of Structures and Machines*, Taylor & Francis, p. 1–24, 3 2020. ISSN 1539-7734. Disponível em: <https://doi.org/10.1080/15397734.2020.1737112>.

AGRAPART, Q. et al. Multi-physics numerical simulation of an experimentally predicted rubbing event in aircraft engines. *Journal of Sound and Vibration*, Elsevier, v. 460, p. 114869, 2019.

ALBER, O.; MARKERT, R. Rotor-stator contact–overview of current research. In: EDP SCIENCES. *MATEC Web of Conferences*. Agadir, Morocco, 2014. v. 16, p. 3001.

AZEEZ, M. F. A.; VAKAKIS, A. F. Numerical and experimental analysis of a continuous overhung rotor undergoing vibro-impacts. *International Journal of Non-linear Mechanics*, Elsevier, v. 34, n. 3, p. 415–435, 1999.

BALACHANDRAN, B.; MAGRAB, E. B. *Vibrations*. 2nd. ed. Toronto, Canada: Cengage Learning, 2008.

BARTHA, A. R. *Dry friction backward whirl of rotors*. Tese (Doutorado) — ETH Zurich, 2000.

BEHZAD, M.; ALVANDI, M. Unbalance-induced rub between rotor and compliant-segmented stator. *Journal of Sound and Vibration*, Elsevier, v. 429, p. 96–129, 2018.

BEHZAD, M.; ALVANDI, M.; MBA, D.; JAMALI, J. A finite element-based algorithm for rubbing induced vibration prediction in rotors. *Journal of Sound and Vibration*, Elsevier, v. 332, n. 21, p. 5523–5542, 2013.

BHATTACHARYA, A.; CHILDS, D. W. Dry-friction whirl and whip between a rotor and a stator: effect of rotor-stator coupling due to seals and rotor rigid-body dynamics. In: AMERICAN SOCIETY OF MECHANICAL ENGINEERS DIGITAL COLLECTION. *ASME Turbo Expo 2009: Power for Land, Sea, and Air*. Orlando, FL, USA, 2009. p. 963–972.

BLACK, H. F. Interaction of a whirling rotor with a vibrating stator across a clearance annulus. *Journal of Mechanical Engineering Science*, SAGE Publications Sage UK: London, England, v. 10, n. 1, p. 1–12, 1968.

CASTRO, H. F. D.; CAVALCA, K. L.; NORDMANN, R. Whirl and whip instabilities in rotor-bearing system considering a nonlinear force model. *Journal of Sound and Vibration*, Elsevier, v. 317, n. 1-2, p. 273–293, 2008.

CHASALEVRIS, A.; PAPADOPOULOS, C. A novel semi-analytical method for the dynamics of nonlinear rotor-bearing systems. *Mechanism and Machine Theory*, Elsevier, v. 72, p. 39–59, 2014.

CHASALEVRIS, A. C.; PAPADOPOULOS, C. A. Nonlinear simulation of continuous rotor bearing systems with multi-step geometry. In: *Proc. Of the 8th IFToMM Int. Conf. on Rotordynamics*. Seoul, Korea: [s.n.], 2010.

CHATELET, E.; LORNAGE, D.; JACQUET-RICHARDET, G. A three dimensional modeling of the dynamic behavior of composite rotors. *International Journal of Rotating Machinery*, Hindawi, v. 8, n. 3, p. 185–192, 2002.

CHEN, G.; ZENG, X.; LIU, X.; RUI, X. Transfer matrix method for the free and forced vibration analyses of multi-step Timoshenko beams coupled with rigid bodies on springs. *Applied Mathematical Modelling*, Elsevier, v. 87, p. 152–170, 2020.

CHEN, L. et al. The visualization of rub-impact characteristics of drill string on casing. *Journal of Petroleum Science and Engineering*, Elsevier, v. 174, p. 1321–1331, 2019.

CHIBA, A. et al. *Magnetic bearings and bearingless drives*. Oxford, UK: Elsevier, 2005.

CHILDS, D. *Turbomachinery rotordynamics: phenomena, modeling, and analysis*. New York: John Wiley & Sons, 1993.

CHILDS, D. W.; BHATTACHARYA, A. Prediction of dry-friction whirl and whip between a rotor and a stator. *Journal of Vibration and Acoustics*, v. 129, n. 3, p. 355–362, 2007.

CHIPATO, E.; SHAW, A. D.; FRISWELL, M. I. Frictional effects on the nonlinear dynamics of an overhung rotor. *Communications in Nonlinear Science and Numerical Simulation*, Elsevier, v. 78, p. 104875, 2019.

CHU, F.; LU, W. Experimental observation of nonlinear vibrations in a rub-impact rotor system. *Journal of Sound and Vibration*, Elsevier, v. 283, n. 3-5, p. 621–643, 2005.

COLE, M. O. T.; KEOGH, P. S. Asynchronous periodic contact modes for rotor vibration within an annular clearance. *Proceedings of the Institution of Mechanical Engineers, Part C: Journal of Mechanical Engineering Science*, Sage Publications Sage UK: London, England, v. 217, n. 10, p. 1101–1115, 2003.

CRANDALL, S. H. From whirl to whip in rotor dynamics. In: *Proceedings of 3rd International Conference on Rotordynamics,(1990-9)*. [S.l.: s.n.], 1990.

CRANDALL, S. H.; YEH, N. A. Automatic generation of component modes for rotordynamic substructures. *Journal of Vibration and Acoustics*, v. 111, n. 1, p. 6–10, 1989.

CRESPO, R. S.; SHAW, A. D.; FRISWELL, M. I.; CHAMPNEYS, A. R. Experimental characterisation of asynchronous partially contacting motion in a multiple-degree-of-freedom rotor system. *Mechanical Systems and Signal Processing*, Elsevier, v. 145, p. 106904, 2020.

DIMAROGONAS, A. D. A study of the Newkirk effect in turbomachinery. *Wear*, Elsevier, v. 28, n. 3, p. 369–382, 1974.

EHEHALT, U.; ALBER, O.; MARKERT, R.; WEGENER, G. Experimental observations on rotor-to-stator contact. *Journal of Sound and Vibration*, v. 446, p. 453–467, 2019. ISSN 0022-460X. Disponível em: <http://www.sciencedirect.com/science/article/pii/S0022460X19300148>.

EHRICH, F. F. High order subharmonic response of high speed rotors in bearing clearance. *Journal of Vibration and Acoustics*, v. 1, n. 110, p. 9–10, 1988.

EHRICH, F. F. Some observations of chaotic vibration phenomena in high-speed rotordynamics. *Journal of Vibration and Acoustics*, American Society of Mechanical Engineers Digital Collection, v. 113, n. 1, p. 50–57, 1991.

ESHLEMAN, R. L.; EUBANKS, R. A. On the critical speeds of a continuous shaft-disk system. *Journal of Engineering for Industry*, v. 89, n. 4, p. 645–652, 1967.

ESHLEMAN, R. L.; EUBANKS, R. A. On the critical speeds of a continuous rotor. *Journal of Engineering for Industry*, v. 91, n. 4, p. 1180–1188, 1969.

EWINS, D. J. *Modal testing: theory, practice and application*. 2nd. ed. Philadelphia, PA: John Wiley & Sons, 2000. ISBN 0863802184.

FANG, H.; YANG, B. Modelling, synthesis and dynamic analysis of complex flexible rotor systems. *Journal of Sound and Vibration*, Elsevier, v. 211, n. 4, p. 571–592, 1998.

FARGHALY, S. H.; EL-SAYED, T. A. Exact free vibration of multi-step Timoshenko beam system with several attachments. *Mechanical Systems and Signal Processing*, Elsevier, v. 72, p. 525–546, 2016.

FONSECA, C. A.; SANTOS, I. F.; WEBER, H. I. Influence of unbalance levels on nonlinear dynamics of a rotor-backup rolling bearing system. *Journal of Sound and Vibration*, Elsevier, v. 394, p. 482–496, 2017.

FRISWELL, M. I.; PENNY, J. E. T.; SEAMUS, D. G.; LEES, A. W. *Dynamics of rotating machines*. New York: Cambridge University Press, 2010. 526 p.

GARVEY, S. D.; PENNY, J. E. T.; FRISWELL, M. I. The relationship between the real and imaginary parts of complex modes. *Journal of Sound and Vibration*, Elsevier, v. 212, n. 1, p. 75–83, 1998.

GASCH, R.; NORDMANN, R.; PFÜTZNER, H. *Rotordynamik*. Berlin: Springer-Verlag Berlin Heidelberg GmbH, 1975.

GENTA, G. A fast modal technique for the computation of the Campbell diagram of multi-degree-of-freedom rotors. *Journal of Sound and Vibration*, Elsevier, v. 155, n. 3, p. 385–402, 1992.

GENTA, G. *Dynamics of rotating systems*. New York: Springer Science & Business Media, 2007. 658 p.

GLASGOW, D. A.; NELSON, H. D. Stability analysis of rotor-bearing systems using component mode synthesis. *Journal of Mechanical Design*, v. 102, n. 2, p. 352–359, 1980.

GOLDMAN, P.; MUSZYNSKA, A. Chaotic behavior of rotor/stator systems with rubs. *Journal of Engineering for Gas Turbines and Power*, American Society of Mechanical Engineers Digital Collection, v. 116, n. 3, p. 692–701, 1994.

GUYAN, R. J. Reduction of stiffness and mass matrices. *AIAA journal*, v. 3, n. 2, p. 380, 1965.

HARTOG, J. P. D. *Mechanical vibrations*. Mineola, NY: Dover Publications, Inc, 1985. 435 p.

HONG, S.-W.; PARK, J.-H. Dynamic analysis of multi-stepped, distributed parameter rotor-bearing systems. *Journal of Sound and Vibration*, Elsevier, v. 227, n. 4, p. 769–785, 1999.

HONG, S.-W.; PARK, J.-H. Modal Analysis of Multi-Stepped Distributed-Parameter Rotor-Bearing Systems Using Exact Dynamic Elements. *Journal of Vibration and Acoustics*, v. 123, n. 3, p. 401–403, 2 2001. ISSN 1048-9002.

HSIEH, S.-C.; CHEN, J.-H.; LEE, A.-C. A modified transfer matrix method for the coupling lateral and torsional vibrations of symmetric rotor-bearing systems. *Journal of Sound and Vibration*, Elsevier, v. 289, n. 1-2, p. 294–333, 2006.

HUNT, K. H.; CROSSLEY, F. R. E. Coefficient of restitution interpreted as damping in vibroimpact. *Journal of Applied Mechanics*, v. 42, n. 2, p. 440–445, 1975.

INMAN, D. J. *Engineering vibration (3rd.)*. [S.l.]: Pearson Education, Inc, 2008.

ISHIDA, Y. Nonlinear vibrations and chaos in rotordynamics. *JSME international journal. Ser. C, Dynamics, control, robotics, design and manufacturing*, The Japan Society of Mechanical Engineers, v. 37, n. 2, p. 237–245, 1994.

ISHIDA, Y.; NAGASAKA, I.; INOUE, T.; LEE, S. Forced oscillations of a vertical continuous rotor with geometric nonlinearity. *Nonlinear Dynamics*, Springer, v. 11, n. 2, p. 107–120, 1996.

ISHIDA, Y.; YAMAMOTO, T. *Linear and nonlinear rotordynamics : a modern treatment with applications*. 2nd enl. a. ed. Weinheim, Germany: Wiley Online Library, 2012. 447 p. ISBN 9783527651894.

JACQUET-RICHARDET, G. et al. Rotor to stator contacts in turbomachines. Review and application. *Mechanical Systems and Signal Processing*, Elsevier, v. 40, n. 2, p. 401–420, 2013.

JANG, S. K.; BERT, C. W. Free vibration of stepped beams: exact and numerical solutions. *Journal of Sound and Vibration*, v. 130, n. 2, p. 342–346, 1989.

JANG, S. K.; BERT, C. W. Free vibration of stepped beams: higher mode frequencies and effects of steps on frequency. *Journal of Sound and Vibration*, v. 132, n. 1, p. 164–168, 1989.

JANSEN, J. D. Non-linear rotor dynamics as applied to oilwell drillstring vibrations. *Journal of Sound and Vibration*, Elsevier, v. 147, n. 1, p. 115–135, 1991.

JAWORSKI, J. W.; DOWELL, E. H. Free vibration of a cantilevered beam with multiple steps: Comparison of several theoretical methods with experiment. *Journal of Sound and Vibration*, Elsevier, v. 312, n. 4-5, p. 713–725, 2008.

JEFFCOTT, H. H. XXVII. The lateral vibration of loaded shafts in the neighbourhood of a whirling speed.—The effect of want of balance. *The London, Edinburgh, and Dublin Philosophical Magazine and Journal of Science*, Taylor & Francis, v. 37, n. 219, p. 304–314, 1919.

JEI, Y.-G.; LEE, C.-W. Finite element model of asymmetrical rotor-bearing systems. *KSME Journal*, Springer, v. 2, n. 2, p. 116–124, 1988.

JEI, Y.-G.; LEE, C.-W. Does curve veering occur in the eigenvalue problem of rotors? *Journal of Vibration and Acoustics*, v. 114, n. 1, p. 32–36, 1992.

JEI, Y.-G.; LEE, C.-W. Modal analysis of continuous asymmetrical rotor-bearing systems. *Journal of Sound and Vibration*, Elsevier, v. 152, n. 2, p. 245–262, 1992.

JIANG, J. Determination of the global responses characteristics of a piecewise smooth dynamical system with contact. *Nonlinear Dynamics*, Springer, v. 57, n. 3, p. 351–361, 2009.

JIANG, J.; SHANG, Z.; HONG, L. Characteristics of dry friction backward whirl—A self-excited oscillation in rotor-to-stator contact systems. *Science China Technological Sciences*, Springer, v. 53, n. 3, p. 674–683, 2010.

JIANG, J.; ULBRICH, H. Dynamics and stability of rotor/stator systems with rubs. In: AMERICAN SOCIETY OF MECHANICAL ENGINEERS DIGITAL COLLECTION. *ASME Turbo Expo 2000: Power for Land, Sea, and Air*. Munich, Germany, 2000.

JIANG, J.; ULBRICH, H. The physical reason and the analytical condition for the onset of dry whip in rotor-to-stator contact systems. *Journal of Vibration and Acoustics*, v. 127, n. 6, p. 594–603, 2005.

JU, F.; LEE, H. P.; LEE, K. H. On the free vibration of stepped beams. *International Journal of Solids and Structures*, Elsevier, v. 31, n. 22, p. 3125–3137, 1994.

JUN, O. S.; KIM, J. O. Free bending vibration of a multi-step rotor. *Journal of Sound and Vibration*, Elsevier, v. 224, n. 4, p. 625–642, 1999.

KANG, Y.; SHIH, Y.-P.; LEE, A.-C. Investigation on the steady-state responses of asymmetric rotors. *Journal of Vibration and Acoustics*, v. 114, n. 2, p. 194–208, 1992.

KHULIEF, Y. A.; MOHIUDDIN, M. A. On the dynamic analysis of rotors using modal reduction. *Finite Elements in Analysis and Design*, Elsevier, v. 26, n. 1, p. 41–55, 1997.

KLEIN, L. Transverse vibrations of non-uniform beams. *Journal of Sound and Vibration*, Elsevier, v. 37, n. 4, p. 491–505, 1974.

KOPLOW, M. A.; BHATTACHARYYA, A.; MANN, B. P. Closed form solutions for the dynamic response of Euler–Bernoulli beams with step changes in cross section. *Journal of Sound and Vibration*, Elsevier, v. 295, n. 1-2, p. 214–225, 2006.

KRÄMER, E. *Dynamics of rotors and foundations*. New York: Springer-Verlag Berlin Heidelberg GmbH, 1993.

KU, D.-M. Finite element analysis of whirl speeds for rotor-bearing systems with internal damping. *Mechanical Systems and Signal Processing*, v. 12, n. 5, p. 599–610, 1998. ISSN 0888-3270.

LALANNE, M.; FERRARIS, G. *Rotordynamics prediction in engineering*. New York: Wiley, 1998. ISBN 0471972886.

LEE, C.-W. A complex modal testing theory for rotating machinery. *Mechanical Systems and Signal Processing*, Elsevier, v. 5, n. 2, p. 119–137, 1991.

LEE, C. W. *Vibration analysis of rotors*. 1st. ed. Dordrecht, Netherlands: Springer Science & Business Media, 1993.

LEE, C.-W.; CHUN, S.-B. Vibration analysis of a rotor with multiple flexible disks using assumed modes method. *Journal of Vibration and Acoustics*, v. 120, n. 1, p. 87–94, 1998.

LEE, C.-W.; JEI, Y.-G. Modal analysis of continuous rotor-bearing systems. *Journal of Sound and Vibration*, Elsevier, v. 126, n. 2, p. 345–361, 1988.

LEE, J. W.; LEE, J. Y. An exact transfer matrix expression for bending vibration analysis of a rotating tapered beam. *Applied Mathematical Modelling*, Elsevier, v. 53, p. 167–188, 2018.

LEE, U. *Spectral Element Method in Structural Dynamics*. Singapore: John Wiley and Sons, 2009. 1–454 p. ISBN 9780470823767.

LEGRAND, M.; JIANG, D.; PIERRE, C.; SHAW, S. W. Nonlinear Normal Modes of a Rotating Shaft Based on the Invariant Manifold Method. *International Journal of Rotating Machinery*, v. 10, n. 4, p. 319–335, 2004.

LEVINSON, M. Free vibration of stepped beams: exact and numerical solutions. *Journal of Sound and Vibration*, v. 49, n. 2, p. 287–291, 1976.

LIN, R. M.; NG, T. Y. Exact vibration modes of multiple-stepped beams with arbitrary steps and supports using elemental impedance method. *Engineering Structures*, Elsevier, v. 152, p. 24–34, 2017.

LU, Z. R. et al. Vibration analysis of multiple-stepped beams with the composite element model. *Journal of Sound and Vibration*, Elsevier, v. 322, n. 4-5, p. 1070–1080, 2009.

LUND, J. W. Stability and Damped Critical Speeds of a Flexible Rotor in Fluid-Film Bearings. *Journal of Engineering for Industry*, v. 96, n. 2, p. 509–517, 5 1974. ISSN 0022-0817.

MAGRAB, E. B. *Vibrations of elastic systems: With applications to MEMS and NEMS*. Dordrecht, Netherlands: Springer Netherlands, 2012. 492 p.

MARTIN, L. B. S.; MENDES, R. U.; CAVALCA, K. L. Model reduction and dynamic matrices extraction from state-space representation applied to rotating machines. *Mechanism and Machine Theory*, Elsevier, v. 149, p. 103804, 2020.

MEIROVITCH, L. *Elements of vibration analysis*. New York: McGraw-Hill, 1975. 495 p.

MEIROVITCH, L. *Computational methods in structural dynamics*. Rockville, USA: Sjithoff & Noordhoff International Publishers, 1980. v. 5.

MEIROVITCH, L. Analytical methods in vibrations. *McMillan, New York*, 1998.

MEIROVITCH, L.; KWAK, M. K. Rayleigh-Ritz based substructure synthesis for flexible multibody systems. *AIAA Journal*, American Institute of Aeronautics and Astronautics, v. 29, n. 10, p. 1709–1719, 10 1991. ISSN 0001-1452. Disponível em: <https://doi.org/10.2514/3.10794>.

MENDES, R. U.; CAVALCA, K. L. On the instability threshold of journal bearing supported rotors. *International Journal of Rotating Machinery*, Hindawi, v. 2014, 2014.

MOKHTAR, M. A.; DARPE, A. K.; GUPTA, K. Analysis of stator vibration response for the diagnosis of rub in a coupled rotor-stator system. *International Journal of Mechanical Sciences*, Elsevier, v. 144, p. 392–406, 2018.

MUSZYNSKA, A. *Rotordynamics*. Boca Raton, FL: Taylor & Francis Group, LLC, 2005. 1054 p.

NAYFEH, A. H.; PAI, P. F. *Linear and nonlinear structural mechanics*. Hoboken, NJ: John Wiley & Sons, 2008. (Wiley series in nonlinear science). ISBN 3527617566. Disponível em: <http://search.ebscohost.com/login.aspx?direct=true&db=cat04198a&AN=unicamp.000886843&lang=pt-br&site=eds-live&scope=sitehttp://dx.doi.org/10.1002/9783527617562>.

NELSON, H. D.; MCVAUGH, J. M. The dynamics of rotor-bearing systems using finite elements. *Journal of Manufacturing Science and Engineering*, v. 98, n. 2, p. 593–600, 1976.

ÖZCSAHIN, O.; ÖZGÜVEN, H. N.; BUDAK, E. Analytical modeling of asymmetric multi-segment rotor–bearing systems with Timoshenko beam model including gyroscopic moments. *Computers & Structures*, Elsevier, v. 144, p. 119–126, 2014.

POPPRATH, S.; ECKER, H. Nonlinear dynamics of a rotor contacting an elastically suspended stator. *Journal of Sound and Vibration*, Elsevier, v. 308, n. 3-5, p. 767–784, 2007.

PRABITH, K.; KRISHNA, I. R. P. The numerical modeling of rotor–stator rubbing in rotating machinery: a comprehensive review. *Nonlinear Dynamics*, Springer, p. 1–47, 2020.

PUST, L.; PETERKA, F. Impact oscillator with Hertz's model of contact. *Meccanica*, Springer, v. 38, n. 1, p. 99–116, 2003.

RAFFA, F. A.; VATTA, F. Gyroscopic effects analysis in the Lagrangian formulation of rotating beams. *Meccanica*, Springer, v. 34, n. 5, p. 357–366, 1999.

RAFFA, F. A.; VATTA, F. Equations of motion of an asymmetric Timoshenko shaft. *Meccanica*, Springer, v. 36, n. 2, p. 201–211, 2001.

RANKINE, W. J. M. On the centrifugal force of rotating shafts. *Van Nostrand's Eclectic Engineering Magazine (1869-1879)*, Center for Research Libraries, v. 1, n. 7, p. 598, 1869.

RAO, S. S. *Mechanical vibrations*. 5th ed. ed. Upper Saddle River, NJ, USA: Pearson Prentice Hall, 2004. 1084 p.

RAO, S. S. *Vibration of continuous systems*. Hoboken, NJ: John Wiley and Sons, Inc, 2007. v. 464.

RIEMANN, B. et al. Oil whip instability control using μ-synthesis technique on a magnetic actuator. *Journal of Sound and Vibration*, Elsevier, v. 332, n. 4, p. 654–673, 2013.

ROQUES, S. et al. Modeling of a rotor speed transient response with radial rubbing. *Journal of Sound and Vibration*, Elsevier, v. 329, n. 5, p. 527–546, 2010.

ROSENBLUM, V. I. Entstehung mehrfacher Wellenbrüche nach dem Bruch einer Laufschaufel oder Radscheibe bei Dampfturbinen. *Allianz Report*, ALLIANZ VERSICHERUNGS-AG, v. 68, p. 176, 1995.

SAWICKI, J. T.; GENTA, G. Modal uncoupling of damped gyroscopic systems. *Journal of Sound and Vibration*, Elsevier, v. 244, n. 3, p. 431–451, 2001.

SHAD, M. R.; MICHON, G.; BERLIOZ, A. Modeling and analysis of nonlinear rotordynamics due to higher order deformations in bending. *Applied Mathematical Modelling*, Elsevier, v. 35, n. 5, p. 2145–2159, 2011.

SHANG, Z.; JIANG, J.; HONG, L. The influence of the cross-coupling effects on the dynamics of rotor/stator rubbing. In: *Dynamical Systems*. [S.l.]: Springer, 2010. p. 121–132.

SHAW, A. D.; CHAMPNEYS, A. R.; FRISWELL, M. I. Asynchronous partial contact motion due to internal resonance in multiple degree-of-freedom rotordynamics. *Proceedings of the Royal Society A: Mathematical, Physical and Engineering Sciences*, The Royal Society Publishing, v. 472, n. 2192, p. 20160303, 2016.

SHAW, S. W.; BALACHANDRAN, B. A review of nonlinear dynamics of mechanical systems in year 2008. *Journal of System Design and Dynamics*, The Japan Society of Mechanical Engineers, v. 2, n. 3, p. 611–640, 2008.

SORRENTINO, S.; MARCHESIELLO, S.; PIOMBO, B. A. D. A new analytical technique for vibration analysis of non-proportionally damped beams. *Journal of Sound and Vibration*, Elsevier, v. 265, n. 4, p. 765–782, 2003.

STEPHENSON, R. W.; ROUCH, K. E. Modeling rotating shafts using axisymmetric solid finite elements with matrix reduction. *Journal of Vibration and Acoustics*, v. 115, n. 4, p. 484–489, 1993.

STRAUSS, W. A. *Partial Differential Equations: An Introduction, 2nd Edition*. 2nd. ed. Hoboken, NJ: John Wiley & Sons, 2007. 464 p.

STROGATZ, S. H. *Nonlinear dynamics and chaos with student solutions manual: With applications to physics, biology, chemistry, and engineering*. Boca Raton, FL: CRC press, 2018. 513 p.

SUN, G. Rotor drop and following thermal growth simulations using detailed auxiliary bearing and damper models. *Journal of Sound and Vibration*, Elsevier, v. 289, n. 1-2, p. 334–359, 2006.

SZOLC, T. On the Discrete–Continuous Modeling of Rotor Systems for the Analysis of Coupled Lateral Torsional Vibrations. *International Journal of Rotating Machinery*, Hindawi, v. 6, 2000.

TALEB, N. J.; SUPPIGER, E. W. Vibration of stepped beams. *Journal of the Aerospace Sciences*, v. 28, n. 4, p. 295–298, 1961.

TIWARI, R. *Rotor Systems: Analysis and Identification*. 1st. ed. Boca Raton, FL: CRC Press, 2017. 1069 p. ISBN 9781138036284.

TORABI, K.; AFSHARI, H.; NAJAFI, H. Vibration Analysis of Multi-Step Bernoulli-Euler and Timoshenko Beams Carrying Concentrated Masses. *Journal of Solid Mechanics*, v. 5, n. 4, p. 336–349, 2013.

TORABI, K.; AFSHARI, H.; NAJAFI, H. Whirling analysis of axial-loaded multi-step Timoshenko rotor carrying concentrated masses. *Journal of Solid Mechanics*, v. 9, n. 1, p. 138–156, 2017.

VAKAKIS, A. Non-linear normal modes (NNMs) and their applications in vibration theory: an overview. *Mechanical Systems and Signal Processing*, v. 11, n. 1, p. 3–22, 1997.

VANCE, J. M.; ZEIDAN, F. Y.; MURPHY, B. G. *Machinery vibration and rotordynamics*. Hoboken, NJ: John Wiley & Sons, Inc, 2010.

VARANIS, M. et al. Rubbing effect analysis in a continuous rotor model. In: CAVALCA, K. L.; WEBER, H. I. (Ed.). *International Conference on Rotor Dynamics*. Rio de Janeiro, Brazil: Springer Nature Switzerland AG, 2018. p. 387–399.

VARANIS, M. et al. Modeling and experimental validation of two adjacent portal frame structures subjected to vibro-impact. *Latin American Journal of Solids and Structures*, v. 16, n. 4, 2019. ISSN 16797825.

VARANIS, M. et al. Impact dynamics models: A short review on nonlinearities effects. *International Review of Mechanical Engineering*, v. 11, n. 3, p. 167–174, 2017. ISSN 25325655.

VARNEY, P.; GREEN, I. Nonlinear phenomena, bifurcations, and routes to chaos in an asymmetrically supported rotor–stator contact system. *Journal of Sound and Vibration*, Elsevier, v. 336, p. 207–226, 2015.

VAZ, J. d. C.; JUNIOR, J. J. de L. Vibration analysis of Euler-Bernoulli beams in multiple steps and different shapes of cross section. *Journal of Vibration and Control*, SAGE Publications Sage UK: London, England, v. 22, n. 1, p. 193–204, 2016.

WAGNER, M. B.; YOUNAN, A.; ALLAIRE, P.; COGILL, R. Model reduction methods for rotor dynamic analysis: a survey and review. *International Journal of Rotating Machinery*, Hindawi, v. 2010, 2010.

WANG, S.; HONG, L.; JIANG, J. Characteristics of stick-slip oscillations in dry friction backward whirl of piecewise smooth rotor/stator rubbing systems. *Mechanical Systems and Signal Processing*, Elsevier, v. 135, p. 106387, 2020.

WANG, X.; WANG, Y. Free vibration analysis of multiple-stepped beams by the differential quadrature element method. *Applied Mathematics and Computation*, Elsevier, v. 219, n. 11, p. 5802–5810, 2013.

WILKES, J. C.; CHILDS, D. W.; DYCK, B. J.; PHILLIPS, S. G. The numerical and experimental characteristics of multimode dry-friction whip and whirl. *Journal of Engineering for Gas Turbines and Power*, American Society of Mechanical Engineers Digital Collection, v. 132, n. 5, 2010.

YU, J. J.; GOLDMAN, P.; BENTLY, D. E. Rotor/Seal Experimental and Analytical Study on Full Annular Rub. In: AMERICAN SOCIETY OF MECHANICAL ENGINEERS DIGITAL COLLECTION. *ASME Turbo Expo 2000: Power for Land, Sea, and Air*. Munich, Germany, 2000.

YU, J. J.; GOLDMAN, P.; BENTLY, D. E.; MUZYNSKA, A. Rotor/seal experimental and analytical study on full annular rub. *Journal of Engineering for Gas Turbines and Power*, v. 124, n. 2, p. 340–350, 2002.

ZILLI, A.; WILLIAMS, R. J.; EWINS, D. J. Nonlinear dynamics of a simplified model of an overhung rotor subjected to intermittent annular rubs. *Journal of Engineering for Gas Turbines and Power*, American Society of Mechanical Engineers Digital Collection, v. 137, n. 6, 2015.

Appendix A – Functions for isotropic rotors

For an arbitrary segment i along the rotor with a kth disk and lth bearing,

$$f_1(\xi_i) = \left(\frac{\rho A_i r_i^2}{EI_i}\left(\lambda^2 - 2j\lambda\Omega\right) + \frac{\kappa G A_i}{EI_i}\right) L_0(\xi_i) \tag{A.1}$$

$$f_2(\xi_i) = L_1(\xi_i) \tag{A.2}$$

$$f_3(\xi_i) = L_3(\xi_i) - \left(\frac{\rho A_i r_i^2}{EI_i}\left(\lambda^2 - 2j\lambda\Omega\right)\right) L_1(\xi_i) \tag{A.3}$$

$$f_4(\xi_i) = L_2(\xi_i) - \left(\frac{\rho A_i r_i^2}{EI_i}\left(\lambda^2 - 2j\lambda\Omega\right) + \frac{\kappa G A_i}{EI_i}\right) L_0(\xi_i) \tag{A.4}$$

$$g_1(\xi_i) = \left(\frac{\kappa G A_i}{EI_i} - \frac{\rho\lambda^2}{\kappa G}\right) L_1(\xi_i) + L_3(\xi_i) \tag{A.5}$$

$$g_2(\xi_i) = L_2(\xi_i) - \left(\frac{\rho\lambda^2}{\kappa G}\right) L_1(\xi_i) \tag{A.6}$$

$$g_3(\xi_i) = -\left(\frac{\rho\lambda^2}{EI_i}\right) L_0(\xi_i) \tag{A.7}$$

$$g_4(\xi_i) = -\left(\frac{\kappa G A_i}{EI_i}\right) L_1(\xi_i) \tag{A.8}$$

$$p_1^{a_k}(\xi_i) = \frac{M^k\lambda^2}{\kappa G A_i}\left[G_2^{a_k}(\xi_i) - \left(\frac{\rho A_i r_i^2}{EI_i}\left(\lambda^2 - 2j\lambda\Omega\right) + \frac{\kappa G A_i}{EI_i}\right) G_0^{a_k}(\xi_i)\right] \tag{A.9}$$

$$p_2^{a_k}(\xi_i) = -\left(\frac{M^k\lambda^2}{EI_i}\right) G_1^{a_k}(\xi_i) \tag{A.10}$$

$$h_1^{a_k}(\xi_i) = \left(\frac{\lambda^2 J_d^k - j\lambda\Omega J_p^k}{EI_i}\right) G_1^{a_k}(\xi_i) \tag{A.11}$$

$$h_2^{a_k}(\xi_i) = \left(\frac{\lambda^2 J_d^k - j\lambda\Omega J_p^k}{EI_i}\right)\left[G_2^{a_k}(\xi_i) - \left(\frac{\rho\lambda^2}{\kappa G}\right) G_0^{a_k}(\xi_i)\right] \tag{A.12}$$

$$p_1^{b_l}(\xi_i) = \frac{k_m^l + \lambda c_m^l}{\kappa G A_i}\left[G_2^{b_l}(\xi_i) - \left(\frac{\rho A_i r_i^2}{EI_i}\left(\lambda^2 - 2j\lambda\Omega\right) + \frac{\kappa G A_i}{EI_i}\right) G_0^{b_l}(\xi_i)\right] \tag{A.13}$$

$$p_2^{b_l}(\xi_i) = -\left(\frac{k_m^l + \lambda c_m^l}{EI_i}\right) G_1^{b_l}(\xi_i) \tag{A.14}$$

$$h_1^{b_l}(\xi_i) = -\left(\frac{k_t^l + \lambda c_t^l}{EI_i}\right) G_1^{b_l}(\xi_i) \tag{A.15}$$

$$h_2^{b_l}(\xi_i) = \left(\frac{k_t^l + \lambda c_t^l}{EI_i}\right)\left[G_2^{b_l}(\xi_i) - \left(\frac{\rho\lambda^2}{\kappa G}\right) G_0^{b_l}(\xi_i)\right] \tag{A.16}$$

where,

$$L_0(\xi_i) = \mathcal{L}^{-1}\left[\frac{1}{(s^2-\delta_i^2)(s^2+\varepsilon_i^2)}\right] = \frac{\varepsilon\sinh(\delta_i\xi) - \delta\sin(\varepsilon\xi_i)}{\delta\varepsilon\,(\delta^2+\varepsilon^2)} \tag{A.17}$$

$$L_1(\xi_i) = \mathcal{L}^{-1}\left[\frac{s}{(s^2-\delta_i^2)(s^2+\varepsilon_i^2)}\right] = \frac{\cosh(\delta_i\xi) - \cos(\varepsilon\xi_i)}{\delta^2+\varepsilon^2} \tag{A.18}$$

$$L_2(\xi_i) = \mathcal{L}^{-1}\left[\frac{s^2}{(s^2-\delta_i^2)(s^2+\varepsilon_i^2)}\right] = \frac{\delta\sinh(\delta_i\xi) + \varepsilon\sin(\varepsilon\xi_i)}{\delta^2+\varepsilon^2} \tag{A.19}$$

$$L_3(\xi_i) = \mathcal{L}^{-1}\left[\frac{s^3}{(s^2-\delta_i^2)(s^2+\varepsilon_i^2)}\right] = \frac{\delta^2\cosh(\delta_i\xi) + \varepsilon^2\cos(\varepsilon\xi_i)}{\delta^2+\varepsilon^2} \tag{A.20}$$

$$G_0^c(\xi_i) = \mathcal{L}^{-1}\left[\frac{e^{cs}}{(s^2-\delta_i^2)(s^2+\varepsilon_i^2)}\right] = \frac{\varepsilon\sinh(\delta_i(\xi-c)) - \delta\sin(\varepsilon(\xi_i-c))}{\delta\varepsilon\,(\delta^2+\varepsilon^2)} \tag{A.21}$$

$$G_1^c(\xi_i) = \mathcal{L}^{-1}\left[\frac{se^{cs}}{(s^2-\delta_i^2)(s^2+\varepsilon_i^2)}\right] = \frac{\cosh(\delta_i(\xi-c)) - \cos(\varepsilon(\xi_i-c))}{\delta^2+\varepsilon^2} \tag{A.22}$$

$$G_2^c(\xi_i) = \mathcal{L}^{-1}\left[\frac{s^2e^{cs}}{(s^2-\delta_i^2)(s^2+\varepsilon_i^2)}\right] = \frac{\delta\sinh(\delta_i(\xi-c)) + \varepsilon\sin(\varepsilon(\xi_i-c))}{\delta^2+\varepsilon^2} \tag{A.23}$$

being $\mathcal{L}^{-1}$ the Inverse Laplace Transform and c is either a_k or b_l. It is worth noting that the operation $\mathcal{L}^{-1}$ in Equations (A.21)-(A.23) also gives the Heaviside step function $H(\xi_i - c)$ $(c = a_k, b_l)$, which is not shown here but considered in Equations (3.38)-(3.39).

Appendix B – Functions for anisotropic rotors

For an arbitrary segment i along the rotor with a kth disk and lth bearing, the functions f_1, f_2, f_3, f_4, g_1, g_2, g_3 and g_4 are the same as in the isotropic case, and are shown in Eqs. (A.1)-(A.8). The remaining functions are obtained as,

$$f_j(\xi_i) = f_{j-4}^{-}(\xi_i) \quad \text{for } j = 5, 6, 7, 8 \tag{B.1}$$

$$g_j(\xi_i) = g_{j-4}^{-}(\xi_i) \quad \text{for } j = 5, 6, 7, 8 \tag{B.2}$$

where $^-$ means interchanging Ω to $-\Omega$, that is, reversing the rotation direction. Note that one also need to interchange the parameters δ_{1i} and ε_{1i} to δ_{2i} and ε_{2i}. The functions $p_1^{a_k}$, $p_2^{a_k}$, $h_1^{a_k}$ and $h_2^{a_k}$ are the same as in the isotropic case, given by Eqs. (A.9)-(A.12). In addition, one has,

$$p_j^{a_k}(\xi_i) = p_{j-2}^{a_k,-}(\xi_i) \quad \text{for } j = 3, 4 \tag{B.3}$$

$$h_j^{a_k}(\xi_i) = h_{j-2}^{a_k,-}(\xi_i) \quad \text{for } j = 3, 4 \tag{B.4}$$

The same is true for $h_2^{b_l}$. The functions, $p_{jf}^{b_l}$, $p_{jf}^{b_l}$, $p_{jb}^{b_l}$ and $p_{jb}^{b_l}$, for $j = 1, 2, 3, 4$, are given as,

$$p_{1f}^{b_l}(\xi_i) = \frac{k_f^l + \lambda c_f^l}{\kappa G A_i}\left[G_2^{b_l}(\xi_i) - \left(\frac{\rho A_i r_i^2}{EI_i}\left(\lambda^2 - 2j\lambda\Omega\right) + \frac{\kappa G A_i}{EI_i}\right) G_0^{b_l}(\xi_i)\right] \tag{B.5}$$

$$p_{2f}^{b_l}(\xi_i) = -\left(\frac{k_f^l + \lambda c_f^l}{EI_i}\right) G_1^{b_l}(\xi_i) \tag{B.6}$$

$$p_{3f}^{b_l}(\xi_i) = \frac{k_f^{l*} + \lambda c_f^{l*}}{\kappa G A_i}\left[G_2^{b_l,-}(\xi_i) - \left(\frac{\rho A_i r_i^2}{EI_i}\left(\lambda^2 + 2j\lambda\Omega\right) + \frac{\kappa G A_i}{EI_i}\right) G_0^{b_l,-}(\xi_i)\right] \tag{B.7}$$

$$p_{4f}^{b_l}(\xi_i) = -\left(\frac{k_f^{l*} + \lambda c_f^{l*}}{EI_i}\right) G_1^{b_l,-}(\xi_i) \tag{B.8}$$

$$p_{1b}^{b_l}(\xi_i) = \frac{k_b^l + \lambda c_b^l}{\kappa G A_i}\left[G_2^{b_l}(\xi_i) - \left(\frac{\rho A_i r_i^2}{EI_i}\left(\lambda^2 - 2j\lambda\Omega\right) + \frac{\kappa G A_i}{EI_i}\right) G_0^{b_l}(\xi_i)\right] \tag{B.9}$$

$$p_{2b}^{b_l}(\xi_i) = -\left(\frac{k_b^l + \lambda c_b^l}{EI_i}\right) G_1^{b_l}(\xi_i) \tag{B.10}$$

$$p_{3b}^{b_l}(\xi_i) = \frac{k_b^{l*} + \lambda c_b^{l*}}{\kappa G A_i}\left[G_2^{b_l,-}(\xi_i) - \left(\frac{\rho A_i r_i^2}{EI_i}\left(\lambda^2 + 2j\lambda\Omega\right) + \frac{\kappa G A_i}{EI_i}\right) G_0^{b_l,-}(\xi_i)\right] \tag{B.11}$$

$$p_{4b}^{b_l}(\xi_i) = -\left(\frac{k_f^{l*} + \lambda c_f^{l*}}{EI_i}\right) G_1^{b_l,-}(\xi_i) \tag{B.12}$$

where care should be taken to interchange δ_{1i} and ε_{1i} to δ_{2i} and ε_{2i} in the functions G^-. Here one can clearly see that in case $k_b^l = c_b^l = 0$, the functions of the bearings becomes the same as in the isotropic case shown in Eq. (A.13) and (A.14). Moreover, the addition

of anisotropic bearings have not such a great influence in the functions, and thus they can easily be applied computationally together with the isotropic case.

Appendix C – Functions for asymmetric rotors

Consider a segment i with a kth disk and lth bearing. Since presenting the full form of the functions in Eqs. (5.28)-(5.31) would not be of great help due to their length; it is instead presented here the way to obtain them. From Eq. (5.21), one may have,

$$\{\hat{\Phi}(s)\} = [L]^{-1}\{b\} = \frac{adj([L])}{det([L])}\{b\} = \frac{1}{det([L])}\{b'\} \tag{C.1}$$

where $\{b'\} = adj([L])\{b\}$, $adj(\cdot)$ means the adjoint matrix and $det(\cdot)$ means the determinant. As shown in Sec. 5.2, one has $det([L]) = (s^2 - \delta_{1i}^2)(s^2 + \varepsilon_{1i}^2)(s^2 - \delta_{2i}^2)(s^2 + \varepsilon_{2i}^2)$, being δ_{1i}^2, δ_{2i}^2, ε_{1i}^2 and ε_{2i}^2 the roots of the polynomial. To arrive at the functions f, g, p and h, one needs to isolate the corresponding variables in the vector $\{b'\}$. For example, to obtain $f_1(\xi_i)$, one needs to gather the terms multiplying $\eta_{1i}(0)$ in the first row of $\{b'\}$ and apply the inverse Laplace transform. In the case of $f_1(\xi_i)$, one may have,

$$f_1(\xi_i) = \mathcal{L}^{-1}\left[\frac{C_1 s^6 + C_2 s^4 + C_3 s^2 + C_4}{(s^2 - \delta_{1i}^2)(s^2 + \varepsilon_{1i}^2)(s^2 - \delta_{2i}^2)(s^2 + \varepsilon_{2i}^2)}\right] \tag{C.2}$$

where C_j are constants with the shaft properties. The above transformation is easily obtained through partial fractions and tabulated transforms (MAGRAB, 2012). The transforms needed for the other functions are similar, and the procedure can be made easier through the help of a symbolic math software.

Note that after obtaining the functions $f_1(\xi_i)$ through $f_8(\xi_i)$ from the first row of $\{b'\}$, the functions $f_9(\xi_i)$ through $f_{16}(\xi_i)$, which are given by the third row of $\{b'\}$, will have the same form but with Ω, δ_{1i} and ε_{1i} interchanged with $-\Omega$, δ_{2i} and ε_{2i}. This is also true for the functions $g_j(\xi_i)$. As for the disks and bearing functions, one needs to obtain p_{1f}^c, p_{2f}^c, h_{1f}^c, h_{2f}^c, p_{1b}^c, p_{2b}^c, h_{1b}^c and h_{2b}^c, being $c = a_k$ for disk and $c = b_l$ for bearing. The remaining functions, namely p_{3f}^c, p_{4f}^c, h_{3f}^c, h_{4f}^c and so on, will have the same form but with the rotation reversed and the mode shape parameters changed.

The final form of the functions in the asymmetric case will not be much different than the ones presented in Appendix A for the isotropic case; they will only have more terms and be much lengthier.